

Causality and Reversibility in Irreversible Time

Sergey Maratovich Korotaev



Scientific Research Publishing, USA

2011

Causality and Reversibility in Irreversible Time

Published by

Scientific Research Publishing, Inc.

ISBN: 978-1-935068-55-6

<http://www.scirp.org>

Copyright © 2011 by Scientific Research Publishing, Inc., USA.

All rights reserved.

This work may not be translated or copied in whole or in part without the written permission of the publisher (Scientific Research Publishing, Inc., USA), except for brief excerpts in connection with reviews or scholarly analysis. Use in connection with any form of information storage and retrieval, electronic adaptation, computer software, or by similar or dissimilar methodology now known or hereafter developed is forbidden.

Requests to the Publisher for permission should be addressed to the SRP Copyrights Manager, Scientific Research Publishing, Inc., USA, E-mail: service@scirp.org.

Biography of Editors

S. M. Korotaev was born 02/18/1950 in Sverdlovsk, Russia. In 1972 he graduated in for honors Leningrad Hydrometeorological Institute with degree of engineer-oceanologist. He was called to military service, after which he went to post-graduate course of the Institute of Terrestrial Magnetism, Ionosphere and Radio Wave Propagation, U.S.S.R. Academy of Sciences (IZMIRAN) in 1974. In 1977 he became junior researcher of IZMIRAN. He earned PhD at IZMIRAN in 1979. He was elected senior researcher in 1984. In 1992 he was elected leading researcher of Geoelectromagnetic Research Centre of Schmidt Institute of Physics of the Earth, Russian Academy of Sciences (GEMRC IPE RAS). He earned Dr. Sci. in 1993 at IPE RAS. From 1994 he is Head of Marine Electromagnetic Research Laboratory of GEMRC RAS. From 1999 he is also Professor of Physics Department of Bauman Moscow State Technical University. In addition, from 2007 he is the main specialist of Kurchatov Institute.

S. M. Korotaev dealt with study of electromagnetic field of the ocean, informational-statistical methods of analysis of the physical experiment, causal mechanics and quantum information. He works in sphere both theory and experiment. The field of his scientific interest covered nature of time, quantum nonlocality, electrodynamics, statistical physics, information theory and their geophysical and astrophysical applications. He deals with the problem of causality and nonlocality of the dissipative processes about 25 years. At the beginning his efforts were directed to the theory, and as a result the method of classical causal analysis had been created. Now this method is utilized in geophysics, astrophysics and economy. Latter he, together with him team, had created the first experimental setup for measurement of the macroscopic nonlocality effect and conducted wide series of the experiments. The main result proved to be revealing of transaction of the non-controlled dissipative processes in reverse time. On the basis of this effect a new method of the solar and geophysical long-term forecasts has been developed now. Recently he has developed the method of quantum causal analysis and has applied it to the various entangled states. Now he develops theory of quantum causality and time reversal phenomena and conducts the related experiments.

S. M. Korotaev is the author of about 200 scientific publications; in particular he is a co-author of the books: "Accounting of Time Variations in Marine Magnetic Survey" (1984), "From Relational to Substantial Time" (1995), "On the Way to Understanding the Time Phenomenon" Part 2 (1996) and Part 3 (2009).

Besides his scientific activity S. M. Korotaev is an active participant of democratic and liberal movement in Russia.

Preface

The problem of time is difficult for investigation because in it as no other, it is difficult to view at the subject “from outside”. Nevertheless usual physical approach, that is verification of a theoretical idea on the base of testing the experimental consequences predicted by it, remains valid. Therewith the deeper theory, the wider range of its consequences, therefore the different researchers may find the different ways to the same summit.

But in spite of obvious importance, up to now the nature of time, its irreversibility (or reversibility?), the causality (real or conventional?) are not in the focus of the physical mainstream. The triumphal procession of modern physics has just evaded these problems. One cannot say that the irreversibility problem is unacknowledged; its accepted solution reduces that irreversibility is a property of the physical systems, and in the most general view represents that time arrow is determined by the expansion of the Universe, pre-determined by its origin, the Big Bang. So all the problems are driven into one corner. With this they are banished from the sphere of everyday experience, but they do not become more intelligible.

The brilliant discoveries of twentieth century physics like proven instantaneous nonlocal correlations or a possibility of wormholes remain the islands in the Ocean Incognita. The philosophers readily fill the wide gaps between the available experimental facts or the reliable theories. But recall the term “philosophic paradox”: if a philosophic question becomes to be subject of concrete science, this question ceases to be a philosophic one!

In contrast to that approach, the fundamental irreversibility of time can be taken as the basis for a new physical approach. Its founder N. A. Kozyrev called this approach “causal mechanics” or “asymmetrical mechanics”. His rather simple theory (too simple from point of view of the physical establishment) predicted a number of absolutely new, but experimentally testable phenomena: existence of the pair longitudinal forces (“forces of causality”) in a gyroscope involved in the irreversible process, correlations of the distant irreversible processes without any local carriers of interaction and unusual time relation of these correlation which can be retarded, instantaneous and advanced, *i.e.* there is a surprising manifestation of reversibility in fundamentally irreversible time. Kozyrev had performed very extensive series of experiments which really confirmed the theoretical predictions, at least qualitatively. Of course these experiments were quite fine, although principally simple (again too simple from point of view of the physical establishment). I was lucky enough to observe most of Kozyrev experiment in his laboratory in 1970-th, and in spite of deficit of rigour in some of them, as a whole they impressed me very much and made sure that regardless of the interpretation, a really new domain of physical phenomena had been discovered. The fact that Kozyrev causal mechanics was not supported during his life is explained simply due to it was born too early.

In this book I describe modern theoretical and experimental approach to the same and related problems. The progress in quantum mechanics has shed a new light on N. A. Kozyrev’s ideas and his experimental results. Irreversible time calls for careful consideration of the concept of causality and the method of classical and quantum causal analysis suggested by the author is described. Quantum mechanical development of the causality concept turned out not only possible, but fruitful in many respects. The possibility of observation of the

future states as the existing reality demonstrated at the last stages of Kozyrev research seems now not only real, but allowing the certain applications. The quantum mechanical principle of weak causality admits availability of the signals in reverse time for the random processes. The macroscopic nonlocality equation reflects this possibility. The series of modern long-terms experiments has revealed availability of the advanced response of random dissipative probe-processes in the lab detectors to large-scale dissipative heliogeophysical processes with big random component. The high level of advanced correlation and the large time shift allowed to set the forecast problem. This problem has been solved and the solution has successfully tested on all obtained experimental data of enough volume for series of the long-term forecasts of solar and geomagnetic activity.

I hope that the readers of bringing to their notice a book will accept it with interest, and, possible, it will be useful to them as an impetus for their own ideas and research.

Sergey Korotaev
August, 2011

Acknowledgements

The author thanks Prof. M. L. Arushanov for collaboration in the classical aspect of this work, Prof. A. N. Morozov for kindly presented his experimental data and theoretical discussion, Dr. J. V. Gorohov for construction and maintenance of the experimental setup, V. O. Serdyuk for data processing and development of the forecasting algorithm, J. M. Abramov, V. A. Machinin and A. V. Novysh for participation in the experiments, and E. O. Kiktenko for fruitful collaboration in development of quantum causal analysis.

Contents at a Glance

Biography of Editors	I
Preface	III
Acknowledgments	V
Introduction	1
Chapter 1 Kozyrev Causal Mechanics and Its Application	3
Chapter 2 Classical Causal Analysis	11
Chapter 3 Quantum Causal Analysis	17
Chapter 4 Macroscopic Entanglement and Signals in Reverse Time	57
Chapter 5 Experimental Approach	63
Chapter 6 Results of the Experiments	71
Conclusion and Discussion	109
References	113
Abbreviations	117

Contents

Introduction	1
Chapter 1 Kozyrev Causal Mechanics and Its Application	
1.1. Kozyrev’s Idea and Results.....	5
1.2. Application of the Force of Causality to the Rotating Earth.....	7
Chapter 2 Classical Causal Analysis	
Chapter 3 Quantum Causal Analysis	
3.1. Kernel of the Method.....	19
3.2. Symmetric States.....	21
3.2.1. Pure States.....	21
3.2.2. Greenberger-Horne-Zeilinger State.....	22
3.2.3. W-State.....	22
3.2.4. Depolarization.....	22
3.2.5. Dephasing.....	23
3.2.6. Bell-Diagonal States.....	23
3.2.7. Werner States.....	26
3.2.8. Maximally Entangled Mixed States.....	27
3.3. Asymmetric Two-Particle States.....	29
3.3.1. Asymmetric Dissipation.....	30
3.3.2. Coffman-Kundu-Wootters State.....	32
3.3.3. WRr-State.....	33
3.3.4. Asymmetric “Quantum-Classical” States.....	33
3.3.5. Thermal Entanglement under a Nonuniform External Magnetic Field.....	36
3.4. Asymmetric Three-Particle States.....	42
3.4.1. Dissipated GHZ States.....	43
3.4.2. Dissipated W-States.....	45
3.4.3. Dissipated CKW States.....	45
3.4.4. Dissipated WRr-States.....	50
3.5. Overview of Causal Analysis.....	54

Chapter 4 Macroscopic Entanglement and Signals in Reverse Time

Chapter 5 Experimental Approach

Chapter 6 Results of the Experiments

6.1. Nonlocality of the Controlled Dissipative Processes.....73

 6.1.1. Statement of the Problem.....73

 6.1.2. Experimental Setup.....74

 6.1.3. The Performance of the Experiment.....74

 6.1.4. Results and Discussion.....75

6.2. Nonlocality of the Natural Dissipative Processes.....77

 6.2.1. Correlation of the Different Detector Signals.....77

 6.2.2. Relation of the Detector Signals with the Internal and External Temperature.....79

 6.2.3. Relation of the Detector Signals with the Synoptic Activity.....83

 6.2.4. Relation of the Detector Signals with the Geomagnetic Activity.....84

 6.2.5. Relation of the Detector Signals with the Ionospheric Activity.....93

 6.2.6. Relation of the Detector Signals with the Solar Activity.....93

 6.2.7. Application of Reversibility in Irreversible Time—Forecasting of the Random Large-Scale Processes.....102

Conclusion and Discussion.....109

References.....113

Abbreviations.....117

Introduction

The obvious reason of interest in the problem of time was and is its inexorable irreversibility. On the other hand the similarity of time and space co-ordinates had been noticed well before the relativity theory creation. The relativity has lent this similarity a dramatic completeness; a little difference has remained to give a place the causality principle. The commonly accepted paradigm brings the problem of time out of most tasks, deeming irreversibility as being a property of the concrete systems, but not a property of time—blessing all the basic physics equations are invariant with reference to the time sign change. From this point of view the sole really irreversible event occurred in the utmost distant past—it was the Big Bang. Since that time the relaxation to the equilibrium has been going, and that prescribes the observed time arrow in the all systems, while time itself is perfectly symmetric. On the other hand nobody denies the known T-noninvariantness of the weak interactions, *i.e.* time irreversibility occurring here and now.

Nikolay Kozyrev (1908-1983) was one of them who held that irreversibility is an inherent property of time. It was formulated in the first and main of three axioms of his causal mechanics [1]. But he was the only to go by this way (though weakly formulating it) to the end. The fact is, by virtue of the known relation of the symmetries and conservation laws, accepting of the time asymmetry inevitably implies violation of the energy conservation. In the traditional paradigm such violation is assumed only at the moment of the Universe birth, and since then the energy has been conserving always and every where absolutely exactly.

But the energy conservation is a usual empirical law established with a finite accuracy. Call attention to the interesting point: the experimental verification accuracy was particularly high for the practically reversible processes (with negligibly small dissipation). Although nowadays nobody performs the special experiments on verification of the energy conservation yet, the obvious violations would be, of course, noticed. But if we look at the wide range of the experiments, where such be it non-special organized verification occurs, we see that the greater dissipativity of a system, the rougher energy conservation is controlled. Wherever the dissipation is the essence of process, e.g. in many of the biological processes, the energy conservation is assured technically with accuracy only of order 10%. Kozyrev, starting from the time asymmetry, arrived at the conclusion on availability of a new form of the energy—the energy of time itself. It is precisely that closes the conservation law. Therefore time becomes an active substance. That involves some interaction, or more precisely transaction of any irreversible, that is dissipative processes.

Irreversible time calls for careful consideration of the concept of causality. That is why the name “causal mechanics” had been emerged. And this consideration had predicted a number of experimentally testable consequences. Kozyrev performed extensive series of the experiments which demonstrated unusual properties of the transaction through active time, for example, availability of instantaneous and advanced correlation of some dissipative processes. The latter means a possibility of observation of the future as the existing reality. It is a striking fact in itself and logically—beginning with the most radical acceptance of time irreversibility, we come to such fantastic manifestation of reversibility!

Causal mechanics was born not as a mental construction. It was challenged by some deep astrophysical problems (in particular of star energy sources), it has clear and very natural axiomatic, which through a few semiclassical theorems leads to the experimentally testable consequences, and it has a wide experimental basis. But its creator fate was dramatic. For his ideas Kozyrev was awarded by 10 years imprisonment in GULAG (1936-1946). Later he won world recognition for his astrophysical works and discoveries. But his causal mechanics was not accepted by most of physical community in due time because of weak formalization of the (semiclassical) theory and doubt of correctness of the experiments.

But the situation became to change in 1990th. Direct classical application of the theory to the rotating Earth, where the time energy manifests itself via the forces of causality was developed [2,3]. Existence of these forces explains in detail the known (and seemed accidental) hemisphere asymmetry of the Earth figure, deep geological structure and atmospheric circulation. Modern formalization of the foundations of

Introduction

causal mechanics, first of all—its concept of causality, has led to creation of the method of classical causal analysis with many the subsequent applications in basic physics, geophysics and astrophysics [4-14]. Next the quantum generalization of causal analysis has been suggested [15]. The causality parameters for the wide series of entangled states are computed. The results were compared with the standard measures of entanglement and degree of mixedness. The role of state asymmetry in quantum information transfer was shown. The quantum causal analysis helped to understand Cramer principle of weak causality [16] which admits extraction of information from the future without the classical paradoxes. Quantum insight in causal mechanics has allowed considering the distant correlations of any irreversible processes as the nonlocal ones originated from a macroscopic entanglement. The equation of macroscopic entanglement motivated by Wheeler-Feynman electrodynamics has been suggested, which turns out agree with the strict quantum mechanical solution at least for a simple model [17-21]. The experimental setup including different types of nonlocal correlation detectors was designed [17-25]. The long-term experiments directed to detection in the solar-terrestrial relationships have been performed [17-21,24-29]. The possibility of long-term forecasting of the random component of solar and geomagnetic activity on the advanced nonlocal correlations has been investigated. The forecasting algorithm, employing advanced correlations (that is signals in reverse time!), was suggested. Its efficiency has been proved on data of the long-term experiments in regime of the real forecast imitation with advancement up to four months. The accuracy of the obtained solar and geomagnetic forecasts is acceptable for all the practical purposes [30-33]. This book is devoted to that modern development of causal mechanics.

In Chapter 1, first, the short review of Kozyrev's idea and results is contained, and, second, the review of their direct classical applications are presented.

The classical causal analysis formalism is described in Chapter 2. Both the theoretical and experimental aspects of its implementation are discussed.

In Chapter 3 the extension of causal analysis to the quantum variables is considered. The question on the possibility of time reversal phenomena is arisen here in a very natural way. Application of causal analysis at the beginning is demonstrated to the symmetrical entangled states, where causality is absent, but nevertheless the quantitative characteristics of the mixed states can be obtained. Then the analysis of asymmetrical mixed entangled states is applied to the examples of increasing complexity, beginning with the illustrative obtaining of causality measure and ending with the nontrivial conclusions about causal connection nature depending on the external magnetic field and temperature, about rather complex causal connections in the many-parties systems, etc.

Chapter 4 is dedicated to the macroscopic entanglement model and related questions of causality and reversibility.

In Chapter 5 the experimental approach to study of macroscopic nonlocality is discussed and design of the experimental setup is described.

The results of experiments on study of macroscopic nonlocal correlations, the signals in reverse time and their practical application to the forecast of large-scale random irreversible processes are expounded in Chapter 6.

The author thanks Prof. M. L. Arushanov for collaboration in the classical aspect of this work, Prof. A. N. Morozov for kindly presented his experimental data and theoretical discussion, Dr. J. V. Gorohov for construction and maintenance of the experimental setup, V. O. Serdyuk for data processing and development of the forecasting algorithm, V. A. Machinin and A. V. Novysh for participation in the experiments, and E. O. Kiktenko for fruitful collaboration in development of quantum causal analysis.

Chapter 1

Kozyrev Causal Mechanics and Its Application

Table of Contents

Kozyrev's Idea and Results

Application of the Force of Causality to the Rotating Earth

1. Kozyrev Causal Mechanics and Its Application

1.1. Kozyrev's Idea and Results

Any naturalist, not limiting himself artificially by bounds of his peculiar tasks and thus not passing over the difficult universal physical problems, must fall to thinking on concordance of time reversibility in the basic physical theories and visible, one can say flagrant irreversibility of the real World. Any solution of this problem gets into one of two classes, namely: 1) irreversibility is the property of the system, and 2) irreversibility the property of time. The solutions from the former class are inevitable particular at variance with universality of the really observed irreversibility. However the most custom modern views are such exactly: irreversibility arises owing to incomplete description, *i.e.* it is the property of the system, including an observer. The solutions from the latter class on the strength of Nother theorem, lead automatically to violation of the energy conservation law. If we interpret this violation as expanding of the low bounds, then the energy of time arises. It is just the heart idea of causal mechanics suggested by Nikolay Kozyrev [1].

So Kozyrev's construction of time was based on its fundamental asymmetry. However, not only general logic of a naturalist had led him to the problem of time, but also reflection on the concrete astrophysical problems. The most important problem of such kind is the question on the energy sources of the stars. Having computed the parameters characterized state of star's interior (the temperature, density and energy emission), Kozyrev has statistically reliable shown, that in the state space almost the all stars are on the free cooling surface. It means that there are no any mechanisms of energy emission independent of the heat relinquishing. In particular (this question has especially been considered) the thermonuclear reactions can not be the energy source. The Kelvin-Gelmgolts mechanism has proved to be useful, but it is not acceptable, because of too short time scale. Kozyrev conclusion is in full contradiction with the conventional theory of thermonuclear mechanism of star fire, but it has nowhere been refuted. It has also been shown by Kozyrev, that planetary energy source is close to the star one. As a result he concluded that only time itself might be the energy source. Preventing stars to come in the equiponderant state, the course of time is the source of their energy. Therefore, time, in addition to the known geometric properties has some active ones. But it was found extremely difficult to obtain these properties by solving the inverse problems, and Kozyrev had suggested development of his concept by usual deductive way.

He had formulated the following 3 axioms:

1) Time has a specific property that distinguishes the causes from the effects and can be called the directionality or the course. This property defines the distinction between the past and the future.

2) The cause and the effect are always separated in space. Thus, there is as much small as is wished $\delta x \neq 0$ between them.

3) The cause and the effect are always separated in time. Thus, there is as much small as is wished $\delta t \neq 0$ between them.

Then Kozyrev had introduced a fundamental conception of the course of time c_2 :

$$c_2 = \delta x / \delta t = ae^2 / \hbar. \quad (1.1)$$

It has sense of the velocity of causal-effect transition at the level of an elementary link, that is, at the microlevel. It has been proven that c_2 is a pseudoscalar, that is, c_2 is the linear velocity of a rotation. Kozyrev also related c_2 with Plank constant and the elementary charge, where a is a dimensionless coefficient. Note than the classical limits of causal and quantum mechanics coincide:

$$\delta t \rightarrow 0 \Leftrightarrow |c_2| \rightarrow \infty \Leftrightarrow \hbar \rightarrow 0. \quad (1.2)$$

Next, Kozyrev has proved the theorem, according to which in the gyroscope, excited by any irreversible process of the enough energy, with the cause Y and effect X , there are new (unknown in classical mechanics) additional forces ΔF_X and ΔR_Y , acting along the axis of rotation j :

$$\Delta \mathbf{F}_X = -\mathbf{j} \frac{u}{c_2} |\mathbf{F}_X| \cos \mathcal{G}, \quad (1.3)$$

$$\Delta \mathbf{R}_Y = \bar{\mathbf{j}} \frac{u}{c_2} |\mathbf{F}_X| \cos \mathcal{G} = -\Delta \mathbf{F}_X. \quad (1.4)$$

They were called the forces of causality. u is the linear velocity of gyro rotation, \mathbf{F}_X is the inelastic force of the cause, affecting on the effect: $\mathbf{F}_X = \mathbf{F}_Y - \delta \mathbf{p}_Y / \delta t = \delta \mathbf{p}_X / \delta t$, \mathbf{F}_Y is the force applied on the point Y , \mathbf{p} is momentum, \mathcal{G} is the angle between \mathbf{j} and \mathbf{F}_X . For the force of causality to be measured in the macroscopic system it is necessary that cause and effect had a finite arm relatively the axis of the gyro. The momentum of the system does not change, but the energy of the system changes! In addition, if there is cross space of the points X and Y , the angular momentum of the system emerges.

Kozyrev had performed series of the experiments with the excited gyros, really discovered the forces of causality and confirmed the theoretical estimation of course of time value (and determined it's *a priori* unknown sign) $c_2 = +(2.2 \pm 0.1) \cdot 10^6$ m/s. The experiment repeated many times at different performance (vertical and horizontal orientation of the gyro axis), different positions the cause and the effect, different kinds of the exciting dissipative process (providing inelastic interaction the gyro and the support).

He also had performed other series of the experiments in which the forces of causality of the rotating Earth were revealed. These forces proved to be parallel to the Earth axis and dependent on the latitude, with the change of the sign near 73° . Kozyrev supposed that asymmetrical figure of the Earth was formed namely by the forces of causality.

On the next stage, Kozyrev had conducted another series of experiments on correlation of any irreversible that is dissipative processes through the active time. The theoretical background of these experiments was weaker, rather intuitive. Nevertheless this background had convincing predictability. Shortly, Kozyrev had invented several types of detectors, included some probe dissipative processes, respondent to the artificial lab and natural astrophysical source-processes. The sign of detector response dependent on the sign of the entropy change in the source. It means, by Kozyrev, that processes progress not only in time, but and with help of time. Specifically, his experimental results can be formulated in the following statements:

- 1) A new type of transaction between the dissipative processes of any nature exists;
- 2) This transaction transmits the energy, the spin, but not the momentum;
- 3) The energy of transaction directly related with the entropy production and inversely related with the squared distance;
- 4) The transaction is screened by the matter, but the screening properties of the matter do not coincide with such properties for the electromagnetic field;
- 5) The transaction can have positive, zero and symmetrical negative time lapse.

The last point says on the possibility of observing the future as the existing reality! This statement is explained as follows. As the Universe is projected on to the time axis in a point, the transaction via time is interaction through a spacelike interval. Formally it admits the time shift equal to \pm classical retardation. Combination of the retarded and advanced signals may lead effectively to the instantaneous interaction.

The statement (5) directly concerning the main topic of this book was late, final Kozyrev result, so was not contained in his single paper on causal mechanics in English [1]. The relevant astrophysical experimental results [34,35] and their theoretical explanation [36] were published only in Russian. There is a review of these works in English in Reference [37]. Kozyrev elaborated [36,37] that time interaction in actually occurs through zero interval, while both time directions are allowed. In particular it can lead to effectively instantaneous correlation of some processes without invoking of the superluminal speed. At this point he independently and exactly converged with the explanation of instantaneous (through zero

interval) quantum nonlocal correlation suggested by Cramer in the same year [16].

It is extremely interesting, but it needs more careful theoretical consideration, while the first part of Kozyrev theory, concerning the force of causality, admits straightforward classical development. And it was the first step in my own work together with M. Arushanov [2].

1.2. Application of the Force of Causality to the Rotating Earth

This application was motivated by rather extensive number of the geophysical facts, difficulty explained from the conventional standpoints. Indeed the geoid has a form of the cardioidal ellipsoid with the depression at the South Pole and the prominence at the North one. The latitudinal distribution of the land and sea is also asymmetrical and described by the cardioid opposite to the geodesic one. And this distribution persists over geological time scale in spite of the continental drift.

In the atmosphere there is a heat asymmetry of the hemispheres. The temperature in the North hemisphere is 3° higher than in the South one. There is an asymmetry of the intertropic convergence zone and so on.

The similar asymmetry is on the other planets, for instance the Mars. All these facts might be explained by some low-governed asymmetrical forces, but there are no such forces in classical mechanics.

Let us consider the force of causality on the Earth. From Equations (1.3, 1.4) follows:

$$\mathbf{F} = \mathbf{j} \frac{\omega r}{c_2} g \rho \cos \varphi |\sin \varphi|, \quad (1.5)$$

where ω is the angular velocity, r is the distance from the center of the Earth, ρ is the density, g is the gravity acceleration, φ is the latitude. The force \mathbf{F} acts over the all points of the Earth parallel to axis to the North. Conservation of the momentum requires force of reaction \mathbf{R} to be directed parallel to the axis to the South:

$$\int \mathbf{F} dV = - \int \mathbf{R} dV. \quad (1.6)$$

The integrals are taken over the all volume of the Earth. A solution of this integral equation is the constant:

$$\mathbf{R} = -\mathbf{j} \frac{\omega r}{\pi c_2}. \quad (1.7)$$

Resulting sum $\mathbf{F} + \mathbf{R}$ is \mathbf{Q} :

$$\mathbf{Q} = \mathbf{j} \frac{\omega r}{c_2} g \rho \left(\frac{1}{2} |\sin 2\varphi| - \frac{1}{\pi} \right). \quad (1.8)$$

For geophysical interpretation of this formula it is essential that \mathbf{Q} has opposite sign for the causes and effects. We may simply determine the positions of the cause and effect objectively by direction of the energy flux, which is directed always from the cause to the effect. The solid Earth losses the heat to the environment and therefore may be considered as the region of the causes. On considering the system the solid Earth-atmosphere, we see that atmosphere is in the region of the effects. In our formula the sign is selected for the causes therefore it should be taken with its sign for the solid Earth and opposite one for the atmosphere.

In **Figure 1.1** the latitudinal distribution of the force \mathbf{Q} is shown. Positive direction is parallel to the Earth axis to the North Note, that force changes its sign at the latitude 71°, close to Kozyrev experimental result.

As the vertical Q_R horizontal Q_φ component of a force (1.8) play in geophysics essentially different roles they should be considered separately:

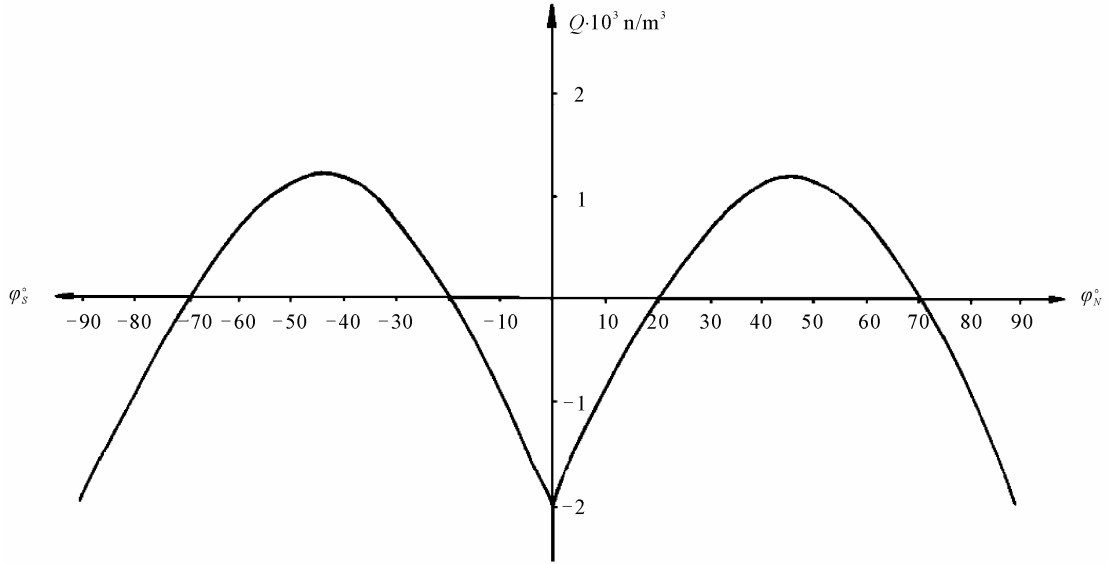


Figure 1.1. Zonal distribution of the force of causality (for $\rho = 1 \text{ kg/m}^3$).

$$Q_R = \frac{\omega r}{c_2} g \rho \left(\frac{1}{2} |\sin 2\varphi| - \frac{1}{\pi} \right) \sin \varphi, \quad (1.9)$$

$$Q_\varphi = \frac{\omega r}{c_2} g \rho \left(\frac{1}{2} |\sin 2\varphi| - \frac{1}{\pi} \right) \cos \varphi. \quad (1.10)$$

In the geological time scale the results of those forces can be noticed via their divergences:

$$\text{div}Q_R = \pm \frac{\omega}{c_2} g \rho \left(\frac{1}{2} |\sin 2\varphi| - \frac{1}{\pi} \sin \varphi \right)_{g \propto r} \quad (1.11)$$

$$\text{div}Q_\varphi = \pm \frac{\omega}{c_2} g \rho \left(\cos 2\varphi \cos \varphi - |\sin 2\varphi \sin \varphi| + \frac{2}{\pi} |\sin \varphi| \right) \quad (1.12)$$

The + is for the North hemisphere, the – for the South one. The signs everywhere are taken for the Solid Earth.

In the Solid Earth, at the process of mantle differentiation, extraction of lighter granitoid fraction goes quicker under condition of vertical stretching. Therefore zones positive $\text{div}Q_R$ are favorable for forming of the continental crust. We may expect concentration of the continents in the zones with positive $\text{div}Q_R$ and the oceans in the zones with negative one.

On the other hand, the horizontal component Q_φ must bring an additional contribution to the continental drift. Therefore we may expect concentration of the movable continents in the zones with negative $\text{div}Q_\varphi$ and deficit in the zones with positive one.

Next, the geodesic figure of the Earth is an equipotential surface. The potential of the force of causality U :

$$U = -\frac{1}{3} \frac{\omega r^2}{c_2} g \rho \left(\frac{1}{2} |\sin 2\varphi| - \frac{1}{\pi} \right) \sin \varphi_{g \propto r} \quad (1.13)$$

has latitudinal distribution opposite to Q_R and $\text{div}Q_R$, and this distribution describes the observed asymmetry of the Earth the figure with the depression at the South pole and the prominence at the North one.

In **Figure 1.2** those theoretical latitudinal distributions are shown together with the real distribution of the land and ocean. The solid line is percentage of the land. The dashed line is $divQ_R$. We see that dashed and solid curves nicely coincide, to detail! So, the theory gives physical explanation of asymmetrical distribution of the land and ocean seemed accidental before.

The dotted line is $divQ_\phi$. It is evidently clear that continental zones qualitatively correspond to its negative value, while the oceanic zones correspond to its positive one.

Thus, both vertical and horizontal components of the force of causality are responsible for the observed geological asymmetry of the Earth.

On the other hand, in atmospheric physics there is well known unsolved problem: why is the inter-tropic convergence zone shifted to the north from the equator? According to the classical theory it must be exactly at the equator. In **Figure 1.2** it is seen, that $divQ_\phi$ has break at the equator and for the atmosphere it is negative to the North. There the convergence zone must be shifted to the North.

Next, the force of causality is remarkable by the fact that it has in addition to the usual potential part, also the solenoidal part. It is the non-conservative force, namely at the expense at time energy! The expressions of $rotQ$ are, for the solid Earth:

$$rotQ = i \frac{\omega}{c_2} g \rho \left(2|\sin 2\varphi| \cos \varphi + |\sin \varphi| \cos 2\varphi - \frac{4}{\pi} \cos \varphi \right)_{g \propto r}, \quad (1.14)$$

and for the atmosphere:

$$rotQ = -i \frac{\omega}{c_2} g \rho \left(\frac{3}{2} |\sin 2\varphi| \cos \varphi + |\sin \varphi| \cos 2\varphi - \frac{3}{\pi} \cos \varphi \right)_{g=const}. \quad (1.15)$$

In **Figure 1.3** the rotor latitudinal distribution is presented, the solid line—for the solid Earth, the dashed line—for the atmosphere.

In the solid Earth the rotor determines intensity of the shift deformation. The extrema of the solid line

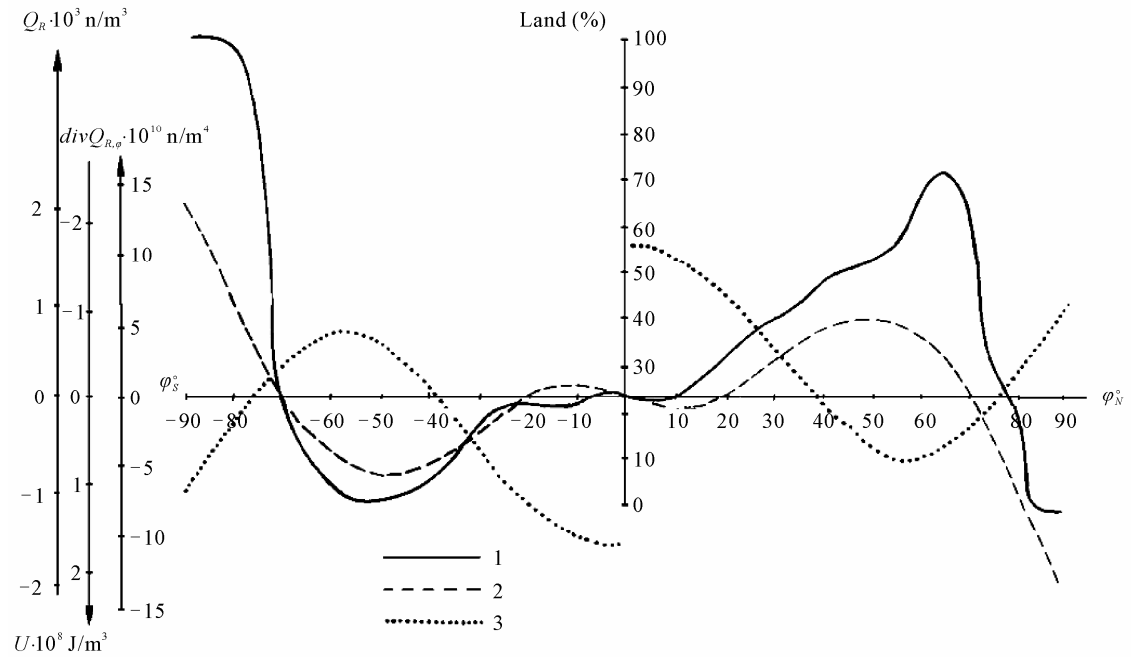


Figure 1.2. Zonal distribution of the land (1), vertical component (2), divergence of vertical (2) and horizontal (3) components and potential (2) of the force of causality (for $\rho = 1 \text{ kg/m}^3$).

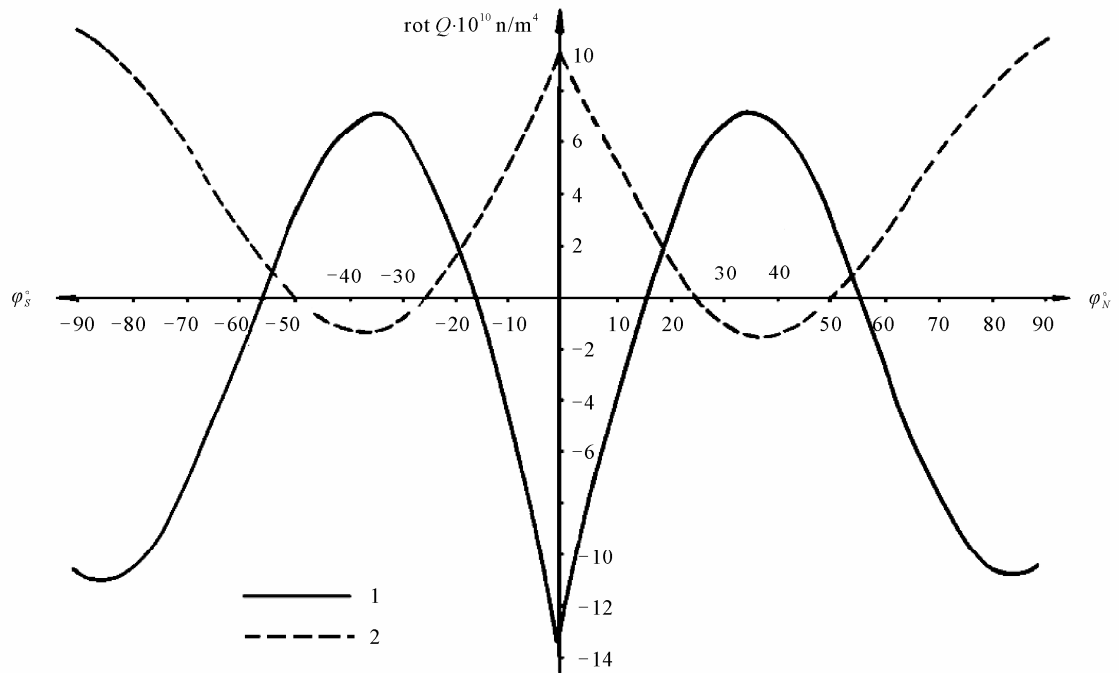


Figure 1.3. Zonal distribution of the rotor the force of causality in the lithosphere (1, $g \propto r$) and in the atmosphere (2, $g = const$) (for $\rho = 1 \text{ kg/m}^3$).

correspond to the well known in geology critical parallels $\pm 35^\circ$ and equator. The parallels $\pm 35^\circ$ of the continents are the orogenic zones. The 0° -parallel is expressed as the global fault zone and called by geologists the equatorial shift zone.

In the atmosphere, the rotor determines intensity of the meridional circulation. From the dashed line it is evident that in the atmosphere the positive values are prevailed. That means existence of the transport directed from the South hemisphere to the North one in the lower layers and the opposite one in the upper layers. As a result the mean temperature near the Earth surface must be higher in the North hemisphere than in the South one.

Thus, causal mechanics explains number of the important facts in global geology and meteorology. Recently it has been demonstrated that inclusion of the force of causality into hydrodynamic equation system leads to improving of exactness of the numerical long-term weather forecasts [3]. In addition from my viewpoint it is important to put into operation the force of causality in dynamics of the Earth core, where it may play essential role in generation of the magnetic field. Indeed, violating symmetry only the force of causality can naturally violate the ban imposed, by Cowling theorem on the field generation by any axial-symmetric movement.

Chapter 2

Classical Causal Analysis

2. Classical Causal Analysis

In spite of the fact, that principle of causality is widely used in physics, it does not mean more than retardation of the effect relative to the cause. However the retardation is necessary but not sufficient condition of the causal connection (“Post hoc non est propter hoc”). But what is a cause and what is an effect remains formally indefinite. Meanwhile in the simple situations we usually well realize what is a cause and what is an effect, not measuring a retardation, but only implicating it (e.g. without any measurement of the retardation, it is obvious causal-effect relation of the current in the lamp and photocell circuits). In the complicated situations, in the systems with feedbacks, usual intuitive understanding of causality may lead to the confusions, and hence the desirability of its formalization is obvious. The fact that in the simple situation location of the causes and effects is clear without retardation measuring indicates that these conceptions are asymmetrical in themselves. The problem is to define this asymmetry formally and not invoking the time relation, which has to be introduced after the definition as an axiom. From the solution of this problem originally directed to formalization of Kozyrev’s causal mechanics, the method of causal analysis was born, turned out to be useful in various classical applications. It was found fruitful in the construction of the models of complicated systems with feedbacks by experimental data, as well as in the estimation of the influence of noise-forming impacts in the real open systems.

Consider the classical variables A and B describing the respective subsystems of the bipartite system AB , their Shannon marginal and conditional entropies:

$$S(A) = -\sum_{j=1}^J P(A_j) \log_2 P(A_j), \quad (2.1)$$

$$S(B) = -\sum_{k=1}^K P(B_k) \log_2 P(B_k),$$

$$S(A|B) = -\sum_{k=1}^K P(B_k) \sum_{j=1}^J P(A_j|B_k) \log_2 P(A_j|B_k), \quad (2.2)$$

$$S(B|A) = -\sum_{j=1}^J P(A_j) \sum_{k=1}^K P(B_k|A_j) \log_2 P(B_k|A_j),$$

where $P(A_j)$, $P(B_k)$ are the probabilities of j -th (k -th) levels of A and B respectively; $P(A_j|B_k)$, $P(B_k|A_j)$ are the respective conditional probabilities. Define the following parameters: the marginal α and conditional β asymmetries:

$$\alpha = \frac{S(B)}{S(A)}, \quad 0 \leq \alpha \leq \infty; \quad \beta = \frac{S(B|A)}{S(A|B)}, \quad 0 \leq \beta \leq \infty; \quad (2.3)$$

and the independence functions:

$$i_{B|A} = \frac{S(B|A)}{S(B)}, \quad i_{A|B} = \frac{S(A|B)}{S(A)}, \quad 0 \leq i \leq 1. \quad (2.4)$$

Meaning of the independence functions is enough transparent: at $i_{B|A} = 1$, B is independent of A , at $i_{B|A} = 0$, B is one-valued function of A . In other words, the values $1-i$ determine the unilateral dependences of the variables. The direct and inversed independences must coincide only in the limiting case: $i_{B|A} = 1 \Leftrightarrow i_{A|B} = 1$.

Next introduce the causality function γ :

$$\gamma = \frac{i_{B|A}}{i_{A|B}}, \quad 0 \leq \gamma \leq \infty. \quad (2.5)$$

The name is derived from the particular values of γ . $\gamma=0$: B is the one-valued function of A , but not the reverse. It is possible to interpret that as the utmost irreversible process $A \Rightarrow B$. $\gamma=1$: A and B to the same extent depend on one another, that is naturally to identify with absence of causality. $\gamma=\infty$: A is one-valued function of B , but not the reverse. It is possible to interpret that is the utmost irreversible process $B \Rightarrow A$.

Consider the space of parameters $\alpha, \beta, i_{B|A}$ ($\gamma = \beta/\alpha$ is equivalent to (2.5)) displayed in **Figure 2.1**. In this space it is possible to obtain the classification of any type of dependence of B on A . Every type is imaged by a point. Analyzing the limiting cases and using the reversibility of information:

$$I = S(B) - S(B|A) = S(A) - S(A|B), \quad (2.6)$$

it is easily to prove, that the forbidden regions are: 1) the subspace $\alpha < 1, \gamma \geq 1$; 2) the subspace $\alpha > 1, \gamma \leq 1$; 3) the plane $\beta = 1$ except the line of intersection with the plane $\alpha = 1$; 4) the plane $\alpha = 1$ except the line of intersection with the plane $\beta = 1$ and except the line of intersection with the plane $i_{B|A} = 0$; 5) the plane $\beta = 0$ except the axis segment $\alpha[0,1]$ and axis $i_{B|A}$; 6) the plane $\alpha = 0$ except the axis $i_{B|A}$; 7) the plane $i_{B|A} = 0$ except the line $\alpha = 1$ and axis segment $\alpha[0,1]$; 8) the plane $i_{B|A} = 1$; except the line $\gamma = 1$; 9) the plane $\gamma = 1$, except the axis $i_{B|A}$, line $i_{B|A} = 1$ and line $\alpha = \beta = 1$.

In the allowed space it is possible to separate out, on parameter meaning grounds, the following regions:

- Subspace of normal causality: $\gamma < 1, \beta < 1, \alpha < 1$.
- Subspace of inversed causality: $\gamma > 1, \beta > 1, \alpha > 1$.
- B -constant line: $B = const$ independently of A .
- One-valued function line: $i_{B|A} = 0, \beta = 0, 0 < \alpha < 1$. Here $S(B|A) = 0$, i.e. B is fully determined by A , but not reverse.

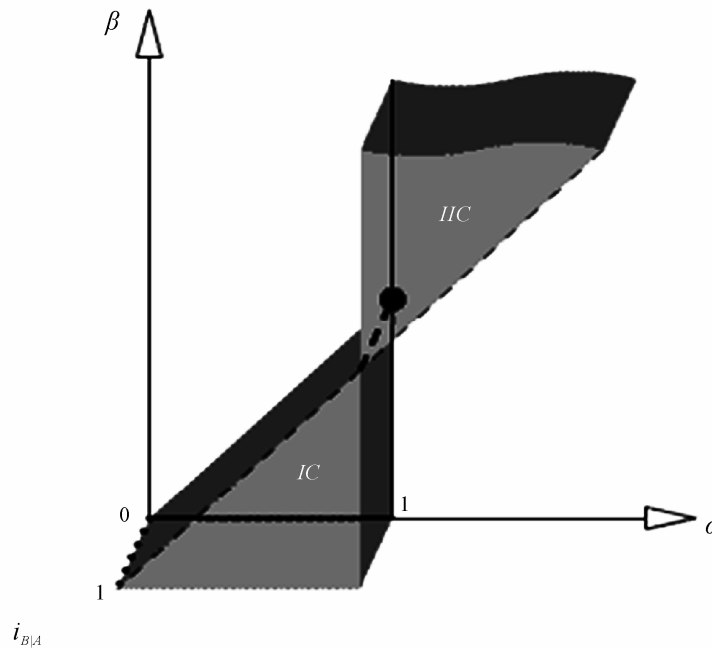


Figure 2.1. Classical entropic diagram (IC is normal causality, IIC is inversed causality, dotted line is the B -constant line, thick solid line is the one-valued function line, fine dashed line is the independence line, thick dashed line is the adiabat, circle is the mutually one-valued function point).

- Independence line: $i_{B|A} = 1, \gamma = 1$.
- Mutually one-valued function point: ($i_{B|A} = 0, \alpha = \beta = 1$). Here $S(B|A) = S(A|B) = 0$.
- Adiat: $\alpha = \beta = 1$, that corresponds to the isentropic process.

It is sufficiently for the formal definition of classical causality.

Definition 1: *The cause A and the effect B are variables for which $\gamma < 1$.*

Analyzing meaning of γ it is not difficult to see that our definition includes usual intuitive understanding of causality (at least with an eye physicist's intuition). Indeed, if we say that A is the cause and B is the effect, we keep in mind fully or partly determined dependence of B on A , such that inversed dependence is absent. Our definition allows refining: the inversed dependence is less than direct one and how much. The causeless functional and statistical dependences are also known. We neatly fix this class: $\gamma = 1$. If, having studied statistics of the arbitrary denoted variables A and B , we find $\gamma > 1$, it simply means that B is the cause and A is the effect. Besides full formality, our definition has an obvious advantage of the quantitative measure over common used the qualitative one. On theoretical and multiplicity of experimental examples of the classical problems (e.g. [5-14]) it had been shown that such formal definition of causality did not contradict its intuitive understanding in the simple situations and could be used in the complicated ones.

Our definition allows formulation of the axiom of classical causality as follows:

$$\gamma < 1 \Rightarrow \tau > 0, \gamma > 1 \Rightarrow \tau < 0, \gamma \rightarrow 1 \Rightarrow \tau \rightarrow 0, \quad (2.7)$$

where τ is time shift of B relative to A .

Note, that $\gamma < 1 \Rightarrow \alpha < 1, \gamma > 1 \Rightarrow \alpha > 1$, (the reversed is wrong, that is why α can not be used for the definition of causality). This necessary condition is a manifestation of 7-th Shannon theorem [38] on decrease of the entropies from a channel input $A(B)$ to its output $B(A)$.

Consider an elementary cause-effect link from information exchange standpoint. According to the theorem about noisy channel capacity, the upper limit of information reception rate in B from A is:

$$\sup v_{A \rightarrow B} = \frac{1}{\delta t} \frac{S(B) - S(B|A)}{S(B)}, \quad (2.8)$$

where δt is duration of an elementary signal, the numerator is maximized by variation of the A distributions. Replacing the rate (2.8) by the lower limit of time and using (4), we have:

$$\inf t_{A \rightarrow B} = \frac{\delta t}{1 - i_{B|A}}. \quad (2.9)$$

In a like manner for the reversed transfer:

$$\inf t_{B \rightarrow A} = \frac{\delta t}{1 - i_{A|B}}. \quad (2.10)$$

By the condition $\gamma < 1 \Leftrightarrow 1 - i_{B|A} > 1 - i_{A|B} \Leftrightarrow t_{A \rightarrow B} < t_{B \rightarrow A}$. The finite difference of times (2.10) and (2.9) means that in any time lapse the effect obtains from the cause more information than the cause does from the effect. Information excess in the effect means the irreversibility of information flow. Than time of information excess reception Δt is:

$$\Delta t = \delta t \left(\frac{1}{1 - i_{A|B}} - \frac{1}{1 - i_{B|A}} \right). \quad (2.11)$$

Supposing that the subsystem A and B are separated by some finite effective distance Δr , one can determine the linear velocity of irreversible information flow $c_2 = \Delta r / \Delta t$ (the notation follows the tradition of Reference [1], where originally, although in less rigorous terms, the course of time pseudoscalar c_2 of the same meaning was introduced):

$$c_2 = k \frac{(1-i_{A|B})(1-i_{B|A})}{i_{A|B} - i_{B|A}} = k \frac{(1-i_{B|A}/\gamma)(1-i_{B|A})}{i_{B|A}(1/\gamma-1)}, \quad (2.12)$$

where $k = \Delta r / \delta t$. It is easy to see that the sign of c_2 is mutually one-valued related with the value of γ relative to 1:

$$\gamma < 1 \Leftrightarrow c_2 > 0, \quad \gamma > 1 \Leftrightarrow c_2 < 0, \quad \gamma \rightarrow 1 \Leftrightarrow c_2 \rightarrow \pm\infty, \quad (2.13)$$

therefore it is possible to replace γ by c_2 in the causality definition and axiom.

The causal analysis apparatus has been generalized to the causal network in the multipartite system [9]. The influence of the different kinds of noise-forming impacts from the non-controlled environment on all the parameters ($\alpha, \beta, i_{B|A}, i_{A|B}, \gamma$), the possibilities of other classical entropy definitions different from Shannon one as well as the foliated spaces of the probability definition have been analyzed [14]. The method has been tested on the problems of classical electrodynamics [5-8] and on data of various classical experiments (e.g. [6-14]).

Chapter 3

Quantum Causal Analysis

Table of Contents

Kernel of the Method

Symmetric States

Asymmetric Two-Particle States

Asymmetric Three-Particle States

Overview of Causal Analysis

3. Quantum Causal Analysis

3.1. Kernel of the Method

For the quantum variables von Neumann entropy is used. Instead of Equations (2.1) and (2.2) we have:

$$S(A) = -\text{Tr} \rho_A \log_2 \rho_A, \quad S(B) = -\text{Tr} \rho_B \log_2 \rho_B, \quad (3.1)$$

$$S(B|A) = S(AB) - S(A), \quad S(A|B) = S(AB) - S(B), \quad (3.2)$$

where $\rho_A = \text{Tr}_B \rho_{AB}$, $\rho_B = \text{Tr}_A \rho_{AB}$, $S(AB) = -\text{Tr} \rho_{AB} \log_2 \rho_{AB}$. Note, that although the conditional entropies can be in principle directly calculated through the conditional entropies by analogy with Equations (2.2) [39], practically it is simple to calculate them indirectly according to Equations (3.2).

For the entangled states the conditional entropies can be negative [39,40]. Therefore $-\infty \leq \beta \leq \infty$, $-1 \leq i \leq 1$, $-\infty \leq \gamma \leq \infty$. In particular, for the bipartite states from Schmidt decomposition it is follows $\alpha = 1$, $\beta = 1$, $\gamma = 1$, $i_{B|A} = i_{A|B} = -1$. The entropic diagram is extended (**Figure 3.1**). Besides the two classical subspaces C the four quantum ones Q are allowed:

$$IC \quad 0 \leq \alpha \leq 1, \quad 0 \leq \beta \leq 1, \quad 0 \leq i_{B|A} \leq 1, \quad 0 \leq i_{A|B} \leq 1, \quad c_2 > 0;$$

$$IIC \quad 1 \leq \alpha \leq \infty, \quad 1 \leq \beta \leq \infty, \quad 0 \leq i_{B|A} \leq 1, \quad 1 \leq \gamma \leq \infty, \quad c_2 < 0;$$

$$IQ \quad 0 \leq \alpha \leq 1, \quad 1 \leq \beta \leq \infty, \quad -1 \leq i_{B|A} \leq 0, \quad 1 \leq \gamma \leq \infty, \quad c_2 > 0;$$

$$IIQ \quad 1 \leq \alpha \leq \infty, \quad 0 \leq \beta \leq 1, \quad -1 \leq i_{B|A} \leq 0, \quad 0 \leq \gamma \leq 1, \quad c_2 < 0;$$

$$IIIQ \quad 0 \leq \alpha \leq 1, \quad -\infty \leq \beta \leq 0, \quad -1 \leq i_{B|A} \leq 0, \quad -\infty \leq \gamma \leq 0, \quad c_2 > 0;$$

$$IVQ \quad 1 \leq \alpha \leq \infty, \quad -\infty \leq \beta \leq 0, \quad 0 \leq i_{B|A} \leq 1, \quad -\infty \leq \gamma \leq 0, \quad c_2 < 0.$$

However in the 3D diagram of **Figure 3.1** it is difficult to show the demarcation of the allowed subspaces. For their indication invoke the fact that the independence function $i_{B|A}$ can be represented as

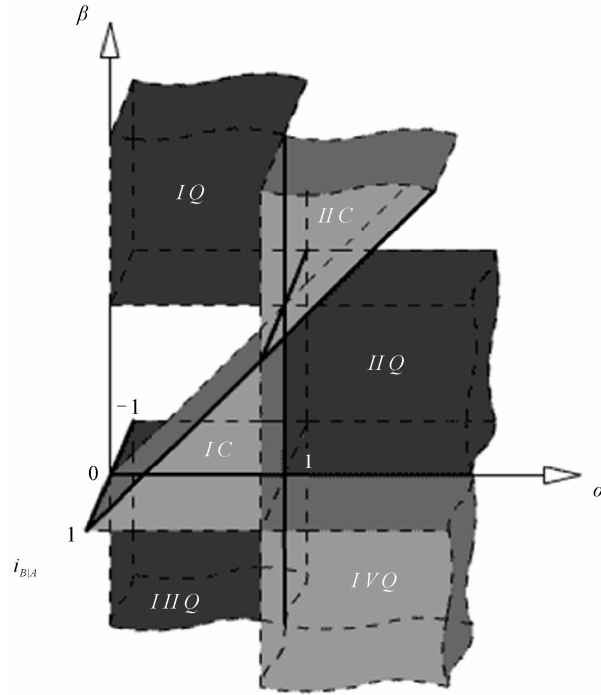


Figure 3.1. Quantum entropic diagram.

follows:

$$i_{B|A} = \frac{\beta(\alpha-1)}{\alpha(\beta-1)}. \quad (3.3)$$

In the subspaces IC, IIC and IVQ $0 \leq i_{B|A} \leq 1$, that according to Equation (16), brings to the system of two inequalities with respect to α, β . Their solutions in the form of sections $i_{B|A} = const$ are presented in **Figure 3.2(a)**. The allowed subspaces are adjacent to the border planes. In the subspaces IQ, IIQ and IVQ $-1 \leq i_{B|A} \leq 0$. The solutions of corresponding couple of the inequalities are presented in **Figure 3.2(b)**. The allowed subspaces are separated from the part of border planes by the hyperbolic surfaces.

At the quantum level the value of γ is insufficient for distinguishing the cause and effect. But by reference to correspondence between c_2 and γ in both the classical subspaces and necessary condition of the 7-th Shannon theorem obeying in all the six subspaces: $c_2 > 0 \Rightarrow \alpha < 1$, $c_2 < 0 \Rightarrow \alpha > 1$ it is possible to give the definition of causality appropriate for the quantum variables.

Definition 2: The cause A and the effect B are the subsystems for which $c_2 > 0$.

Then, introducing the demand of the effect retardation τ , we can formulate the axiom of strong causality, embracing local and nonlocal correlations, as follows:

$$c_2 > 0 \Rightarrow \tau > 0, \quad c_2 < 0 \Rightarrow \tau < 0, \quad |c_2| \rightarrow \infty \Rightarrow \tau \rightarrow 0. \quad (3.4)$$

Notice, that nonlocal correlations are often treated as instantaneous and causeless ones. Our approach includes such treatment, but only as a particular case.

The axiom (3.4) is the principle namely of strong causality. Cramer was the first to distinguish the principles of strong and weak causality [16]. The strong causality corresponds to the usual condition of retardation of the effect relative to the cause. Without this axiom we have the weak causality. The weak causality corresponds only to nonlocal correlations and implies a possibility of information transmission in reverse time, but only related with unknown states (hence “the telegraph to the past” is impossible).

Equations (2.8)-(2.12) remain true by virtue of the parallelism of classical and quantum information theory [40]. A justified in Reference [41] interpretation of entanglement of a quantum system as the re-

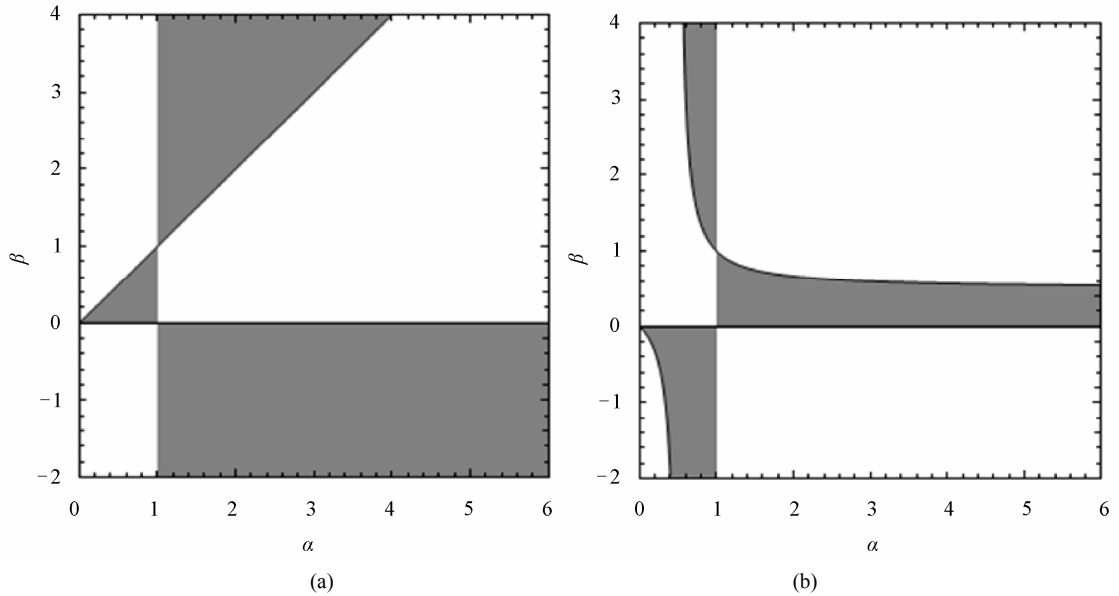


Figure 3.2. The allowed subspaces in the sections $i_{B|A} = const$: (a) the subspaces IC, IIC and IVQ ; (b) the subspaces IQ, IIQ and $IIIQ$.

source serving for information transfer through it, gives them the additional physical meaning. Specifically in Reference [41] it has been proven that negative conditional entropy is “an amount of information which can be transmitted through <the subsystems>1 and 2 from a system interacting with 1 to another system interacting with 2. The transmission medium is quantum entanglement between 1 and 2.” Causality characterized by c_2 value reflects the asymmetry of this process (the greater causality is expressed by the less $|c_2|$).

But though defined by Equation (2.12) c_2 with accuracy to the coefficient k is of great interest by itself, it is desirable to show the way of its full determination for the natural processes. For this there is no remain δt to be duration of “an elementary signal”, that is pertinent only for a technical channel. Since δt in any case plays a role of some elementary time it is natural to suppose it, according to Reference [42] to be time of brachistochrone evolution. In the case of time independent Hamiltonian this time is easily expressed explicitly:

$$\delta t = \frac{\hbar \theta}{2\omega}, \quad (3.5)$$

where 2ω is the difference between the largest and smallest eigenvalues of the Hamiltonian and θ is the length of geodesic (according to Fabini-Study metric) connecting the initial and final states. If they are orthogonal, $\theta = \pi$. In realistic Hamiltonian ω depends on distance Δr and k becomes definite. It is readily shown [4] that for the simplest Coulomb interaction $k = e^2/\hbar$, that corresponds to Kozyrev order estimation of c_2 obtained from the semiclassical reasoning.

To keep the examples described bellow from becoming too involved; we shall restrict ourselves by calculations of c_2 with accuracy to $k = 1$. Only in the last example of Section 3 I shall demonstrate the more precise estimation with regard to δt , which variable dependent on eigenvalues of Hamiltonian (remaining $\Delta r = 1$).

3.2. Symmetric States

By the symmetric two-partite states are meant the states with equal subsystem entropies: $S(A) = S(B)$, $\alpha = \beta = \gamma = 1$, $|c_2| \rightarrow \infty$. The causality is absent (adiabatic state connection). However the value $i_{B|A} = i_{A|B}$ is finite and can be related to the mixedness measures $\text{Tr}\rho_{AB}^2$ or $S(AB)$ and to the standard entanglement measure-concurrence C [43]:

$$C = \max\left(\sqrt{\lambda_1} - \sqrt{\lambda_2} - \sqrt{\lambda_3} - \sqrt{\lambda_4}, 0\right), \quad (3.6)$$

where λ_i are eigenvalues of the matrix $\rho\tilde{\rho}$. Spin-flip matrix $\tilde{\rho}$ is defined as:

$$\tilde{\rho} = (\sigma_y \otimes \sigma_y) \rho^* (\sigma_y \otimes \sigma_y). \quad (3.7)$$

I show below that employment of causal analysis make sense, naturally, only for the mixed states. At the beginning I consider the elementary systems, when mixedness emerges as a result of extraction of the two subsystems from a three-partite pure state, thereupon—more containable situations, when the mixedness is a result of interaction with a non-controlled environment. Since such interaction leads to decoherence, analysis of these situation we shall begin with the basic mechanisms of decoherence—depolarization and dephasing (dissipation, which may lead to the asymmetry is considered in Section 3.2.1). Next we consider typical mixed states in their initial and asymptotic species (after long-run dissipation).

3.2.1. Pure States

The entropic symmetry is evident from Schmidt decomposition. Consider the arbitrary pure states:

$$|\Phi\rangle = \alpha|00\rangle + \beta|11\rangle, \quad (3.8)$$

or

$$|\Psi\rangle = \alpha|01\rangle + \beta|10\rangle, \quad (3.9)$$

where $|\alpha|^2 + |\beta|^2 = 1$. Since the state is pure, $\text{Tr}\rho_{AB}^2 = 1$, $S(AB) = 0$, concurrence C varies according to ratio of α and β . But at any nonzero α and β the independence function is constant: $i_{B|A} = -1$. Therefore for the pure states the causal analysis is of no interest.

3.2.2. Greenberger-Horne-Zeilinger State

It is known, that Greenberger-Horne-Zeilinger (GHZ state):

$$|GHZ\rangle = \frac{1}{\sqrt{2}}(|000\rangle + |111\rangle) \quad (3.10)$$

is marked by that in spite of the maximal entanglement of three particles (ABC), the pairwise entanglement is absent: $C = 0$. The two-partite state is mixed: $\text{Tr}\rho_{AB}^2 = \frac{1}{2}$, $S(AB) = 1$. Therewith $i_{B|A} = 0$. The entanglement is absent but the particles A and B are maximally classically correlated.

3.2.3. W -State

$$|W\rangle = \frac{1}{\sqrt{3}}(|001\rangle + |010\rangle + |100\rangle). \quad (3.11)$$

Similar to GHZ state, W -state is entangled three-partite state, but the pairwise concurrence $C = \frac{2}{3}$ (moreover, (3.11) and in general N -partite W -state represents the case of arranged in pairs and equal entanglement of the all N particles [44]). The mixedness of the two-partite subsystem is somewhat weaker than for GHZ: $\text{Tr}\rho_{AB}^2 = \frac{5}{9}$, $S(AB) = -\frac{1}{3}\log_2 \frac{1}{3} - \frac{2}{3}\log_2 \frac{2}{3} \approx 0.918$. However, likewith GHZ state: $i_{B|A} = 0$.

3.2.4. Depolarization

Depolarization reduces to the following transformation [45,46]:

$$\begin{aligned} |0\rangle\langle 0| &\rightarrow (1-p)|0\rangle\langle 0| + p\frac{I}{2}, \\ |1\rangle\langle 1| &\rightarrow (1-p)|1\rangle\langle 1| + p\frac{I}{2}, \\ |1\rangle\langle 0| &\rightarrow (1-p)|1\rangle\langle 0|, \\ |0\rangle\langle 1| &\rightarrow (1-p)|0\rangle\langle 1|. \end{aligned} \quad (3.12)$$

where $0 \leq p \leq 1$ is decoherence degree. Take the singlet for the initial state:

$$|\Psi^-\rangle = \frac{1}{\sqrt{2}}(|01\rangle - |10\rangle). \quad (3.13)$$

And let us assume that only the second particle (B) is depolarized. The depolarized density is:

$$\rho_{AB} = \left(\frac{1-p}{2} - \frac{p}{4}\right)(|01\rangle\langle 01| + |10\rangle\langle 10|) - \left(\frac{1-p}{2}\right)(|01\rangle\langle 10| + |10\rangle\langle 01|) + \frac{p}{4}(|00\rangle\langle 00| + |11\rangle\langle 11|) \quad (3.14)$$

In spite of the fact that only one particle is depolarized, both the reduced densities are equal to each other, *i.e.* the system is symmetric:

$$\rho_A = \rho_B = \frac{1}{2}(|0\rangle\langle 0| + |1\rangle\langle 1|) \quad (3.15)$$

On finding the eigenvalues, we obtain:

$$S(AB) = -\frac{3p}{4} \log_2 \frac{p}{4} - \left(1 - \frac{3p}{4}\right) \log_2 \left(1 - \frac{3p}{4}\right), \quad (3.16)$$

$$S(A) = S(B) = 1. \quad (3.17)$$

The independence function is:

$$i_{B|A} = S(AB) - 1. \quad (3.18)$$

The concurrence is:

$$C = \max\left(1 - \frac{3p}{2}, 0\right). \quad (3.19)$$

The dependence of $i_{B|A}$, C , $\text{Tr}\rho_{AB}^2$ on p is shown in **Figure 3.3**. It is seen that $i_{B|A}$ varies with decoherence degree in the full range from -1 at $p=0$ to $+1$ at $p=1$ (full depolarization), when correlation of the subsystems fully disappears. The independence increases according to the increase of mixedness in both its measures (exactly proportional for $S(AB)$) and to the decrease of concurrence. It is the most interesting that there is an interval $\frac{1}{4} < p < \frac{2}{3}$, where $i_{B|A} > 0$ and $C > 0$. On this interval the system is in an entropic sense is classical but nevertheless entangled.

3.2.5. Dephasing

The transformation is [45,46]:

$$\begin{aligned} |1\rangle\langle 0| &\rightarrow (1-p)|1\rangle\langle 0|, \\ |0\rangle\langle 1| &\rightarrow (1-p)|0\rangle\langle 1|. \end{aligned} \quad (3.20)$$

The state (3.13) after dephasing of the particle B is:

$$\rho_{AB} = \frac{1}{2} \left[|01\rangle\langle 01| + |10\rangle\langle 10| - (1-p)(|01\rangle\langle 10| + |10\rangle\langle 01|) \right]. \quad (3.21)$$

Equations (3.15), (3.17) and (3.18) are true, but

$$S(AB) = -\left(1 - \frac{p}{2}\right) \log_2 \left(1 - \frac{p}{2}\right) - \frac{p}{2} \log_2 \frac{p}{2}, \quad (3.22)$$

$$C = 1 - p. \quad (3.23)$$

Therefore by full dephasing $i_{B|A} = 0$, *i.e.* the subsystems remain classically maximally correlated. By partial dephasing C and negative $i_{B|A}$ are the characteristics of entanglement on equal terms (**Figure 3.4**).

3.2.6. Bell-Diagonal States

Initial Bell-diagonal states are:

$$\rho_{AB} = p_1 |\Phi^+\rangle\langle \Phi^+| + p_2 |\Phi^-\rangle\langle \Phi^-| + p_3 |\Psi^+\rangle\langle \Psi^+| + p_4 |\Psi^-\rangle\langle \Psi^-|, \quad (3.24)$$

where

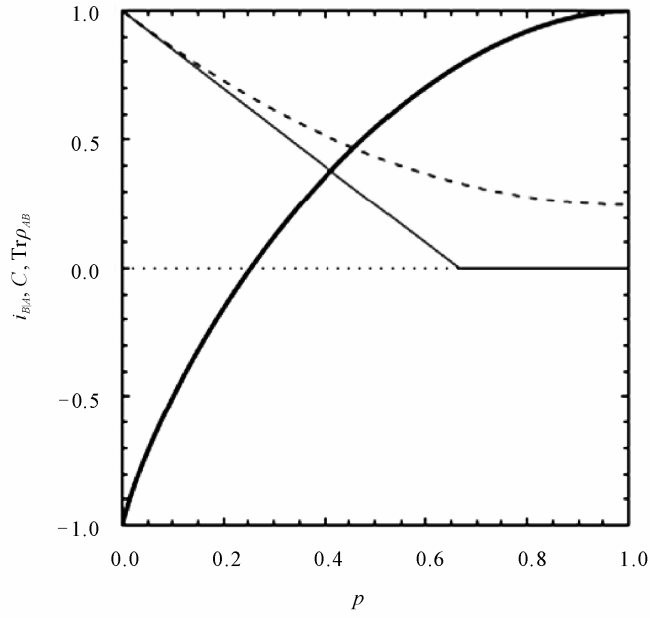


Figure 3.3. Dependence of $i_{B|A}$ (thick solid line), C (fine solid line), and $\text{Tr}\rho_{AB}^2$ (dashed line) on degree of depolarization p of the state (3.13).

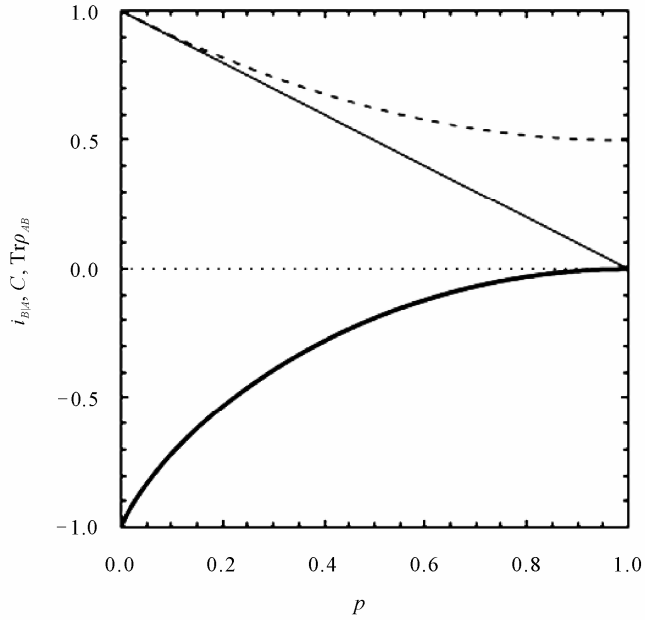


Figure 3.4. Dependence of $i_{B|A}$ (thick solid line), C (fine solid line) and $\text{Tr}\rho_{AB}^2$ (dashed line) on degree of dephasing p of the state (3.13).

$$|\Phi^\pm\rangle = \frac{1}{\sqrt{2}}(|00\rangle \pm |11\rangle), \quad |\Psi^\pm\rangle = \frac{1}{\sqrt{2}}(|10\rangle \pm |01\rangle). \quad (3.25)$$

Equations (3.15), (3.17) and (3.18) are true again, but

$$S(AB) = -\sum_{i=1}^4 p_i \log_2 p_i. \quad (3.26)$$

$$C = \max(2 \max\{p_i\} - 1, 0). \quad (3.27)$$

Behavior of $i_{B|A}$, C and $\text{Tr}\rho_{AB}^2$ in deciding on $p_4 = p$, $p_1 = p_2 = p_3 = (1-p)/3$ is shown in **Figure 3.5**. It is seen that $i_{B|A}$ reflects the mixedness achieving 1 at equality of the all p_i . But more important, that there is an interval $0.5 < p < 0.81$, where $i_{B|A} > 0$ and $C > 0$. On this interval the system is entangled in spite of the entropic classiness.

Now consider dissipation of the states (3.24) at the presence of a common bath. It is known that against before accepted views, dissipation may not reduce to decoherence, but on the contrary, may play a constructive role in entanglement generation [47-54]. Following Reference [52], suppose that the qubits represent the two-level atoms separated by a distance small compared to the radiation wavelength. Dissipation occurs at the expense of spontaneous emission of the photons, which have a substantial probability to be absorbed by the other atom. In Reference [52] the system dynamic equation is solved and the asymptotic solutions $t \rightarrow \infty$ are analyzed in detail. In particular the asymptotic density matrix at the initial one (3.24) is:

$$\rho_{AB}^{as} = \begin{pmatrix} 0 & 0 & 0 & 0 \\ 0 & \frac{p_4}{2} & -\frac{p_4}{2} & 0 \\ 0 & -\frac{p_4}{2} & \frac{p_4}{2} & 0 \\ 0 & 0 & 0 & 1-p_4 \end{pmatrix}. \quad (3.28)$$

Hence

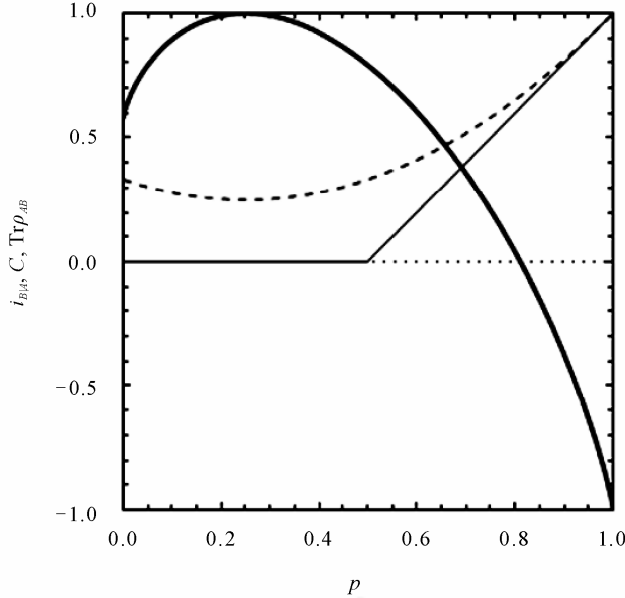


Figure 3.5. Dependence of $i_{B|A}$ (thick solid line), C (fine solid line) and $\text{Tr}\rho_{AB}^2$ (dashed line) on $p = p_4$ of initial Bell-diagonal states (3.24).

$$S(AB) = -p_4 \log_2 p_4 - (1-p_4) \log_2 (1-p_4), \quad (3.29)$$

$$S(A) = S(B) = -\frac{p_4}{2} \log_2 \frac{p_4}{2} - \left(1 - \frac{p_4}{2}\right) \log_2 \left(1 - \frac{p_4}{2}\right), \quad (3.30)$$

$$i_{B|A} = \frac{S(AB)}{S(A)} - 1, \quad (3.31)$$

$$C = p_4. \quad (3.32)$$

The constructive role of dissipation is that even the initial state was separable ($C = 0$) the asymptotic one is entangled in the all range of finite p_4 . **Figure 3.6** demonstrates that in this case the independence function does not reflect the mixedness, but does reflect the concurrence. Therewith $i_{B|A} \leq 1$, *i.e.* the system is correlated at almost any p_4 ($\max i_{B|A} = 1$) is achieved at $p_4 = 0$). On the interval $0 \leq p_4 < 0.67$ $i_{B|A} > 0$ (classical) at rather strong entanglement.

3.2.7. Werner States

The initial Werner states

$$\rho_{AB} = p \frac{I}{4} + (p-1) |\Phi^+\rangle \langle \Phi^+| \quad (3.33)$$

represent a depolarized triplet, for which as well as for the singlet, the expressions (3.15)-(3.19) and **Figure 3.3** are true.

Consider the result of described in above subsection dissipation process of the states (46). According to Reference [52] in the asymptotic limit $t \rightarrow \infty$:

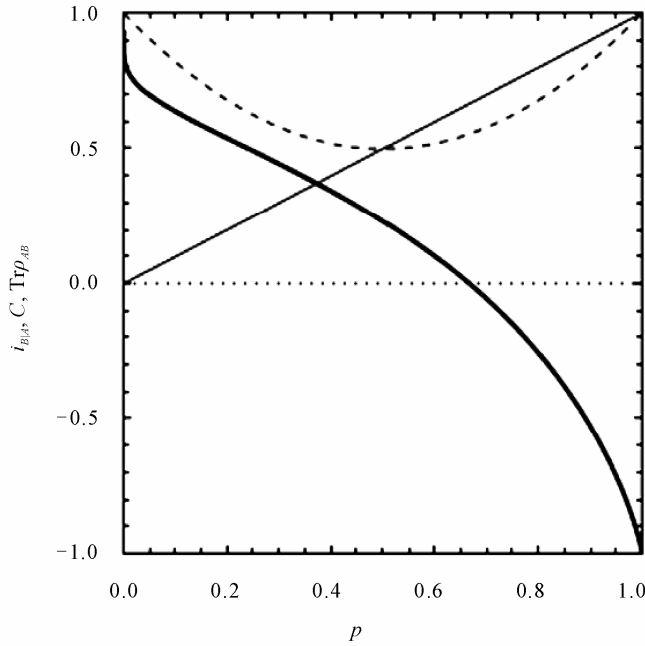


Figure 3.6. Dependence of $i_{B|A}$ (thick solid line), C (fine solid line) and $\text{Tr} \rho_{AB}^2$ (dashed line) on $p = p_4$ of asymptotic Bell-diagonal states (3.28).

$$\rho_{AB}^{as} = \begin{pmatrix} 0 & 0 & 0 & 0 \\ 0 & \frac{p}{8} & -\frac{p}{8} & 0 \\ 0 & -\frac{p}{8} & -\frac{p}{8} & 0 \\ 0 & 0 & 0 & 1 - \frac{p}{4} \end{pmatrix} \quad (3.34)$$

Hence:

$$S(AB) = -\frac{p}{4} \log_2 \frac{p}{4} - \left(1 - \frac{p}{4}\right) \log_2 \left(1 - \frac{p}{4}\right), \quad (3.35)$$

$$S(A) = S(B) = -\frac{p}{8} \log_2 \frac{p}{8} - \left(1 - \frac{p}{8}\right) \log_2 \left(1 - \frac{p}{8}\right), \quad (3.36)$$

$$C = \frac{p}{4}. \quad (3.37)$$

Figure 3.7 shows that asymptotic Werner states radically differ from the initial ones: They are not only entangled at any $p > 0$, but the concurrence increases with the increase of p —the smaller entangled initial state the greater entangled dissipated one. Therewith $i_{B|A}$ is positive (classical) at any p ($\max i_{B|A} = 1$ at $p = 0$, $\min i_{B|A} \approx 0.493$ at $p = 1$). It is remarkable that the decrease of $i_{B|A}$ and the increase of C are practically proportional to the increase of mixedness.

3.2.8. Maximally Entangled Mixed States

In Reference [55] it is conjectured that at fixed $\text{Tr} \rho_{AB}^2$ the maximally entangled are the states:

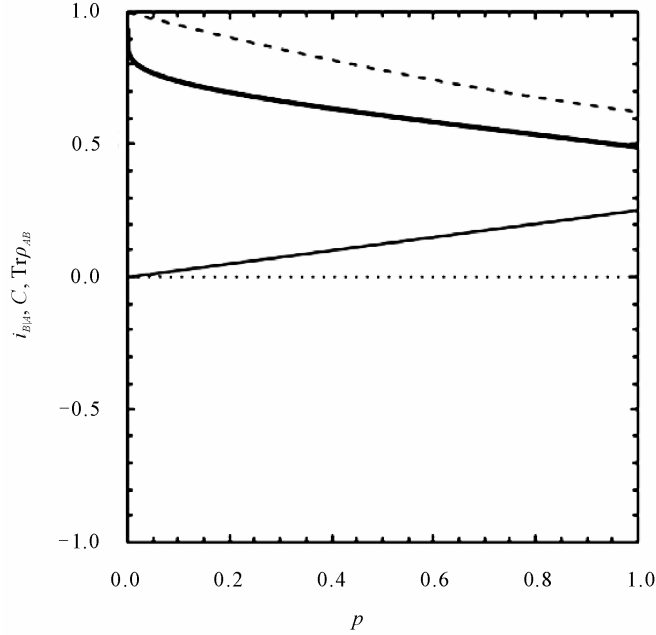


Figure 3.7. Dependence of $i_{B|A}$ (thick solid line), C (fine solid line) and $\text{Tr} \rho_{AB}^2$ (dashed line) on p of asymptotic Werner states (3.34).

$$\rho_{AB} = \begin{pmatrix} h(\delta) & 0 & 0 & \frac{\delta}{2} \\ 0 & 1-2h(\delta) & 0 & 0 \\ 0 & 0 & 0 & 0 \\ \frac{\delta}{2} & 0 & 0 & h(\delta) \end{pmatrix}, \quad h(\delta) = \begin{cases} \frac{1}{3}, & \delta \in \left[0, \frac{2}{3}\right] \\ \frac{\delta}{2}, & \delta \in \left[\frac{2}{3}, 1\right] \end{cases}. \quad (3.38)$$

Hence:

$$S(AB) = -(1-2h)\log_2(1-2h) - \left(h - \frac{\delta}{2}\right)\log_2\left(h - \frac{\delta}{2}\right) - \left(h + \frac{\delta}{2}\right)\log_2\left(h + \frac{\delta}{2}\right), \quad (3.39)$$

$$S(A) = S(B) = -h\log_2 h - (1-h)\log_2(1-h), \quad (3.40)$$

$i_{B|A}$ is determined by Equation (3.31), the concurrence is

$$C = \delta. \quad (3.41)$$

The dependence of $i_{B|A}$, C , $\text{Tr}\rho_{AB}^2$ on δ is shown in **Figure 3.8**. $i_{B|A}$ changes from +0.725 at $\delta = 0$ to -1, at $\delta = 1$ and its decrease as whole reflects the decrease of mixedness. Therewith on the interval $0 < \delta < \frac{2}{3}$ $i_{BA} > 0$ at $C > 0$ —the states are entangled in spite of the entropic classicness.

According to solution of Reference [52], the asymptotic result of dissipation of the state (3.38) is:

$$\rho_{AB}^{as} = \begin{pmatrix} 0 & 0 & 0 & 0 \\ 0 & \frac{1}{4}(1-2h) & -\frac{1}{4}(1-2h) & 0 \\ 0 & -\frac{1}{4}(1-2h) & \frac{1}{4}(1-2h) & 0 \\ 0 & 0 & 0 & \frac{1}{2}+h \end{pmatrix}. \quad (3.42)$$

Hence:

$$S(AB) = -\left(\frac{1}{2}+h\right)\log_2\left(\frac{1}{2}+h\right) - \left(\frac{1}{2}-h\right)\log_2\left(\frac{1}{2}-h\right), \quad (3.43)$$

$$S(A) = S(B) = -\left(\frac{1}{4}-\frac{h}{2}\right)\log_2\left(\frac{1}{4}-\frac{h}{2}\right) - \left(\frac{3}{4}+\frac{h}{2}\right)\log_2\left(\frac{3}{4}+\frac{h}{2}\right), \quad (3.44)$$

$i_{B|A}$ is determined by Equation (3.31), the concurrence is:

$$C = \frac{1}{2}(1-2h). \quad (3.45)$$

Figure 3.9 shows that dissipated maximally entangled mixed states are characterized by radically different dependence of C on δ , hence at small δ they are more entangled than the initial ones. As this takes place, as a result of dissipations the system has become in entropic terms classical ($0.571 \leq i_{B|A} \leq 1$ at all δ). In contrast to the initial states the independence function varies inversely to the degree of mixedness. In the pure state limit $\delta \rightarrow 0$: $S(AB) \rightarrow 0$, $\text{Tr}\rho_{AB}^2 \rightarrow 1$, but also $S(A) = S(B) \rightarrow 0$, therefore $i_{B|A} = i_{A|B} \rightarrow 1$.

Qualitatively asymptotic maximally entangled mixed states are close to asymptotic Werner states by the relation of independence, concurrence and mixedness.

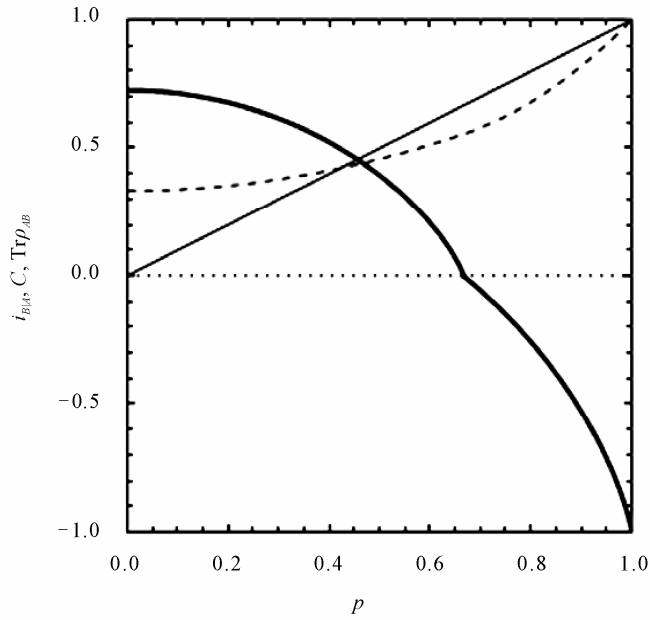


Figure 3.8. Dependence of $i_{B|A}$ (thick solid line), C (fine solid line) and $\text{Tr}\rho_{AB}^2$ (dashed line) on δ of initial maximally entangled mixed states (3.38).

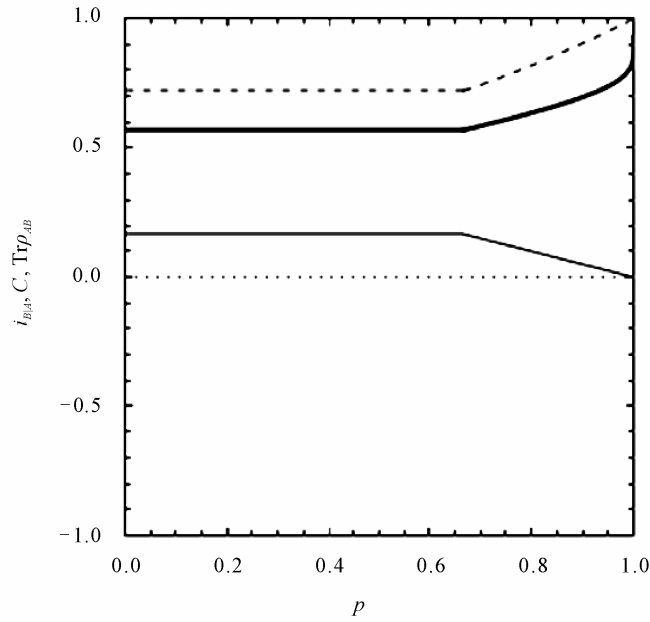


Figure 3.9. Dependence of $i_{B|A}$ (thick solid line), C (fine solid line) and $\text{Tr}\rho_{AB}^2$ (dashed line) on δ of asymptotic maximally entangled mixed states (3.42).

3.3. Asymmetric Two-Particle States

Hereafter we consider the examples of asymmetric states, for which application of causal analysis is

the most substanceble. The examples are considered in ascending order of nontriviality. In the computations of c_2 we shall suppose $k=1$ until the last example, where we shall consider the variable k . Note, that in those examples we shall nowhere use the axiom of strong causality (3.4). Reverse time is allowed.

3.3.1. Asymmetric Dissipation

Consider the third possible way of decoherence that is dissipation by the same manner as in Section 3.2.4 and 3.2.5: only one particle B is dissipated. Therein lies dissimilarity from the symmetric dissipation considered in Sections 3.2.6-3.2.8.

The dissipation reduces to the following transformation [45,46]:

$$\begin{aligned} |0\rangle\langle 0| &\rightarrow |0\rangle\langle 0|, \\ |1\rangle\langle 1| &\rightarrow (1-p)|1\rangle\langle 1| + p|0\rangle\langle 0|, \\ |1\rangle\langle 0| &\rightarrow \sqrt{1-p}|1\rangle\langle 0|, \\ |0\rangle\langle 1| &\rightarrow \sqrt{1-p}|0\rangle\langle 1|. \end{aligned} \quad (3.46)$$

As well as in Sections 3.2.4 and 3.2.5 the singlet (3.13) is taken as the initial state. The dissipated density is:

$$\rho_{AB} = \frac{1}{2} \left[|10\rangle\langle 10| + (1-p)|01\rangle\langle 01| + p|00\rangle\langle 00| - \sqrt{1-p}(|01\rangle\langle 10| + |10\rangle\langle 01|) \right]. \quad (3.47)$$

The reduced densities are:

$$\rho_A = \frac{1}{2} (|0\rangle\langle 0| + |1\rangle\langle 1|), \quad (3.48)$$

$$\rho_B = \frac{1}{2} \left[(1+p)|0\rangle\langle 0| + (1-p)|1\rangle\langle 1| \right]. \quad (3.49)$$

The entropies are:

$$S(AB) = -\frac{p}{2} \log_2 \frac{p}{2} - \left(1 - \frac{p}{2}\right) \log_2 \left(1 - \frac{p}{2}\right), \quad (3.50)$$

$$S(A) = 1, \quad (3.51)$$

$$S(B) = -\frac{1+p}{2} \log_2 \frac{1+p}{2} - \frac{1-p}{2} \log_2 \frac{1-p}{2}. \quad (3.52)$$

The independence functions are:

$$i_{B|A} = \frac{S(AB) - 1}{S(B)}, \quad i_{A|B} = S(AB) - S(B). \quad (3.53)$$

The concurrence is:

$$C = \sqrt{1-p} \quad (3.54)$$

From **Figure 3.10** it is clear that dissipation differs from depolarization and dephasing by greater values of C in the all p range, while $i_{B|A}$ is negative everywhere similar to the dephasing case. But the main interest represents **Figure 3.11**, where the measures of causality c_2 and γ are presented. $c_2 > 0$, therefore the particle A is the cause and B is the effect. It is in full agreement with the intuitive expectation—the irreversible flow of information is directed to the dissipating particle B . The decrease of

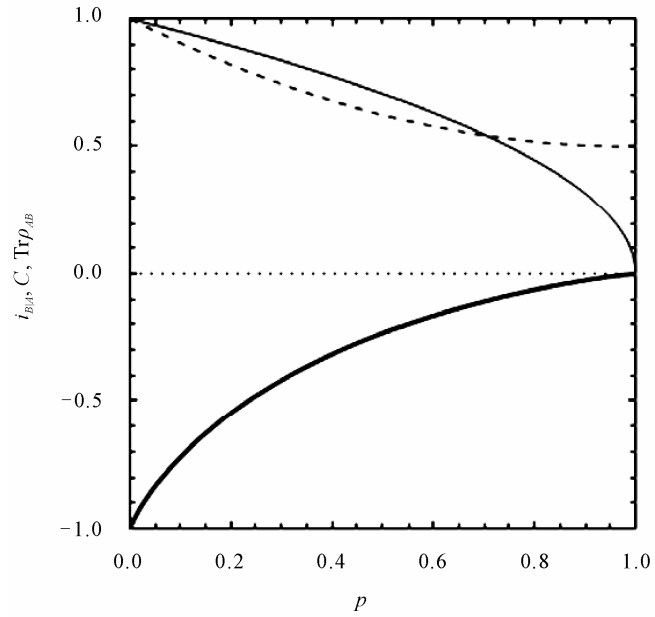


Figure 3.10. Dependence of $i_{B|A}$ (thick solid line), C (fine solid line) and $\text{Tr}\rho_{AB}^2$ (dashed line) on degree of dissipation p of the states (3.47).

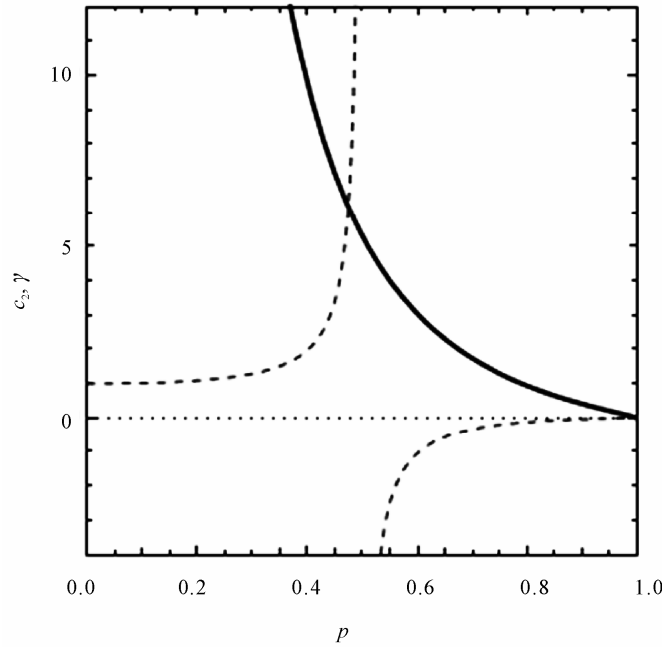


Figure 3.11. Dependence of c_2 (solid line) and γ (dashed line) on degree of dissipation p of the states (3.47).

c_2 with the increase of p also responds to intuitive expectation of amplification of causal connection with the increase of dissipation. But employment of the classical measure γ would lead at $0 < p < \frac{1}{2}$

to the opposite conclusion about directionality of the causal connection, while at $\frac{1}{2} < p < 1$ γ becomes classically meaningless.

In the entropic diagram (**Figure 3.1**) the states (3.47) correspond to subspaces IQ (at $0 \leq p \leq \frac{1}{2}$) and $IIIQ$ (at $\frac{1}{2} \leq p \leq 1$). The transition between the subspaces does not break smoothness of $c_2(p)$.

3.3.2. Coffman-Kundu-Wootters State

Coffman, Kundu and Wootters [56] have discovered the (CKW) state:

$$|CKW\rangle = \frac{1}{\sqrt{2}}|100\rangle + \frac{1}{2}(|001\rangle + |010\rangle), \quad (3.55)$$

which is notable by maximal pairwise entanglement (measured by concurrence) of the subsystems AB and AC . The entanglement properties of this remarkable state have also been considered in Reference [44].

Take the pair AB (the pair AC is identical). The reduced densities are:

$$\rho_{AB} = \frac{1}{2}|10\rangle\langle 10| + \frac{1}{4}(|00\rangle\langle 00| + |01\rangle\langle 01|) + \frac{1}{2\sqrt{2}}(|10\rangle\langle 01| + |01\rangle\langle 10|), \quad (3.56)$$

$$\rho_A = \frac{1}{2}(|0\rangle\langle 0| + |1\rangle\langle 1|), \quad (3.57)$$

$$\rho_B = \frac{3}{4}|0\rangle\langle 0| + \frac{1}{4}|1\rangle\langle 1|. \quad (3.58)$$

The entropies are:

$$S(AB) = S(B) = -\frac{3}{4}\log_2 \frac{3}{4} - \frac{1}{4}\log_2 \frac{1}{4} \approx 0.811, \quad (3.59)$$

$$S(A) = 1. \quad (3.60)$$

The independences are:

$$i_{B|A} \approx -0.233, \quad i_{A|B} = 0. \quad (3.61)$$

The measures of causality are:

$$\gamma = -\infty, \quad c_2 \approx 5.299 \quad (3.62)$$

The concurrence is:

$$C = \frac{1}{\sqrt{2}}. \quad (3.63)$$

According to the quantum measure c_2 A is the cause and B is the effect, while the classical measure γ is meaningless (the subspace $IIIQ$ in the entropic diagram). In the pair AC the result is the same and thus A is the common cause for B and C . Classical intuition in this case would be powerless to distinguish the common cause from the common effect.

Intuition gives only true, by virtue of the symmetry, answer about the absence of causal connection of B and C . The similar mathematics for this couple give: $i_{B|C} = i_{C|B} \approx 0.233$, $\gamma = 1$, $|c_2| = \infty$, $C = \frac{1}{2}$.

The particles B and C are entangled and classically correlated due to availability of the common cause. Note that the mixedness, according to both the measures in the pairs AB (AC) is less than in the pair BC : $S(AB) \approx 0.811$, $\text{Tr}\rho_{AB}^2 \approx 0.625$, $S(BC)=1$, $\text{Tr}\rho_{AB}^2 = \frac{1}{2}$.

3.3.3. WRr-State

In References [57,58] the different three-partite states related by the symmetry transformations, the particular cases of which are GHZ and W-states, have been investigated.

In particular the duplet has been obtained:

$$|WRr\rangle = \frac{1}{\sqrt{6}}(|001\rangle + |010\rangle - 2|100\rangle). \quad (3.64)$$

This state differs by the entanglement distribution from W-state considered in Section 3.2.3, for which $C_{AB} = C_{AC} = C_{BC} = \frac{1}{3}$, and the state considered in Section 3.3.2, for which $C_{AB} = C_{AC} = \frac{1}{\sqrt{2}}$, $C_{BC} = \frac{1}{2}$.

For the state (3.64) $C_{AB} = C_{AC} = \frac{2}{3}$, $C_{BC} = \frac{1}{3}$ [57,58], that is the pair BC has entanglement twice smaller than two another pairs have.

For the state (3.64):

$$\rho_{AB} = \frac{1}{6}(4|10\rangle\langle 10| - 2|10\rangle\langle 01| - 2|01\rangle\langle 10| + |01\rangle\langle 01| + |00\rangle\langle 00|), \quad (3.65)$$

$$S(AB) = S(B) = -\frac{1}{6}\log_2 \frac{1}{6} - \frac{5}{6}\log_2 \frac{5}{6} \approx 0.651, \quad (3.66)$$

$$S(A) = -\frac{1}{3}\log_2 \frac{1}{3} - \frac{2}{3}\log_2 \frac{2}{3} \approx 0.918, \quad (3.67)$$

$$i_{B|A} \approx -0.412, \quad i_{A|B} = 0, \quad (3.68)$$

$$\gamma = -\infty, \quad c_2 \approx 3.43. \quad (3.69)$$

The same is true for the pair AC . Therewith $\text{Tr}\rho_{AB}^2 = \text{Tr}\rho_{AC}^2 \approx 0.722$.

As in Section 3.3.2, A is the cause for B and C and only the quantum measure of causality has a meaning (the subspace IIIQ in **Figure 3.1**). The quantitative difference implies that according to both the measures of mixedness in the causal links of the state (3.64) it is less than in (3.55), and though the concurrence is less, the independence functions $i_{B|A} = i_{C|A} < 0$ are lower, i.e. quantum correlations are stronger, and c_2 is lower, i.e. causal connection is expressed stronger.

For the particles B and C in the state (3.64) we have: $S(BC) \approx 0.918$, $\text{Tr}\rho_{BC}^2 \approx 0.556$,

$i_{B|C} = i_{C|B} \approx 0.412$, $\gamma = 1$, $|c_2| = \infty$, $C = \frac{1}{3}$. As with the state (3.55), causality in the pair BC is absent, and although the mixedness is lower, but the entanglement and classical ($i_{B|C} = i_{C|B} > 0$) correlations are weaker.

3.3.4. Asymmetric "Quantum-Classical" States

The question on the peculiarities of behavior of the asymmetric states was the first to set in reference [59], where the case of "quantum-classical" two-partite states was considered. The subsystem A is called quantum if $S(A) > S(AB)$, and classical $-B$ if $S(B) \leq S(AB)$. The strange fact has been discovered: the decoherence may go faster by interaction of the environment with the classical subsystem.

This has been called in Reference [59] anomalous entanglement decay. As a result a number of open questions about nontrivial behavior of the open systems have been set, among them on asymmetry in the transfer of quantum information with respect to its direction.

In Reference [59] asymmetric states were considered:

$$\rho_{AB} = q|\Psi_1\rangle\langle\Psi_1| + (1-q)|\Psi_2\rangle\langle\Psi_2|, \quad 0 < q < 1. \quad (3.70)$$

with normalized $|\Psi_1\rangle = a|00\rangle + \sqrt{1-a^2}|11\rangle$ and $|\Psi_2\rangle = a|10\rangle + \sqrt{1-a^2}|01\rangle$ with $0 < a < 1$. From Equation (3.70) it is seen that mixedness depends on q only, while the concurrence—on q and a . The expanded Equation (3.70) is:

$$\rho_{AB} = \begin{pmatrix} qa^2 & 0 & 0 & qa\sqrt{1-a^2} \\ 0 & (1-q)(1-a^2) & (1-q)a\sqrt{1-a^2} & 0 \\ 0 & (1-q)a\sqrt{1-a^2} & (1-q)a^2 & 0 \\ qa\sqrt{1-a^2} & 0 & 0 & q(1-a^2) \end{pmatrix}. \quad (3.70a)$$

Hence:

$$S(AB) = -q \log_2 q - (1-q) \log_2 (1-q), \quad (3.71)$$

$$S(A) = -(a^2 - 2qa^2 + q) \log_2 (a^2 - 2qa^2 + q) - (1 - a^2 + 2qa^2 - q) \log_2 (1 - a^2 + 2qa^2 - q), \quad (3.72)$$

$$S(B) = -a^2 \log_2 a^2 - (1 - a^2) \log_2 (1 - a^2), \quad (3.73)$$

$$i_{B|A} = \frac{S(AB) - S(A)}{S(B)}, \quad i_{A|B} = \frac{S(AB) - S(B)}{S(A)}, \quad (3.74)$$

$$C = 2\sqrt{a^2(1-a^2)}|1-2q|. \quad (3.75)$$

Always $S(A) \geq S(AB)$, $S(B)$ may be greater as well as less than $S(AB)$. According to definition of Reference [59] the subsystem A is almost always quantum, while the subsystem B may be either quantum or classical. In **Figure 3.12** the dependences of $i_{B|A}$, C and $\text{Tr}\rho_{AB}^2$ on q and a^2 which have the expected appearance. Only the dependence of $i_{B|A}$ on a^2 is nontrivial. That the $i_{B|A}$ is almost always negative (except of the case $q = \frac{1}{2}$) just reflects the fact that the subsystem A is almost

always quantum. At the maximal mixedness, achieved at $q = \frac{1}{2}$, the subsystem are not entangled but classically maximally correlated ($i_{B|A} = 0$) at any a^2 .

The dependences of c_2 and γ on q and a^2 are presented in **Figure 3.13**. The positive value of c_2 shows that at almost all q and a^2 A is the cause and B is the effect. Causality disappears ($c_2 = \infty$) only at $q = 0$ or 1 (the pure states) and $a^2 = \frac{1}{2}$ (the symmetric states). The direction of causal connection $A \rightarrow B$ clears up a conclusion of Reference [59] about bigger fragility to decoherence of the classical subsystem B . Certainly the runoff quantum information occurs mainly in the effect B .

The states correspond to the subspaces IQ and $IIIQ$ (**Figure 3.1**), accordingly, the classical measure of causality γ in **Figure 3.13** shows either mistakenly opposite direction of causal connection or loses its meaning where γ is negative. Classical causality is absent ($\gamma = 1$) at $a^2 = q$ and $a^2 = 1 - q$. The negative values of γ (subspace $IIIQ$) correspond to the positive values of the independence function

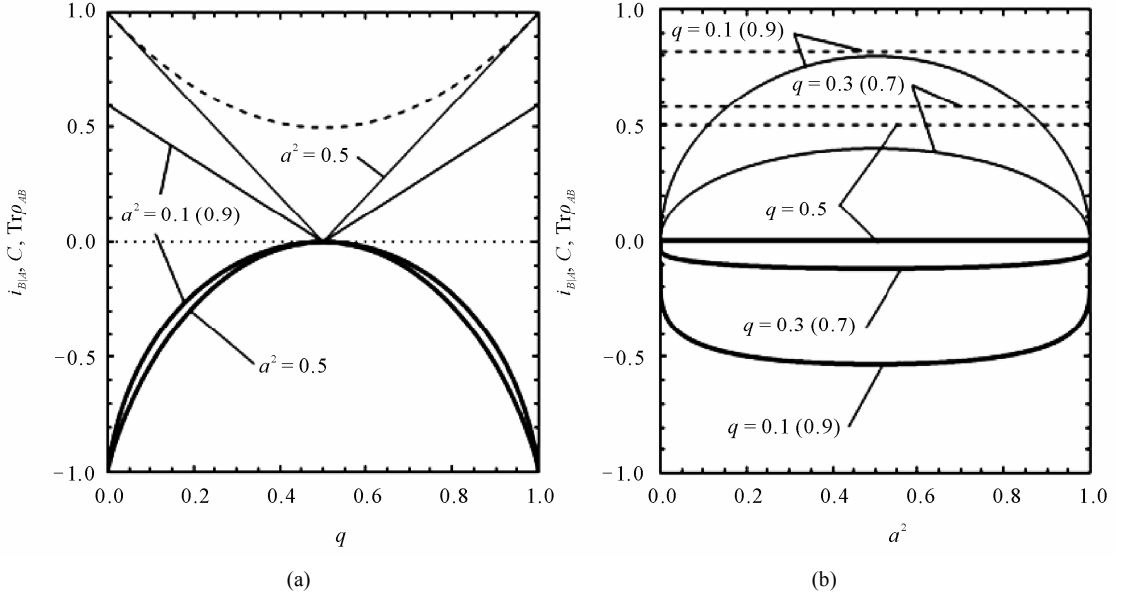


Figure 3.12. Dependence of $i_{B|A}$ (thick solid lines), C (fine solid lines) and $\text{Tr}\rho_{AB}^2$ (dashed lines) (a) on q and (b) on a^2 of the asymmetric “quantum-classical” states (3.70).

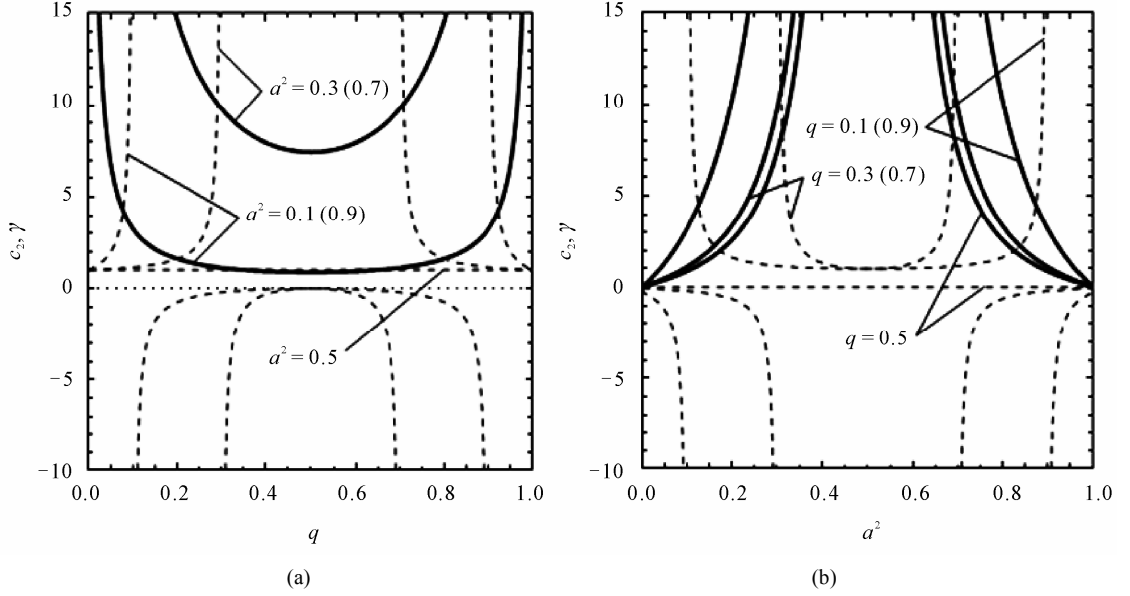


Figure 3.13. Dependence of c_2 (solid lines), and γ (dashed lines) (a) on q and (b) on a^2 of the asymmetric “quantum-classical” states (3.70).

$i_{A|B}$ or in other words, to the classicness of subsystem B by the definition of Reference [59]. But since $c_2 > 0$ is *always* positive we conclude that anomalous entanglement decay by Reference [59] is not anomalous, because it is only a particular case of general and natural phenomenon of greater quantum information runoff on the more dissipative subsystem.

A nontrivial quantitative conclusion (which is impossible to make simply from appearance of the states

(3.70) or (3.70a)) is that maximal mixed states $q = \frac{1}{2}$ correspond to the one-valued function line (**Figure 2.1**). At any a^2 here $\gamma = 0$ (**Figure 3.13**), that corresponds to the utmost irreversible transition $A \Rightarrow B$. This one-valued dependence of B on A is achieved at zero concurrence (**Figure 3.12**). Therewith c_2 has any positive value depending on a^2 . In other words, the case of the utmost strong classical causality can correspond to different degree of uniformly directed quantum causality—from the strongest one for the utmost asymmetry of the state ($a^2 \rightarrow 0$ or $a^2 \rightarrow 1$) to its absence at the symmetry ($a^2 = \frac{1}{2}$).

3.3.5. Thermal Entanglement under a Nonuniform External Magnetic Field

It is generally believed that increase of the temperature, as well as the magnetic field, destroy entanglement. But recently [60] it has been discovered that nonuniform magnetic field, on the contrary, play a constructive role and entanglement is maintained at the high temperature as well as under the strong magnetic field. It has been found that just nonuniform magnetic field of opposite direction at the subsystem A and B has such decoherence suppression property.

Consider, according to Reference [60], thermal entanglement of the two qubits with spin $\frac{1}{2}$ related by XY -Heisenberg interaction with the following Hamiltonian:

$$H = J(S_A^x S_B^x + S_A^y S_B^y) + B_A S_A^z + B_B S_B^z, \quad (3.76)$$

where the spin operator $S^j = \sigma^j / 2$ ($j = x, y, z$), J is the strength of Heisenberg interaction, B_A and B_B are the external magnetic fields at the particles A and B . The eigenvalues and eigenvectors of Hamiltonian (3.76) are:

$$\begin{aligned} H|00\rangle &= -(B_A + B_B)|00\rangle, \\ H|11\rangle &= (B_A + B_B)|11\rangle, \\ H|\Psi^\pm\rangle &= \pm\sqrt{D}|\Psi^\pm\rangle, \end{aligned} \quad (3.77)$$

where

$$\begin{aligned} |\Psi^\pm\rangle &= \frac{1}{N_\pm} \left[|01\rangle + \frac{(B_A - B_B) \pm \sqrt{D}}{J} |10\rangle \right], \\ D &= (B_A - B_B)^2 + J^2. \end{aligned}$$

The density matrix of the thermal states is:

$$\rho_{AB} = \frac{1}{Z} \begin{pmatrix} e^{(B_A + B_B)/k_B T} & 0 & 0 & 0 \\ 0 & m + n & -s & 0 \\ 0 & -s & m - n & 0 \\ 0 & 0 & 0 & e^{-(B_A + B_B)/k_B T} \end{pmatrix}, \quad (3.78)$$

$$Z = \text{Tr} e^{-H/k_B T},$$

$$m = \text{ch} \left(\frac{\sqrt{D}}{k_B T} \right),$$

$$n = \frac{B_A - B_B}{\sqrt{D}} \operatorname{sh} \left(\frac{\sqrt{D}}{k_B T} \right),$$

$$s = \frac{J \operatorname{sh} \left(\frac{\sqrt{D}}{k_B T} \right)}{\sqrt{D}}.$$

In the next calculations we accept $k_B = J = 1$. The state asymmetry is determined by n . From Equation (3.78) follows:

$$S(AB) = -\frac{m + \sqrt{n^2 + s^2}}{Z} \log_2 \frac{m + \sqrt{n^2 + s^2}}{Z} - \frac{m - \sqrt{n^2 + s^2}}{Z} \log_2 \frac{m - \sqrt{n^2 + s^2}}{Z} - \frac{\exp\left(\frac{B_A + B_B}{T}\right)}{Z} \log_2 \frac{\exp\left(\frac{B_A + B_B}{T}\right)}{Z} - \frac{\exp\left(-\frac{B_A + B_B}{T}\right)}{Z} \log_2 \frac{\exp\left(-\frac{B_A + B_B}{T}\right)}{Z}, \quad (3.79)$$

$$S(A) = -\frac{\exp\left(\frac{B_A + B_B}{T}\right) + m + n}{Z} \log_2 \frac{\exp\left(\frac{B_A + B_B}{T}\right) + m + n}{Z} - \frac{\exp\left(-\frac{B_A + B_B}{T}\right) + m - n}{Z} \log_2 \frac{\exp\left(-\frac{B_A + B_B}{T}\right) + m - n}{Z}, \quad (3.90)$$

$$S(B) = -\frac{\exp\left(\frac{B_A + B_B}{T}\right) + m - n}{Z} \log_2 \frac{\exp\left(\frac{B_A + B_B}{T}\right) + m - n}{Z} - \frac{\exp\left(-\frac{B_A + B_B}{T}\right) + m + n}{Z} \log_2 \frac{\exp\left(-\frac{B_A + B_B}{T}\right) + m + n}{Z}. \quad (3.91)$$

The independence functions are determined by the general formulae (87). The concurrence is:

$$C = 2 \frac{s-1}{Z} \quad (3.92)$$

For investigation of the nonuniform field impact, accept at the beginning $T = 1$, $B_A = 5$, $B_B = 5p$.

The maximal mixedness both by $\max S(AB)$ derived from Equation (3.79), and by $\min \operatorname{Tr} \rho_{AB}^2$ (**Figure 3.14**) is achieved at $p \approx 0.010$. The concurrence in **Figure 3.14** demonstrates noted in Reference [60] the most entanglement at oppositely directed fields at A and B , but the maximum is achieved not at the exact antisymmetry ($p = -1$) as presumed in Reference [60], but at $p \approx -0.253$. Note, that according to Equations (3.90) and (3.91) $\max S(A)$ ($p \approx -0.149$) is close to $\max C$, while $\max S(B)$ is close to $\min \operatorname{Tr} \rho_{AB}^2$ ($p \approx 0.08$), therewith $\max \alpha \approx 26.5$ is observed at $p \approx 0.176$. The independence function $i_{B|A}$ in **Figure 3.14** demonstrates similarity neither with the mixedness nor with the concurrence. $i_{B|A} \rightarrow -1$ that is quantum correlation increases at deeply negative p , where C decreases. At $-0.54 < p < 0.5$ $i_{B|A}$ is classically positive in spite of $C > 0$. $\max i_{B|A}$ that is the least correlation of the subsystem is observed at $p \approx 0.379$, where C is still finite. At big p $i_{B|A}$ goes down at the expense of classical correlations under the parallel fields. The independence function $i_{A|B}$ is also shown in **Figure 3.14**. Although $i_{A|B} = 0$ at $p = 0$ there are no antisymmetry by p , $\min i_{A|B}$ is observed at $p \approx -1.115$, while $i_{A|B} \rightarrow 1$ at big positive p . In the interval $0 < p < 0.5$ the states are entangled though classically correlated (the both i are positive). Thus, the independence functions

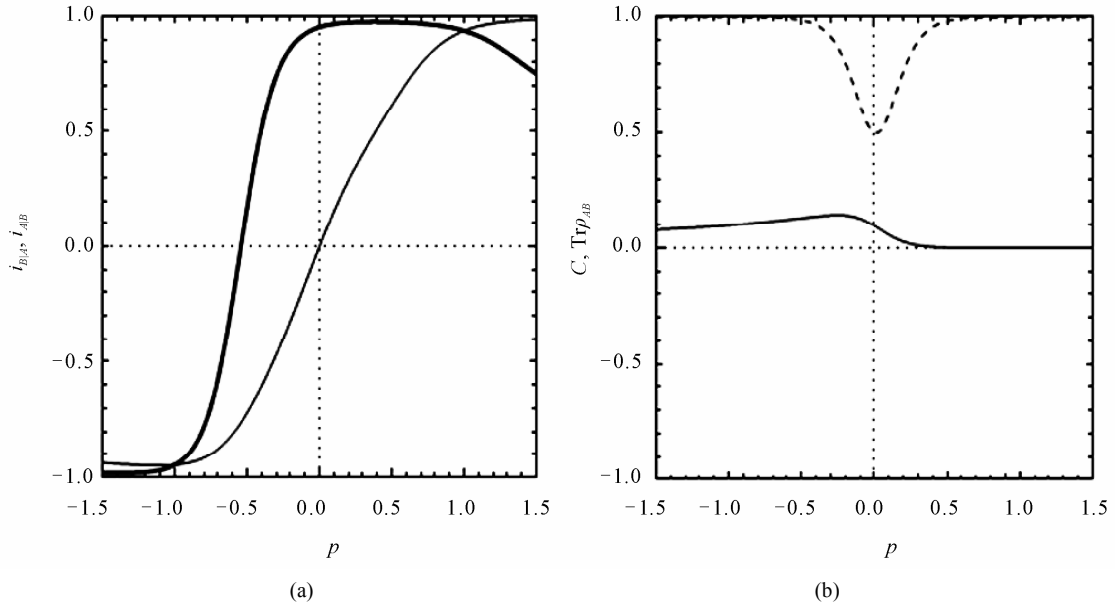


Figure 3.14. Dependence of (a) $i_{B|A}$ (thick solid line) and $i_{A|B}$ (fine solid line), (b) C (solid line) and $\text{Tr}\rho_{AB}^2$ (dashed line) on $p = B_B/B_A$ of the states (3.78) ($T = 1$).

demonstrate nontrivial relation between quantum and classical correlations, which is impossible to reveal from consideration of the concurrence only.

Consider the causal connection of the subsystems. In this case determine c_2 not only at $k = \Delta r/\delta t = 1$ in Equation (2.12), but drawing on the eigenvalues of Hamiltonian (3.77), compute δt according to Equation (3.5). Supposing now $\Delta r = 1$, determine $c'_2 = c_2/\delta t$. In **Figure 3.15** c_2 , c'_2 and γ are presented. The former two as convenience (to show their maxima) are presented at two different scales for the parallel and antiparallel fields. According to all the three measures causality is absent at $p = \pm 1$, that is under equal parallel and antiparallel fields at A and B . The interval $p(-\infty, -1)$ corresponds to the subspace IQ , $p(-1, 0.54] - IIQ$, $p[-0.54, 0] - IVQ$, $p(0, 1) - IIC$, $p(1, \infty) - IC$. According to both the quantum measures at $|p| > 1$ A is the cause, B is the effect, and inversely at $|p| < 1$. In other words, the effect is always in the region of stronger field. It can be understood as stabilizing polarization of the qubit in the strong field, as a result of which the qubit becomes to a greater degree the sink of information than the source. At directionality of causal connection $A \rightarrow B$ and $|p| \rightarrow \infty$ causality is amplified: $c_2 \rightarrow +0$, $c'_2 \rightarrow +0$. But at directionality $B \rightarrow A$ $\min|c_2|$ and $\min|c'_2|$ are not at $p = 0$ as could be supposed intuitively, but at finite $p \approx 0.364$ for c_2 and $p \approx 0.266$ for c'_2 . These values of p are determined by the chosen temperature $T = 1$. Calculation shows that specific field ratio p at which causality is strongest decreases as the temperature increases. The causality function γ gives the right answer about directionality of causal connection only at $p > 0$. At last from **Figure 3.15** it is seen that there is no a qualitative difference between c_2 and c'_2 .

Consider the temperature influence more closely. It can be expected that any correlations decrease as the temperature increases. On the other hand, namely finite temperature leads to mixing, which is a necessary condition of quantum causality. Indeed, as the temperature increases $S(AB)$ increases, however the subsystem entropies increases too, but by different manner, and one can expect nontrivial behavior of the entropic functions.

From **Figure 3.16** it is seen that mixedness increases with the temperature, but the magnetic field at the subsystem B suppresses this temperature influence. The concurrence (**Figure 3.17**) under antiparallel fields, in accordance with the main conclusion of Reference [60] is maintained at the high temperature.

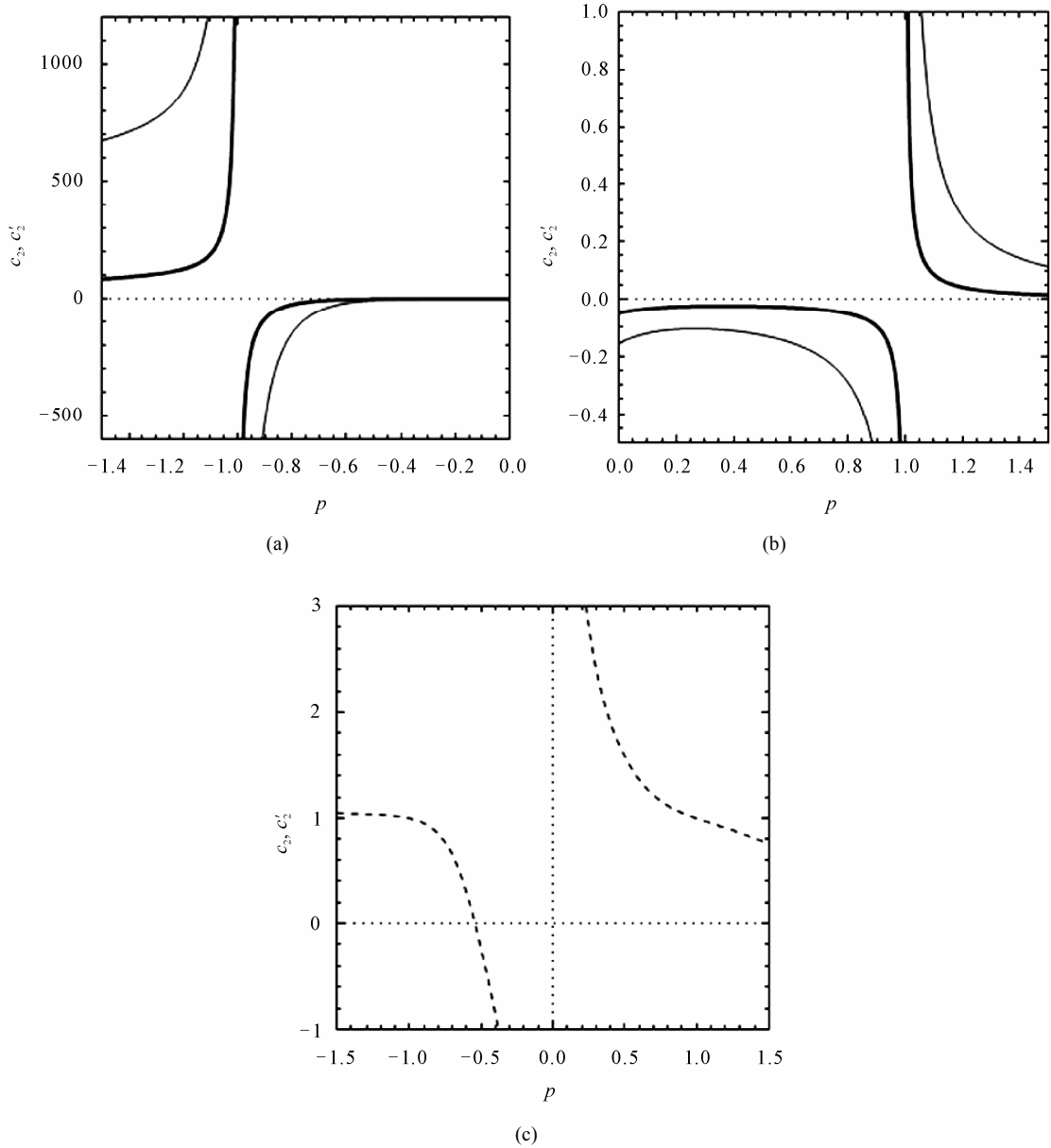


Figure 3.15. Dependence of (a, b) c_2 (thick solid line) and c_2' (fine solid line), and (c) γ (dashed line) on $p = B_B/B_A$ of the states (3.78) ($T=1$).

However the most suppression of decoherence is achieved not in the antisymmetric case ($p = -1$), but under stronger field at B ($p = -1.5$). At $T \rightarrow 0$, on the contrary, the highest concurrence is achieved under zero field at B . At positive p the concurrence steeply disappears in accordance with common view about suppression of entanglement by the magnetic field. The independence function $i_{B|A}$ (**Figure 3.18**) points out monotonous amplification of quantum and classical correlations with amplification of negative field ratio p . At positive p correlations are classical and the temperature dependence is not monotonous—there is a minimum of positive $i_{B|A}$ (maximum of classical correlation) at the finite temperature. The inversed independence function $\tilde{i}_{B|A}$ (**Figure 3.19**) has much smaller sensitivity of the

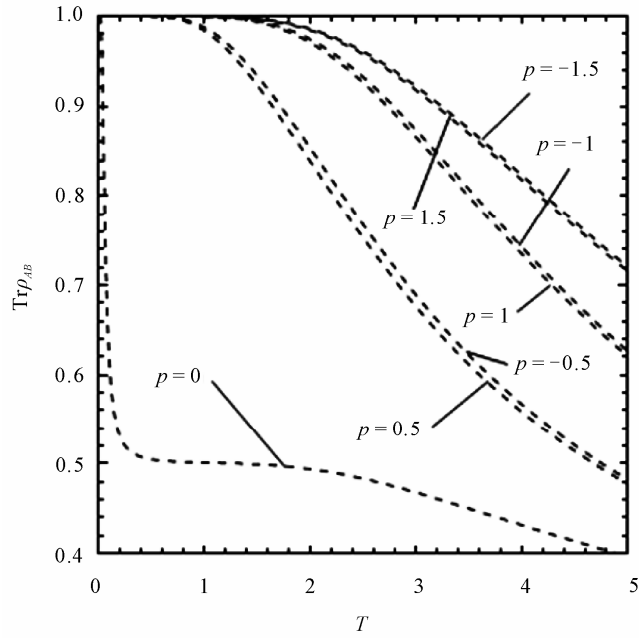


Figure 3.16. Dependence of $\text{Tr} \rho_{AB}^2$ on T of the states (3.78).

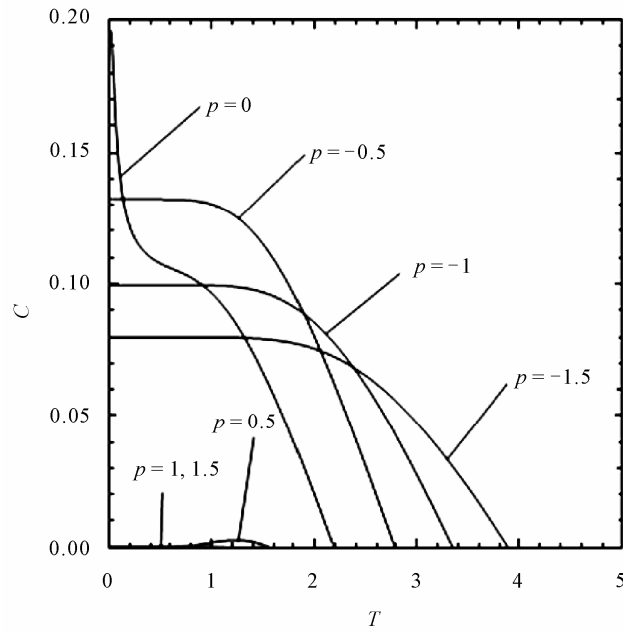


Figure 3.17. Dependence of C on T of the states (3.78).

temperature variation to the negative p , but much greater sensitivity to the positive p . At $p = 0$ the curve $i_{A|B}(T)$ has the inflection point (at $T \approx 0.8$), which is absent in the curve $i_{B|A}$.

The classical measure of causality γ (**Figure 3.20**) demonstrates that in the domain of its correct implementation ($p > 0$) directionality of causal connection is exactly independent of the temperature.

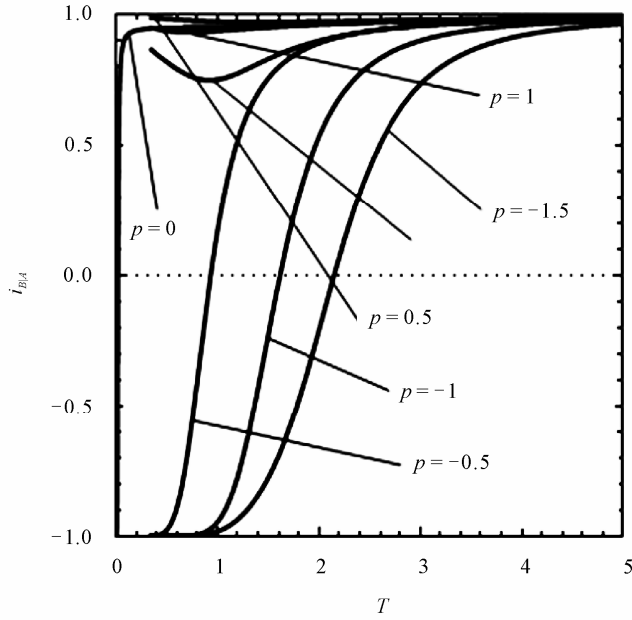


Figure 3.18. Dependence of $i_{B|A}$ on T of the states (3.78).

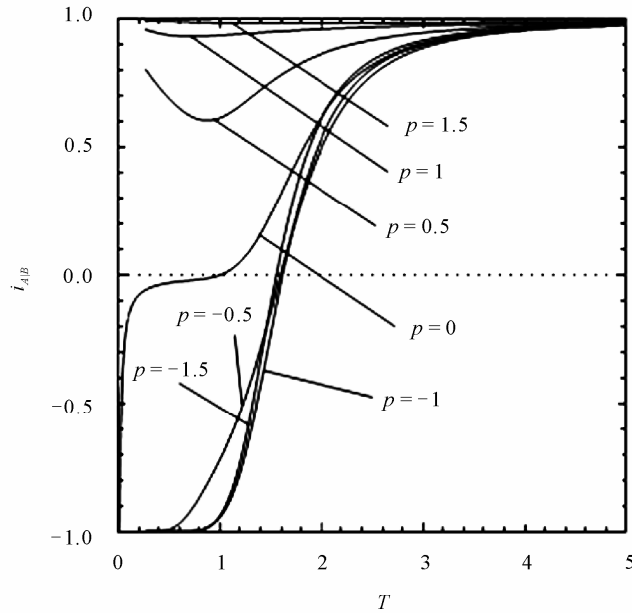


Figure 3.19. Dependence of $i_{A|B}$ on T of the states (3.78).

There is only a weak amplification of the causal connection at $T \approx 0.9$. In the domain of its incorrect implementation ($p < 0$) γ demonstrates the breaks and causality reversals. In **Figure 3.21** behavior of c_2 and c'_2 against the temperature is shown. At any p directionality of the causal connection is independent of the temperature, but its value depends on it. At $p > 0$, that is under the parallel fields, causality utmostly amplifies at the temperature tending to zero and remains almost steady at $T > 1.3$ (at

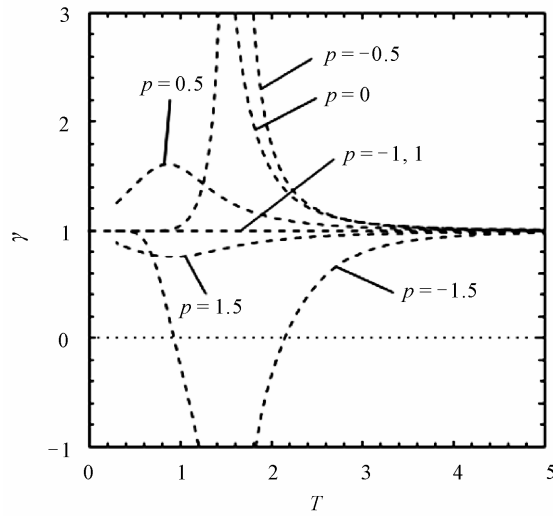


Figure 3.20. Dependence of γ on T of the states (3.78).

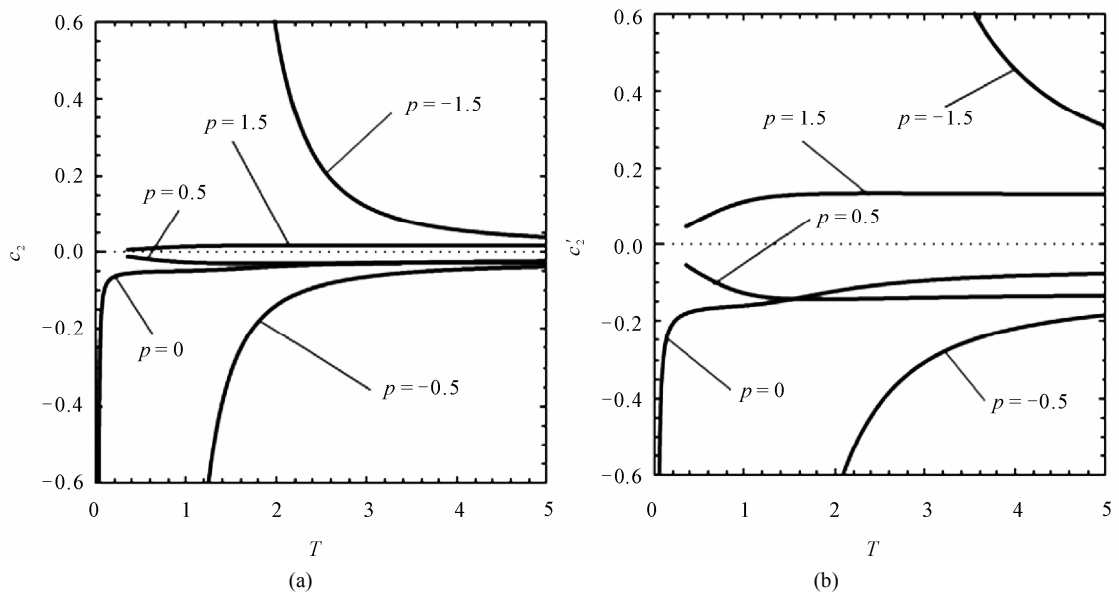


Figure 3.21. Dependence of c_2 (a) and c'_2 (b) on T of the states (3.78).

$p = 0.5$ there is a very weak amplification of causality at the high temperature). Under the antiparallel fields ($p \leq 0$) causality, on the contrary considerably amplifies at the high temperature. The stronger field nonuniformity, the sharper this amplification. As it was accepted $J = 1$, $B_A = 5$ in the computations, hence it follows that Heisenberg interaction is essential for the causal connection only under the parallel fields.

3.4. Asymmetric Three-Particle States

Above the series of examples of two-qubit causeless (symmetric) and causal (asymmetric) states has

been considered. In this section we consider more complicated three-qubit states. In fact this consideration demonstrates the qualitative peculiarities of the many-qubit states as compared to two-qubit ones.

As before the first qubit we call the subsystem A , the second and third—the subsystems B and C respectively. We consider the bipartite states, where one party may consist of two particles, that is some more complicated in comparison to Section 3, where only one-particle partition has been analyzed. Thus the rather simple three-qubit examples will help to understand the peculiarities of many-particle causality in comparison to two-particle ones.

Naturally, instead of the concurrence every example we shall provide with the negativity N as a standard measure of bipartite entanglement between two groups of qubits which is defined as (e.g. [61]):

$$N(\rho) = \sum_i |\mu_i| \quad (3.93)$$

where μ_i is the negative eigenvalue of ρ^T , and T denotes the partial transpose with respect to another subsystem. And in this section the entropy of full system $S(ABC)$ (or two-particle subsystems $S(AC)$ etc.) as a measure of mixedness is more convenient.

At last, after rather detailed description of the above examples, below we can afford the less detailed style.

3.4.1. Dissipated GHZ States

Let's apply the transformation (3.46) to one of the particles of (3.10), for example, C . By the influence of dissipation the state becomes mixed, so its density matrix is:

$$\rho_{GHZ}^{diss} = \frac{1}{2} \left[|000\rangle\langle 000| + (1-p)|111\rangle\langle 111| + p|110\rangle\langle 110| + \sqrt{1-p}(|000\rangle\langle 111| + |111\rangle\langle 000|) \right] \quad (3.94)$$

The full set of marginal and conditional entropies is calculated from the matrix (14) and corresponding reduced matrices. Then the independence functions (1) for the all bipartitions are calculated, which in their turn are used in calculation of corresponding c_2 .

Because of the symmetry there are only four unique links: $A-B$, $AB-C$, $A-C$, $AC-B$. The $A-B$ link is symmetric ($i_{A|B} = i_{B|A}$) so there is no causality in it. The causalities characterized by c_2 of three other links are presented in **Figure 3.22(a)** (hereafter we follow the notation of c_2 arguments ordering: $c_2(X, Y) > 0$ corresponds to that X is cause and Y is effect).

As we see in the links $AB-C$ and $A-C$ the dissipated particle C always corresponds to the effect ($c_2(AB, C) > 0$, $c_2(A, C) > 0$) and with the increase of the degree of dissipation p the causality amplifies ($c_2 \rightarrow 0$ at $p \rightarrow 1$). It is in full agreement with the intuitive expectation—the irreversible flow of information is directed to the dissipated particle. The fact that $c_2(AB, C) > c_2(A, C)$ is explained by stronger mixedness of the reduced state $\rho(AC)$ as compared to $\rho(ABC)$: $S(AC) > S(ABC)$ (**Figure 3.22(b)**), because mixedness is a necessary condition of causality. In its turn stronger mixedness of $\rho(AC)$ is the consequence of both interaction with B and dissipation of C *i.e.* interaction with the non-controlled environment; while mixedness of $\rho(ABC)$ is the consequence of only the latter. Note that in the case of dissipation of one of the particles of two-particle counterpart of GHZ state (that is Bell state) all the corresponding entropies and therefore all the other parameters, including c_2 exactly coincides with those of GHZ $AB-C$ partition.

In the link $AC-B$ the behavior of causality is nontrivial. In contrast to the above case the couple AC including the dissipated particle C constitutes the cause. The fact is the dissipation of C decreases $S(C)$ (the state approaches to the certain ground state according to Equation (3.46)). On the other hand the dissipation of C opens the subsystem AC to the environment and $S(AC)$ increases and has the maximum at $p = \frac{1}{2}$ equal to $\frac{3}{2}$ (**Figure 3.22(b)**), while $S(B) = const = 1$. The particle B always corresponds to the effect but c_2 is not monotonous: it has the minimum at $p \approx 0.594$. To

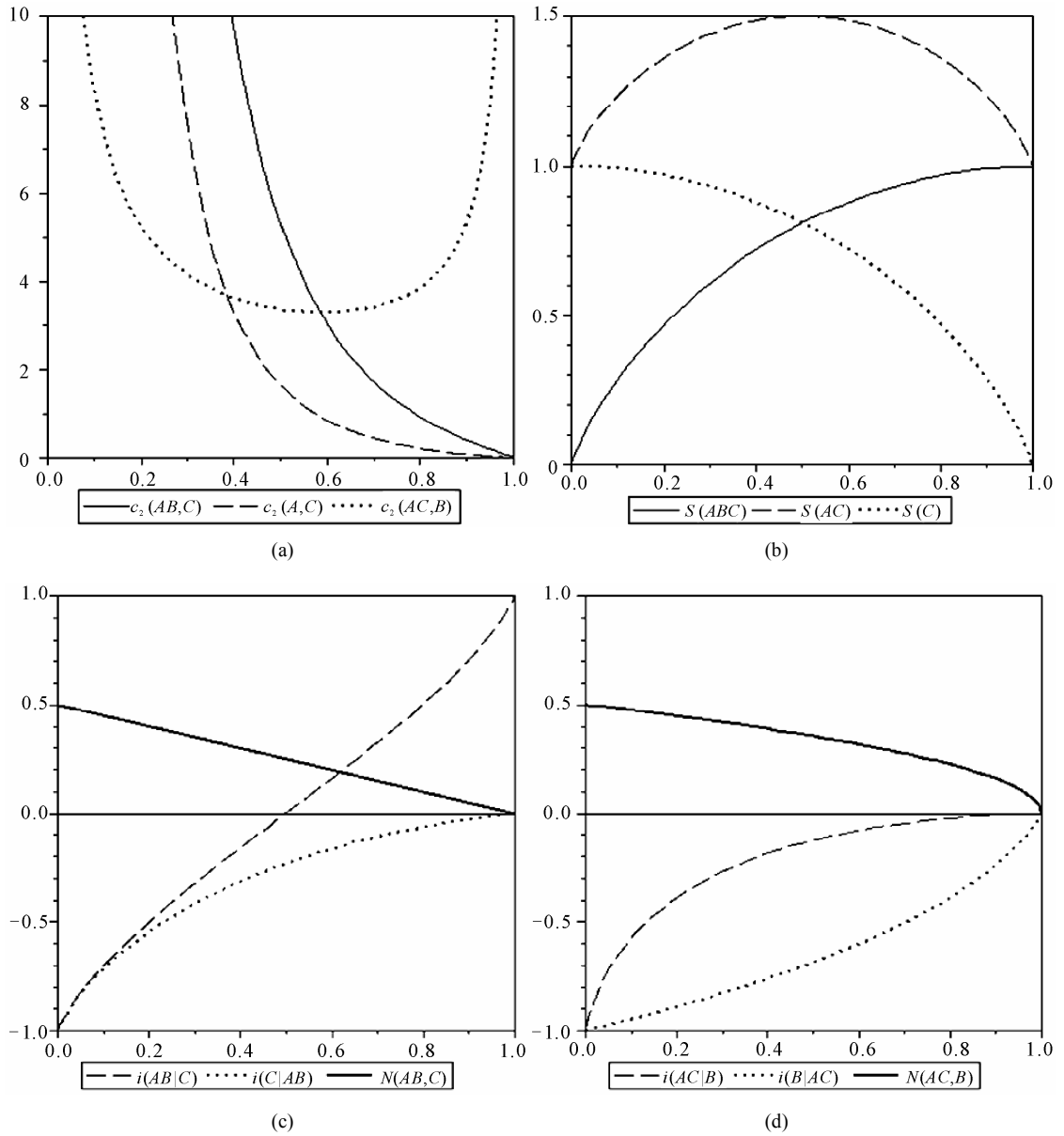


Figure 3.22. Dependence of c_2 (a), S (b), i and N (c, d) on degree of dissipation p of the particle C for the different partition of the states (3.94).

explain this fact, note that at $p=0$ the state (3.94) is pure therefore $c_2(AC,B) \rightarrow \infty$; at $p=1$ the state (3.94) is maximally mixed, but $S(AC) = S(B)$ (the fully dissipated particle C has “disappeared”) therefore $c_2(AC,B) \rightarrow \infty$ too. The denominator of Equation (2.12) for $c_2(AC,B)$: $i_{AC|B} - i_{B|AC}$ has the maximum at $p \approx 0.401$ (**Figure 3.22(d)**), while the nominator that is correlation $(1 - i_{AC|B})(1 - i_{B|AC})$ decreases as p increases, therefore $\min c_2$ is shifted to a higher p relative to $\frac{1}{2}$. But by comparison with other links causality in the link $AC - B$ is prevailing, as it is seen from **Figure 3.22(a)**, at small

dissipation ($p < 0.387$).

A comparison of the negativity N and independence functions i , which are presented in **Figures 3.22(c)** and **3.22(d)**, shows that the latter's are more sensitive to partition. In addition one could expect that since a maximally entangled state is pure (and therefore causeless) then the weaker entanglement the stronger causality. But a comparison of **Figures 3.22(c)**, **3.22(d)** and **3.22(a)** shows that in general such is not the case.

3.4.2. Dissipated W-States

Applying transformation (3.46) to the third particle C , of W-state (3.11) we come to the dissipated states:

$$\begin{aligned} \rho_W^{diss} = \frac{1}{3} [& |010\rangle\langle 010| + |010\rangle\langle 100| + |100\rangle\langle 010| + |100\rangle\langle 100| + (1-p)|001\rangle\langle 001| \\ & + p|000\rangle\langle 000| + \sqrt{1-p} (|001\rangle\langle 010| + |001\rangle\langle 100| + |010\rangle\langle 001| + |100\rangle\langle 001|)]. \end{aligned} \quad (3.95)$$

Similar to dissipated GHZ in the links $AB-C$ and $A-C$ the dissipated particle C always corresponds to the effect ($c_2(AB, C) > 0$, $c_2(A, C) > 0$) and with the increase of the degree of dissipation p the causality amplifies ($c_2 \rightarrow 0$ at $p \rightarrow 1$) (**Figure 3.23(a)**). The fact that $c_2(AB, C) > c_2(A, C)$ is explained by more mixedness of the reduced state $\rho(AC)$ as compared to $\rho(ABC)$: $S(AC) > S(ABC)$ (**Figure 3.23(b)**) by the same reasons as in the above case. And in the link $AC-B$ the couple AC , including the dissipated particle C , constitutes the cause by the same reasons as in the case of dissipated GHZ state. The distinction is that c_2 has the minimum at $p \approx 0.576$ and c_2 in this link is higher, *i.e.* causality is weaker, than in the two other links at any p (**Figure 3.23(a)**).

When **Figures 3.23(c)** and **3.23(d)** are compared with **Figure 3.23(a)** it is apparent that for the different partitions the higher negativity, the stronger quantum correlations and the weaker causality: $N(AC, B) > N(AB, C) > N(A, C)$, $c_2(AC, B) > c_2(AB, C) > c_2(A, C)$. It is quite expectable, but within the same partition such is not the case: at $p > 0.576$ $N(AC, B)$ goes down, while $c_2(AC, B)$ goes up.

Of particular interest is negativity and independence function comparison of the reduced state $\rho(AC)$. In **Figure 3.24** it is seen that at any $p < 1$ the both i and N are positive. It means that subsystem AC is in an entropic sense is classical but nevertheless entangled.

3.4.3. Dissipated CKW States

In Section 3.3.2 it has been found that subsystems of the CKW-state (3.55) are causal, a party A is a common cause for B and C : $c_2(A, B) = c_2(A, C) \approx 5.30$ (the link $B-C$ is causeless: $|c_2(A, B)| = \infty$). Since the original state (3.55) is asymmetric, the causality picture will be richer. Let the particle C is dissipated as in above examples. Then the states are:

$$\begin{aligned} \rho_{CKW}^{dissC} = \frac{1}{4} & |010\rangle\langle 010| + \frac{1}{2\sqrt{2}} (|010\rangle\langle 100| + |100\rangle\langle 010|) + \frac{1}{2} |100\rangle\langle 100| + \frac{1}{4} (1-p) |001\rangle\langle 001| \\ & + \frac{1}{4} p |000\rangle\langle 000| + \sqrt{1-p} \left(\frac{1}{4} |001\rangle\langle 010| + \frac{1}{2\sqrt{2}} |001\rangle\langle 100| + \frac{1}{4} |010\rangle\langle 001| + \frac{1}{2\sqrt{2}} |100\rangle\langle 001| \right). \end{aligned} \quad (3.96)$$

One may expect that as a result of dissipation of C $c_2(A, C)$ must be lowered, while $c_2(A, B)$ must remain constant; the finite causality must appear in all the other links. The results of all calculations are presented in **Figure 3.25** (except the link $A-B$, where all the parameters are constants: $c_2(A, B) \approx 5.30$,

$$S(AB) \approx 0.811, \quad i_{B|A} \approx -0.233, \quad i_{A|B} = 0, \quad N(A, B) = \frac{1}{4}.$$

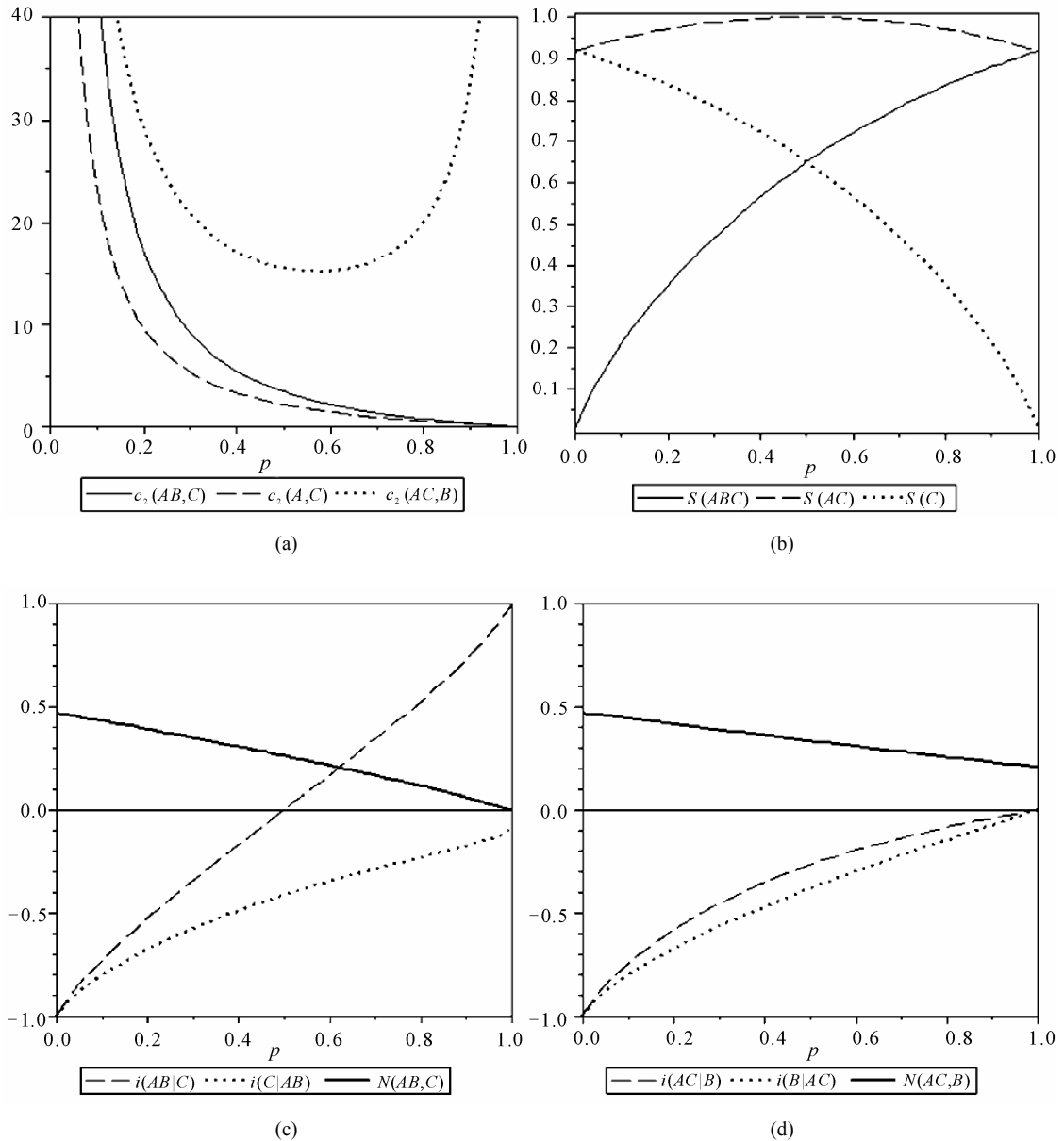


Figure 3.23. Dependence of c_2 (a), S (b), i and N (c, d) on degree of dissipation p of the particle C for the different partition of the states (3.95).

In **Figure 3.25(a)** it is seen that indeed $c_2(A,C)$ lowers from 5.30 as p increases and tends to 0 at $p \rightarrow 1$. $c_2(A,C)$ is minimal among the others at any p . Indeed, just in the link $A-C$ directionality of causal connection owing to original asymmetry and owing to dissipation is the same and resulting causality turns out the strongest. In the link $B-C$ causality is only due to dissipation and, accordingly, it is weaker: $c_2(B,C) > c_2(A,C)$ at any p . Next, in **Figure 3.25(a)** it is seen that causality in both the two-particle links $A-C$ and $B-C$ is stronger (c_2 is less) than in the three-particle links $AB-C$, $A-BC$ and $AC-B$. It is explained by the fact that mixedness of the formers is more—the both $S(AC)$ and $S(BC)$ are more than $S(ABC)$ (**Figure 3.25(b)**). It should be stressed that the rela-

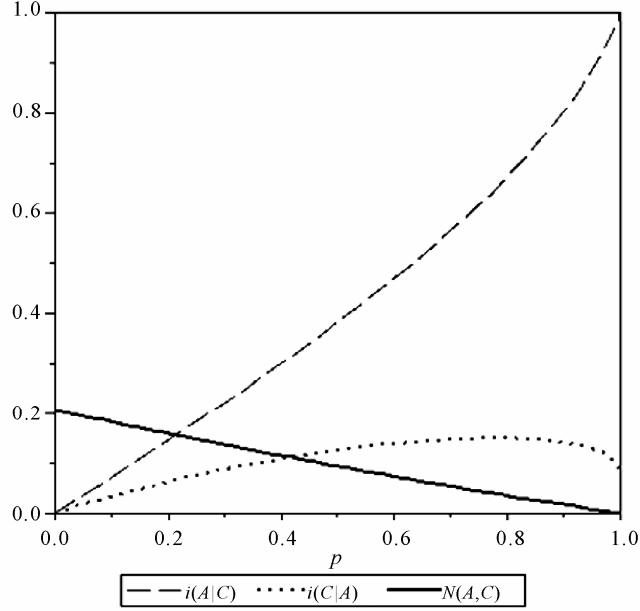


Figure 3.24. Dependence of i and N on degree of dissipation p of the particle C for reduced $\rho(AC)$ of the states (3.95).

tionship between causality and mixedness is only a tendency, but not a rule, e.g. $c_2(B, C)$ and $S(BC)$ both decrease as p increases.

A nontrivial result, as well as in the cases of GHZ and W-states, is that dissipated particle C can belong not only to the party-effect (in the partitions $AB-C$ and $A-BC$), but to the party-cause too (in the partition $AC-B$). At full dissipation ($p=1$) the particle C “disappears” from its two particle party and as a result $c_2(AC, B) = c_2(A, BC) = c_2(A, B) \approx 5.30$.

When **Figure 3.25(a)** is compared with **Figures 3.25(c)-(e)** it is apparent that for most of the partitions the stronger entanglement the weaker causality: $N(A, C) < N(AB, C) < N(AC, B) < N(A, BC)$ correspond to $c_2(A, C) < c_2(AB, C) < c_2(AC, B) < c_2(A, BC)$. But the partitions $A-B$ and $B-C$ do not obey this relationship. That is the relationship between causality and entanglement is only a tendency, but not a rule too.

In **Figure 3.25(f)** it is seen that in the link $B-C$ at any $p < 1$ the both i and N are positive. The subsystem BC is entangled in spite of the entropic classiness.

Now consider dissipation of the particle A :

$$\begin{aligned} \rho_{SKW}^{dissA} = & \frac{1}{4}(|001\rangle\langle 001| + |001\rangle\langle 010| + |010\rangle\langle 001| + |010\rangle\langle 010|) + \frac{1-p}{2}|100\rangle\langle 100| \\ & + \frac{p}{2}|000\rangle\langle 000| + \frac{1}{2}\sqrt{\frac{1-p}{2}}(|001\rangle\langle 100| + |010\rangle\langle 100| + |100\rangle\langle 001| + |100\rangle\langle 010|) \end{aligned} \quad (3.97)$$

One may expect that as a result of increasing dissipation of A , the original causal connection $A \rightarrow C$ will at the beginning attenuate until disappear at some p , after that direction of causality will reverse with further utmost amplification of the connection $C \rightarrow A$ as p will tend to 1. The finite causality must appear in all the other links, except $B-C$ because of its symmetry. The results of calculations are presented in **Figure 3.26**, except the link $B-C$, where all the parameters are constants:

$$c_2(A, B) \rightarrow \pm\infty, \quad S(BC) = 1, \quad i_{B|C} = i_{C|B} \approx 0.233, \quad N(B, C) = \frac{\sqrt{2}-1}{4} \quad (\text{the particles } B \text{ and } C \text{ are en-})$$

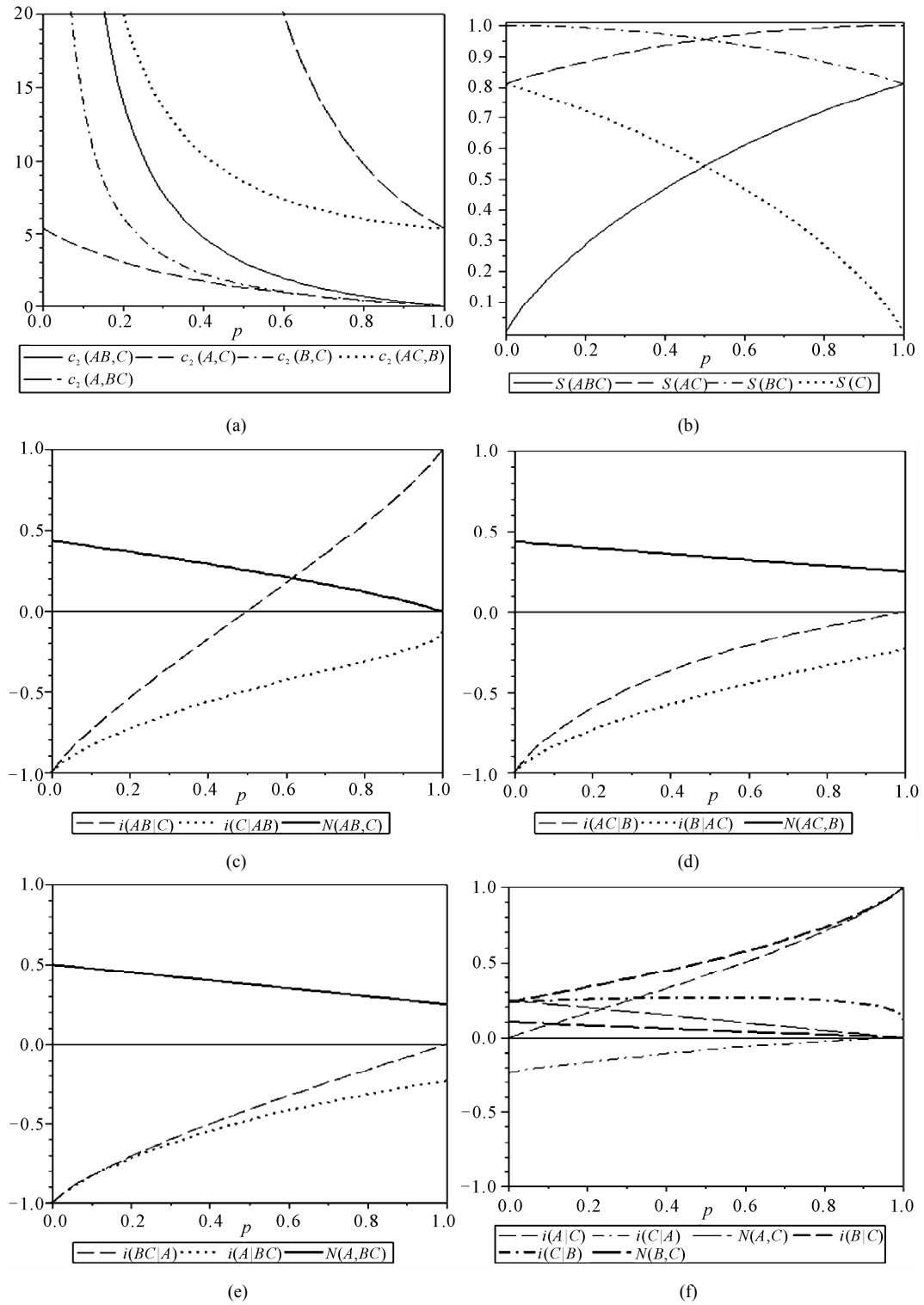


Figure 3.25. Dependence of c_2 (a), S (b), i and N (c, d, e, f) on degree of dissipation p of the particle C for the different partition of the states (3.96).

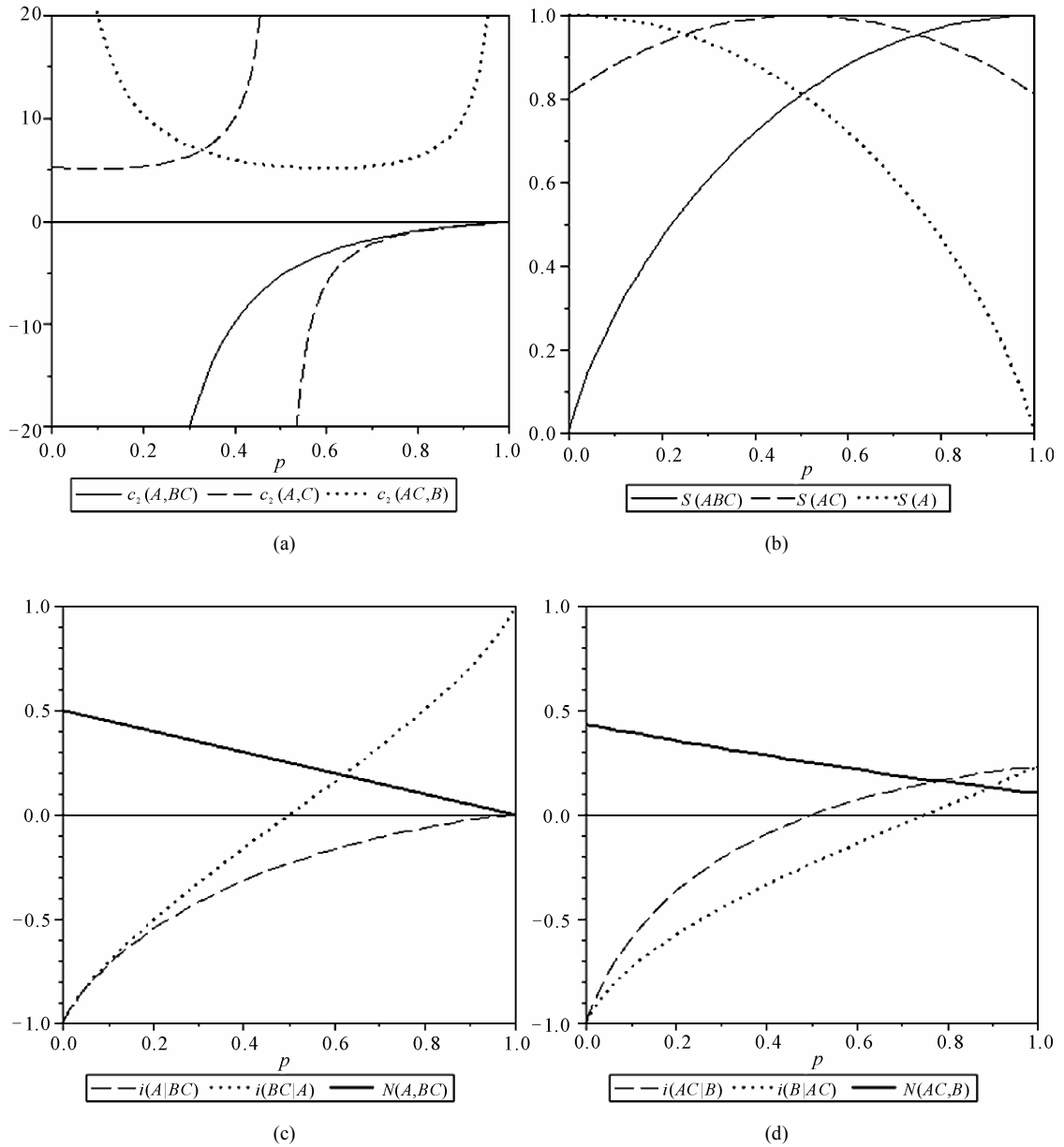


Figure 3.26. Dependence of c_2 (a), S (b), i and N (c, d) on degree of dissipation p of the particle A for the different partition of the states (3.97).

tangled and classically correlated due to availability of the common cause). The partition $AB-C$ is equivalent to the presented one $AC-B$.

In **Figure 3.26(a)** it is seen that indeed $c_2(A,C)$ changes its sign at $p = \frac{1}{2}$. But the variation of positive $c_2(A,C)$ (corresponding to directionality of the causal connection $A \rightarrow C$) proves to be not monotonous; it has the intuitively unexpected minimum equal to 5.08 at $p = 0.103$. The monotonous increase of negative $c_2(A,BC)$ simply reflects amplification of causality along with increase of dissipa-

tion of the effect A . The nontrivial behavior of causality in the link $AC-B$ is explained by the same way as in the GHZ and W examples. It is notable that $\min c_2(AC, B) = \min c_2(A, C)$. There is an interesting relation, which is valid not only in this example:

$$p(\min c_2(AC, B)) = 1 - p(|c_2(A, C)| = \infty) + p(\min c_2(A, C)).$$

There is no a relationship between different c_2 with the degree of mixedness (**Figure 3.26(b)**). There is only a relationship between $c_2(AC, B)$ and $c_2(A, BC)$ with the degree of entanglement (**Figure 3.26(c) and (d)**): at $p < \frac{1}{2}$ $N(AC, B) < N(BC, A)$ corresponds to $|c_2(AC, B)| < |c_2(A, BC)|$; at $p > \frac{1}{2}$ $N(AC, B) > N(BC, A)$ corresponds to $|c_2(AC, B)| > |c_2(A, BC)|$.

In **Figure 3.26(d)** it is seen that on the interval $\frac{3}{4} < p < 1$ the partition $AC-B$ is classically correlated (the both i are positive), but entangled. The same is observed in the subsystem AC (**Figure 3.27**), but on the wider interval $\frac{1}{4} < p < 1$.

A comparison between the cases $AB-C^{diss}$ and $BC-A^{diss}$ shows:

1) $|c_2(AB, C^{diss})| \rightarrow 0$ at $p \rightarrow 1$ quicker than $|c_2(A^{diss}, BC)|$. It reflects the influence of the original (at $p=0$) causality in the link $A-C$ (where A is the cause and C is the effect).

2) $S(A^{diss}BC)$ grows up more than $S(ABC^{diss})$ as p increases that is dissipation of the original cause enhances mixedness more than of the effect. Therefore opening of the system through the cause (information source) is more dramatic than through the effect (information sink).

3) $i_{A^{diss}|BC} \rightarrow 0$ at $p \rightarrow 1$ quicker than $i_{C^{diss}|AB}$. Therefore dissipation of the original cause quicker destroys quantum correlation than of the effect.

4) At $0 < p < \frac{3}{4}$ $N(AB, C^{diss}) < N(BC, A^{diss})$, but at $\frac{3}{4} < p < 1$ $N(AB, C^{diss}) > N(BC, A^{diss})$.

Therefore dissipation of the original cause destroys entanglement to a greater extent than of the effect.

3.4.4. Dissipated WRr-States

In Section 3.3.3 it has been found that in the WRr-state, similar to CKW state, the subsystems AB and AC are causal, a party A is a common cause for B and C , but quantitatively the causality is expressed stronger: $c_2(A, B) = c_2(A, C) \approx 3.43$ (the link $B-C$ is also causeless: $|c_2(B, C)| = \infty$).

Again at the beginning let the particle C is dissipated. Then the states are:

$$\begin{aligned} \rho_{WRr}^{dissC} = & \frac{1}{6}|010\rangle\langle 010| - \frac{1}{3}(|010\rangle\langle 100| + |100\rangle\langle 010| - 2|100\rangle\langle 100|) + \frac{1-p}{6}|001\rangle\langle 001| \\ & + \frac{1}{6}p|000\rangle\langle 000| + \frac{\sqrt{1-p}}{6}(|001\rangle\langle 010| - 2|001\rangle\langle 100| + |010\rangle\langle 001| - 2|100\rangle\langle 001|) \end{aligned} \quad (3.98)$$

The results of calculations are presented in **Figure 3.28** (except the link $A-B$, where all the parameters are constants: $c_2(A, B) \approx 3.43$, $S(AB) \approx 0.650$, $i_{B|A} \approx -0.413$, $i_{A|B} = 0$, $N(A, B) = \frac{\sqrt{17}-1}{12}$).

It is easy to see, that the states (3.98) qualitatively are similar to (3.96). The quantitative distinctions are stemmed from stronger causality in (3.98).

Then consider dissipation of the particle A :

$$\begin{aligned} \rho_{WRr}^{dissA} = & \frac{1}{6}(|001\rangle\langle 001| + |001\rangle\langle 010| + |010\rangle\langle 001| + |010\rangle\langle 010|) + \frac{2}{3}(1-p)|100\rangle\langle 100| \\ & + \frac{2}{3}p|000\rangle\langle 000| - \frac{1}{3}\sqrt{1-p}(|001\rangle\langle 100| + |010\rangle\langle 100| + |100\rangle\langle 001| + |100\rangle\langle 010|) \end{aligned} \quad (3.99)$$

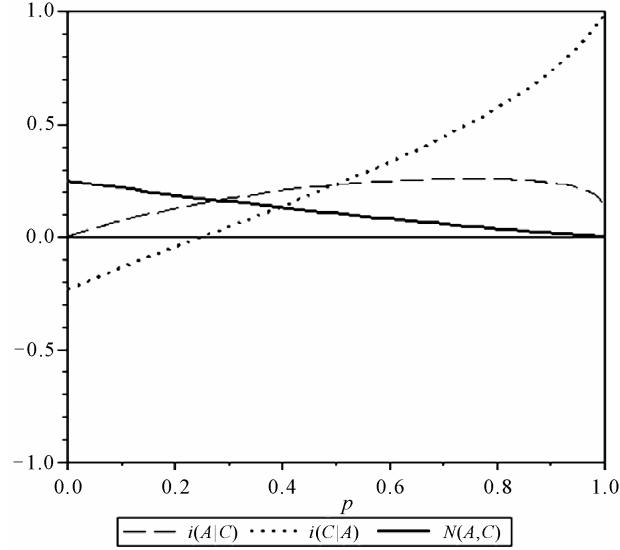


Figure 3.27. Dependence of i and N on degree of dissipation p of the particle A for reduced $\rho(AC)$ of the states (3.97).

The results of calculations are presented in **Figure 3.29** except the link $B-C$, where all the parameters are constants: $c_2(B,C) \rightarrow \pm\infty$, $S(BC) \approx 0.918$, $i_{B|C} = i_{C|B} \approx 0.412$, $N(B,C) = \frac{\sqrt{5}-2}{6}$, that is again particles B and C are entangled and classically correlated due to availability of the common cause. The partition $AB-C$ is equivalent to $AC-B$.

In contrast to dissipation of C , dissipation of A leads to a number of qualitative distinctions in **Figure 3.29** as compared to **Figure 3.26**. Contrary to all the above cases, the entropy of dissipated particle $S(A)$ does not decrease monotonously, but has a maximum at $p = \frac{1}{4}$, while mixedness of the whole system $S(ABC)$ does not increase monotonously, but has a maximum at $p = \frac{3}{4}$ (**Figure 3.29(b)**). Therewith $S(AC)$ is the same (with a maximum at $p = \frac{1}{2}$).

The causality set in **Figure 3.29(a)** notably differs from that in **Figure 3.26(a)**. $c_2(A,C)$ changes its sign at $p = \frac{3}{4}$, that is original pairwise causality in WRr-state is more robust than in CKW one.

$\min c_2(A,C) \approx 2.12$ is deeper and observed now at $p = 0.377$. In contrast to dissipated CKW state, $c_2(A,BC)$ changes its sign at $p = \frac{1}{2}$. At less p direction of causal connection is $A \rightarrow BC$, at higher p it is $A \leftarrow BC$. The minimum of $c_2(A,BC) \approx 15.2$ corresponding to $A \rightarrow BC$ is observed at $p = 0.288$. The curve of $c_2(AC,B)$ in **Figure 3.29(a)** is similar to that in **Figure 3.26(a)**, although $\min c_2(AC,B) \approx 1.97$ at $p = 0.627$ is not equal to $\min c_2(A,C)$ but their position also obey the relation: $p(\min c_2(AC,B)) = 1 - p(|c_2(A,C)| = \infty) + p(\min c_2(A,C))$.

The same relationship of $c_2(AC,B)$ and $c_2(A,BC)$ with the negativity is observed in **Figure 3.29(c)** and **(d)**: at $p < \frac{3}{4}$ $N(AC,B) < N(BC,A)$ corresponds to $|c_2(AC,B)| < |c_2(A,BC)|$; at $p > \frac{3}{4}$

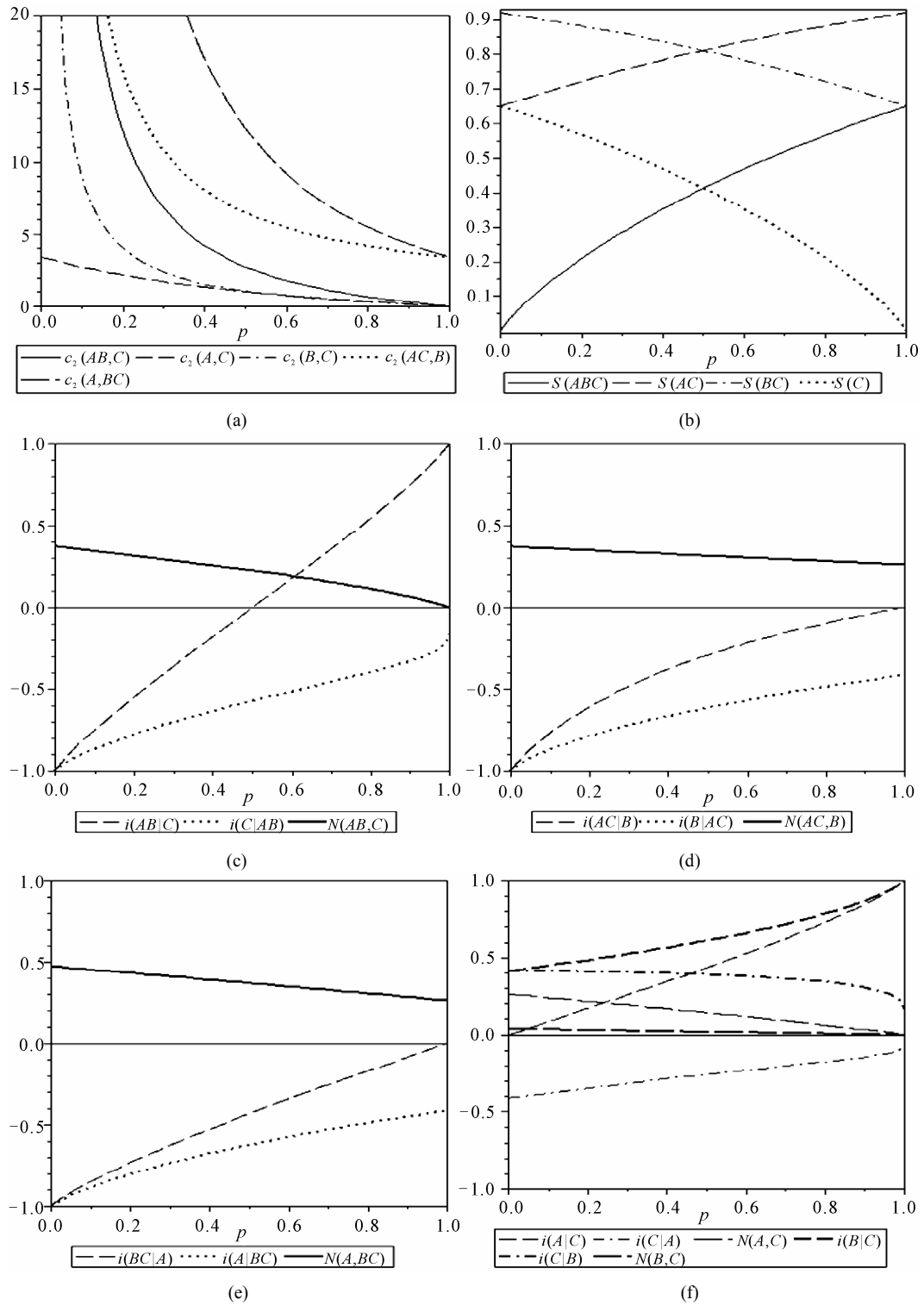


Figure 3.28. Dependence of c_2 (a), S (b), i and N (c, d) on degree of dissipation p of the particle C for the different partition of the states (3.98).

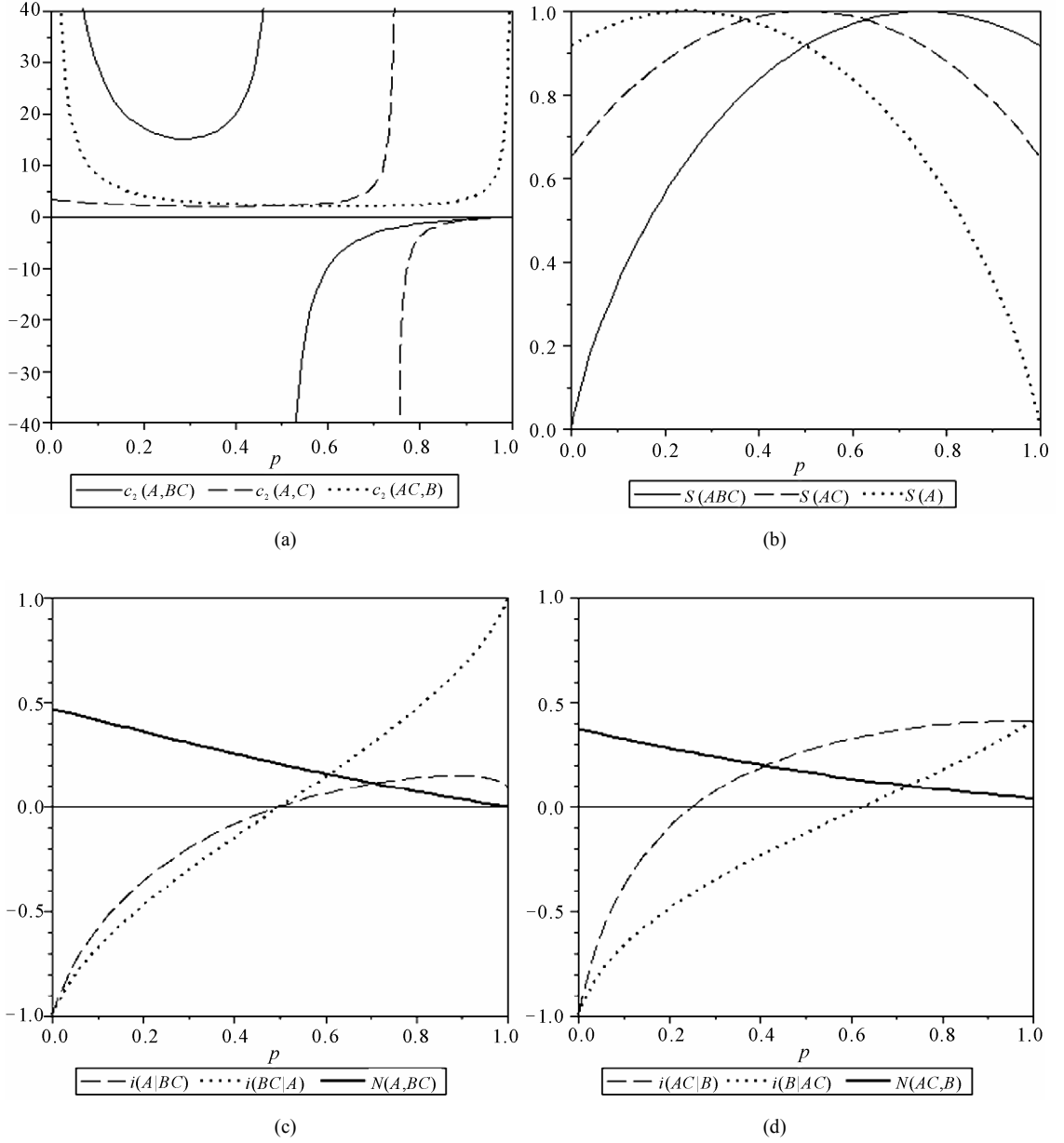


Figure 3.29. Dependence of c_2 (a), S (b), i and N (c, d) on degree of dissipation p of the particle A for the different partition of the states (3.99).

$N(AC, B) > N(BC, A)$ corresponds to $|c_2(AC, B)| > |c_2(A, BC)|$. Note, that the inversion points: $p = \frac{3}{4}$ in this case, and $p = \frac{1}{2}$ in the case of CKW state dissipation, exactly coincide with break points $c_2(A, C) \rightarrow \pm\infty$.

In **Figure 3.29(c)** it is seen that on the interval $\frac{1}{2} < p < 1$ the partition $A-BC$ is classically corre-

lated (the both i are positive, unlike **Figure 3.26(c)**), but entangled. The same is observed in **Figure 3.29(d)** at $p > 0.625$ for the partition $AC-B$. The subsystem AC (**Figure 3.30**) is classically correlated, but entangled, but on the wider interval $0.375 < p < 1$.

The conclusions (1)-(4) concerning dissipated CKW state remains true for WRr one (with less $p = 0.390$ in the quantitative justification of (4)) and obviously are general.

3.5. Overview of Causal Analysis

The classical causal analysis had formalized the intuitive understanding of causality that, first, gave the possibility of its application to the complicated system analysis and, second, gave a quantitative measure of causality. The quantum extension of causal analysis has shown a richer picture of the subsystem causal connections, where the usual intuitive approach is hampered more commonly. The direction of causal connection is determined by the direction of irreversible information flow, and the quantitative measure of this connection c_2 is determined as the velocity of such flow. The absence of causality corresponds to $|c_2| \rightarrow \infty$, accordingly the degree of causal connection is inversely related to c_2 . This formal definition of causality is valid at any time direction.

The independence functions used in the causal analysis allow classification of quantum and classical correlations of the subsystems, and their employment is of interest in any quantum systems, including those where causality is absent.

The possibilities of causal analysis have been demonstrated by the two series of examples of the two-partite two-state systems (qubits). The examples in both the series have been arranged in order from the simplest to the most nontrivial ones.

In the first series of the examples (Section 3.2) causality is absent; only the relationship between the independence function and the usual measures of entanglement and mixedness is revealed. It has been demonstrated that the independence function often but not always is determined by the state mixedness. Most important of all, in a number of cases the state can appear classical in entropic sense, but neverthe-

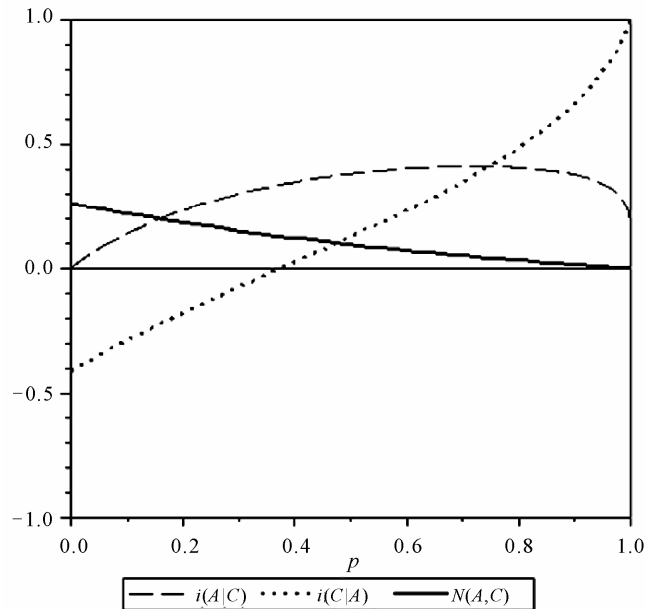


Figure 3.30. Dependence of i and N on degree of dissipation p of the particle A for reduced $\rho(AC)$ of the states (3.99).

less be entangled.

In the second series of the examples (Section 3.3) the systems with finite causality have been considered, beginning with the simplest example with asymmetric dissipation and ending with the enough complicated case of the qubits under a nonuniform external magnetic field at the different temperature. In every case the quantum measure of causality has been related with the classical one and it has been demonstrated that the latter often leads to apparent inversion of causal connection or meaninglessness. It has been shown the manner in which the distribution of entanglement in a three-partite system leads to the pairwise causal connection. For the case of asymmetric “quantum-classical” states the positive answer to the question, stated in Reference [59] about availability of an asymmetry in the transfer of quantum information with respect to its direction, has been obtained. For the case of qubits under an external magnetic field the conclusions about nonuniformity field control of directionality of the causal connection have been obtained, which can be physically explained by the causal analysis results, but which could not be drawn without them. It has been demonstrated that directionality of causal connection is unaffected by temperature, but its value is affected by temperature oppositely under the parallel and antiparallel fields.

In the third series of the examples (Section 3.4) the possibilities of causal analysis have been demonstrated by the series of examples of the three-qubit states. The examples have been arranged in order of increasing asymmetry. We could demonstrate the specific causal properties of the compound parties of the quantum systems. In the simplest cases the results of formal causal analysis correspond to the intuitively expected ones, but even at small complication of a quantum system the intuition fails. Thus its employment leads to the nontrivial conclusions about quantum information propagation.

In contrast to the classical case, a finite causality can exist only in the open systems, because a necessary condition of quantum causality is a finite mixedness. Correspondingly consideration of various causal links in the different states has shown that often (although not always) the greater mixedness the less c_2 . The mixedness of the asymmetric subsystems inside even closed quantum system leads to their original causal connection. In the case of asymmetric interaction of a system with the environment, e.g. by dissipation of one of the particles, causality emerges inside even originally symmetric causeless systems. In the originally causal systems the dissipation leads to nontrivial redistribution of the causal connections. Opening of the system through the cause (information source) leads to more mixedness of the state than through the effect (information sink). Dissipation of the original cause destroys quantum correlations and entanglement to a greater extent than of the effect.

In addition we have found that some states can be entangled but classically correlated. This fact is important for theoretical insight into the results of experiments on macroscopic entanglement of the dissipative systems described below.

Application of the causal analysis to the systems with the number of states more than two should present no problems in itself, except the usual build-up of calculation cumbersomeness of the density matrix eigenvalues.

Chapter 4

**Macroscopic Entanglement and Signals in
Reverse Time**

4. Macroscopic Entanglement and Signals in Reverse Time

The progress in quantum mechanics shed a new light on Kozyrev's results described in Chapter 1, Section 1.1 (statements (1)-(5)). His results obtained in the framework of causal mechanics concept, demonstrated phenomena very similar to macroscopic nonlocality (interpreted now in another terms). Next I shall consider Kozyrev's correlations of the dissipative processes, as macroscopic manifestation of quantum nonlocality.

Since its discovery phenomenon of quantum nonlocality has been attracting attention, above of all, in connection with apparent violation of relativity. Indeed quantum correlations occur through a spacelike interval. If it possible namely due to the absence of any local carriers of interaction. But it remains to be strange, because such correlations imply possible reversal of time ordering. The mainstream of quantum information research avoids this question, because from outset it had been realized that quantum nonlocal channel could transmit only *unknown* information. Therefore for the communication purposes one should use an ancillary classical channel. That is why this question became irrelevant.

In 1980 Cramer put forward an elegant transactional interpretation of quantum nonlocality leaned upon Wheeler-Feynman action-at-a-distance electrodynamics and its generalization on quantum amplitudes [16]. He conservatively pointed out that it was the only interpretation allowed to explain all basic quantum phenomena, but did not predict any new ones [62]. However his idea proved to be much richer. Cramer was the first who explicitly distinguished the principles of strong (local) and weak (nonlocal) causality. The latter implies a possibility of advanced correlations, but only related with unknown states, or in other terms with genuine fluctuating (random) processes. The weak causality admits the extraction of information from the future without the well known classical paradoxes. It allowed Elitzur and Dolev to suggest an experimental detection of time reversed causal events [63]. Another way of account of time reversed correlation has been suggested and experimentally verified as applied to quantum teleportation by Laforest *et al.* [64]. Although Cramer's works had some internal contradiction—the explanation of quantum phenomena on the base of classical Wheeler-Feynman theory, now the successive quantum version of action-at-a-distance theory has been developed [65].

In addition take notice to likeness of axioms of causal mechanics and action-at-a-distance electrodynamics. In this electrodynamics transaction of the charges separated by finite distance δx and lapse δt (with zero interval) is postulated. Self-action of the charges is absent. Two from three Kozyrev's axioms (there are $\delta x \neq 0$ and $\delta t \neq 0$ between any cause and effect) assert the same, replacing only terms "charges" by "cause" and "effect".

On the other hand, as it was generally believed that quantum nonlocality existed only at the micro-level, Cramer addressed the weak causality only to this level. However the idea about persistence of nonlocality in the macroscopic limit was recently put forward from different standpoints [66-70] and was realized experimentally [71-73]. The experimental results obtained by Kozyrev before the emergence of these ideas demonstrated phenomena very similar to macroscopic entanglement induced by dissipation and understood in terms of transactional interpretation.

Our idea was to include dissipation in the framework of Cramer interpretation of quantum nonlocality by Wheeler-Feynman action-at-a-distance electrodynamics. This theory considers the direct particle field as superposition of the retarded E^{ret} and advanced E^{adv} ones. The advanced field of a charge q is unobservable and manifests itself only via radiation damping [65]:

$$E^{adv} = E^{ret} - \frac{4e^2}{3qc^3} \ddot{x}. \quad (4.1)$$

On the other hand, radiation power is:

$$P = \frac{2}{3} \frac{e^2}{c^3} \langle \dot{x}^2 \rangle = -\frac{2}{3} \frac{e^2}{c^3} \langle \ddot{x}\dot{x} \rangle, \quad (4.2)$$

The entropy (dimensionless) production per a particle at temperature T is $\dot{S} = P/kT$, where k is Boltzman constant. Therefore, the third time derivative of position $\ddot{\ddot{x}}$ can be related via radiation power with the entropy production per particle:

$$\langle \ddot{\ddot{x}} \rangle = -\frac{3c^3}{2e^2} kT\dot{S}. \quad (4.3)$$

The radiation damping presents a typical dissipative process. Moreover, any dissipative processes is ultimately related with radiation, and therefore with the radiation damping. Hence it can be asserted from Equations (4.1)-(4.3) that advanced fields carry out the relationship between the dissipative processes.

Although a successive theory is absent yet, the following heuristic equation of macroscopic entanglement, describing factual Kozyrev's results) has been suggested by us:

$$\dot{S}_d = \sigma \int_x \dot{s} \delta \left(t^2 - \frac{x^2}{v^2} \right) dV, \quad (4.4)$$

where \dot{S}_d is the entropy production per particle in a probe process (that is a detector), \dot{s} is the density of total entropy production in the sources, the integral is taken over the source volume, σ is cross-section of transaction (it is of an atom order and goes to zero in the classical limit): $\sigma \approx \hbar^4/m_e^2 e^4$, m_e is the electron mass, e is the elementary charge. δ -function shows that transaction occurs with symmetrical retardation and advancement. The propagation velocity v for diffusion entanglement swapping can be very small. Accordingly, the retardation and advancement can be very large.

As this equation is heuristic, let us consider its correspondence with the particular but strict quantum-mechanical result developed for a dilute spin gas by Calsamiglia and coauthors [70]. They have obtained for partition of the system $A-B$ following equation for the entropy of entanglement between a part A and the rest of the system B :

$$S_A \approx \frac{N_A N_B}{N-1} r t (2 - \log_2 e), \quad (4.5)$$

where N is the number of particles, $N = N_A + N_B$, r is the collision rate.

For an adaptation of Equation (4.4) to the conditions of the model (4.5), consider the steady-state regime (integrate over time, neglecting the irrelevant integration constant). Then (4.4) reduces to:

$$S_d = \sigma \int \frac{s}{x^2} dV. \quad (4.6)$$

Consider the detector as a small part A of the large system. Correspondingly the source proves to be the part B . Then:

$$S_d = \frac{S_A}{N_A} = \sigma \frac{S_B}{L^2}, \quad (4.7)$$

where L is the space size of the system.

Now slightly transform (4.5), taking into account the assumption that the mean free path is compatible to the size of the enclosing volume [70]. That is $t = L/\langle v_r \rangle$, therefore $rt = \sigma Ln$, where $n = N/V$. On the other hand, $Ln \approx N/L^2$, $rt \approx \sigma N/L^2$. Assume $N \gg 1$. At last use \ln (not \log_2) in the entropy definition for further convenience. As a result we can rewrite (4.5):

$$\frac{S_A}{N_A} \approx \sigma \frac{0.3863 N_B}{L^2}. \quad (4.8)$$

We have the obvious correspondence between (4.7) and (4.8) with $S_B \approx 0.3863 N_B$. This correspondence encourages considering the equation of macroscopic entanglement (4.4) as at least a not too bad approximation of reality in terms of macroscopic correlations.

But it should be noted that our equation in its simplest form does not take into account the absorption by the intermediate medium. Its influence, however, is very peculiar. Although the equations of action-at-a-distance electrodynamics are time symmetrical, the fundamental time asymmetry is represented by an absorption efficiency asymmetry: the absorption of retarded field is perfect, while the absorption of advanced one must be imperfect. Indeed, having accepted that total field E is superposition of the retarded and advanced:

$$E = AE^{ret} + BE^{adv}, \quad (4.9)$$

it is possible [65] to express the constants A and B via corresponding absorption efficiencies a and b :

$$A = \frac{1-b}{2-a-b}, \quad B = \frac{1-a}{2-a-b}. \quad (4.10)$$

Since we observe only retarded field ($A=1, B=0$) then $a=1$, but $b \leq 1$. It should be stressed wide a priori arbitrariness in value b , which may be close as to unit so to zero. Therefore the screening properties of the matter must be in one degree or another attenuated. The fact itself of imperfect absorption of the advanced field means a possibility of its separate detection.

Thus observed time asymmetry emerges from absorption asymmetry: efficiency of absorption of the advanced field is less than (perfect) of the retarded one (although the theory does not predict how much less). Hoyle and Narlikar [65] have explained it by the cosmological reasons: the fact is only Steady-state and Quasi-steady-state cosmological models provide such asymmetry. But their proof itself did not refer to any cosmological conditions and could be applied, e.g. for a radiating charge in a cavity. Therefore absorption asymmetry reflects time asymmetry at more deep level in spirit of Kozyrev [1]. Observational consequence of the absorption asymmetry, if there is an intermediate medium, has to be prevailing advanced nonlocal correlation over retarded one.

Nonlocal nature of macroscopic correlations can be tested by two ways. They both are based on the causal analysis.

The first way is verification of violation of strong causality (3.4). Moreover, since we use only classical output of measuring device, we may employ γ instead of c_2 without limitations (in this we follow the accepted way of the use of Shannon entropies for proof of nonlocality [74,75]). That is the first way is violation of the inequalities (2.7) like this:

$$B \rightarrow A: \gamma > 1 \Rightarrow \tau < 0, \quad (4.11)$$

where τ is time shift of B relative to A (the arrow is symbol of direction of the causal connection). Violation of (4.11) means signaling in reverse time, which is sufficient condition of nonlocality.

Thus, calculating by experimental data $i_{A|B}$ and $i_{B|A}$ as the functions of time shift τ , it is possible, by their minima, to find optimal time shifts corresponding to connection of A and B . Then, by value of γ relative to 1, it is possible to establish the direction of the causal connection. In the case if B is known to be the cause (e.g. B is some measure of a source-process), while A is to be the effect (e.g. A is a detector signal), then for any classical interaction $\min i_{A|B}$ would observe only at $\tau < 0$, and this minimum would correspond to $\max \gamma > 1$. Only for nonlocal transaction of A and B it is possible $\gamma > 1$ at $\tau > 0$.

The second way is verification of the Bell-like inequality which is derived as follows. Suppose some process C acts upon a distant process A by means of any local interaction by the causal chain $C \rightarrow B \rightarrow A$. The intermediate process B is situated so that local carriers of interaction can not come A avoiding B (e.g. B occupies a spherical layer around A). Then the claim of locality in terms of conditional entropies is:

$$S(A|BC) = S(A|B). \quad (4.12)$$

Transform the left-hand side of this equation:

$$S(A|BC) = S(ABC) - S(BC) = S(AC) + S(B|AC) - S(C) - S(B|C) = S(A|C) + S(B|AC) - S(B|C)$$

Substituting the last expression into Equation (4.12), we obtain:

$$S(A|C) - S(A|B) = S(B|C) - S(B|AC) \quad (4.13)$$

As $S(B|C) - S(B|AC) \geq 0$, then $S(A|C) \geq S(A|B)$. Normalize on $S(A)$:

$$i_{A|C} = S(A|C)/S(A) \geq S(A|B)/S(A) = i_{A|B}. \quad (4.14)$$

Next, rearrange terms $i_{A|C}$ in Equation (4.13):

$$S(A|C) - S(B|C) = S(A|B) - S(B|AC). \quad (4.13a)$$

Transform the right-hand side of this equation:

$$S(A|B) - S(B|AC) = S(AB) - S(B) - S(ABC) + S(AC) = S(AB) + S(AC) - S(AC|B).$$

Since $S(AB) \geq 0$ and $S(AC) - S(AC|B) \geq 0$, then in the left-hand side of Equation (4.13a) $S(A|C) \geq S(B|C)$. By 7-th Shannon theorem [38] $S(A) \leq S(B)$, hence

$$i_{A|C} = S(A|C)/S(A) \geq S(B|C)/S(B) = i_{B|C}. \quad (4.15)$$

In Equations (4.14) and (4.15) bring to a Bell-like inequality; its violation is a sufficient condition of nonlocality of correlation A and C :

$$i_{A|C} \geq \max(i_{A|B}, i_{B|C}). \quad (4.16)$$

In the derivation, the quantum property of negativity of von Neumann conditional entropies has nowhere been used. It means that the derivation holds in terms of Shannon entropies as well, so the well known usual entropic Bell inequalities do [74,75]. Next, only the notion of locality but not of the hidden variables has been used. Similar to usual Bell inequalities, violation of (4.16) does not forbid existence of *nonlocal* hidden variables. A typical hidden nonlocal variable is advanced Wheeler-Feynman field and its generalization on the quantum amplitudes [16,62,65].

In spite of the above arguments, it may appear unusual that both the ways of verification of nonlocal nature of correlations, *i.e.* violation of (4.11) and (4.16), are leaned upon positive that is classical independence functions i . The strongest additional argument in favor of this is revealed on many examples of Chapter 3 availability of classically positive i for the entangled states as rather ordinary phenomenon.

Chapter 5

Experimental Approach

5. Experimental Approach

The experimental problem is to establish a correlation of the entropy changes in a probe-process and in the source-processes, according to the nonlocality Equation (4.4) under condition of suppression of all classical local impacts. As it is not possible to measure \dot{S}_d and \dot{s} in (4.4) directly, we have to evaluate for the concrete source and probe processes the theoretical expressions relating the entropies with the observables: $\dot{S}_d = F(P_d, \{p_d\})$, $\dot{s} = f(P_s, \{p_s\})$, where P_s is a measured parameter of the source-process, P_d is a measured parameter in the probe-process (detector signal), $\{p\}$ is set of other parameters of the processes, influencing on the entropy, which must be known unless they are stable.

Although any dissipative process may be used as the probe one, its choice is dictated by relative value of effect and theoretical distinctness, allowing to relate the measured macro-parameter (signal) with the left-hand side of Equation (4.4) and consciously to take steps on screening and/or control of all possible local impacts. From these reasons three types of detectors had been chosen: the first was based on the spontaneous variations of self-potentials of weakly polarized electrodes in an electrolyte, the second—on the spontaneous variations of dark current of the photomultiplier and the third—on the fluctuations of ion mobility in a small electrolyte volume (the latter was suggested and designed by Morozov [76]).

Consider theory of the electrode detector. The self-consistent solution for the potential u in the liquid phase is [76]:

$$u = \frac{2kT}{q} \ln \cos \left(z \arccos \exp \frac{q\zeta}{2kT} \right), \quad (5.1)$$

where q is ion charge, z is dimensionless length ($z=1$ corresponds to, half of the distance between the electrodes) and ζ is full (electrokinetic) potential. The entropy can be expressed in terms of the normalized potential Φ as:

$$\Phi = \frac{u}{\int_0^1 u dz}, \quad (5.2)$$

$$S = - \int_0^1 \Phi \ln \Phi dz. \quad (5.3)$$

After substituting Equation (5.1) into Equations (5.2) and (5.6) one may express the entropy in the elementary functions:

$$S \approx \ln 6 - 2 \ln(\arccos \exp w) + \frac{6 \left(\ln |w| w \arcsin \exp w - \exp w \ln w - \exp w + \ln |w| + w + \frac{w^2}{4} + 1 \right)}{(\arccos \exp w)^3}, \quad (5.4)$$

where

$$w = \frac{q\zeta}{2kT}, \quad (5.5)$$

and as signs of q and ζ are always opposite, $w < 0$. For weakly polarized electrodes it is easily attainable $|w| \ll 1$. Then Equation (5.4) is simplified:

$$S \approx \ln 6 - 2 \ln(\arccos \exp w). \quad (5.6)$$

Note if $w \rightarrow -0$, then $S \rightarrow +\infty$, that corresponds to expectative (space distribution aspires to uniform one). From Equation (5.6) the entropy production is

$$\dot{S} \approx \frac{\exp w}{\arccos \exp w \sqrt{1 - \exp 2w}} \dot{w}. \quad (5.7)$$

The prefactor before \dot{w} is always positive, therefore from Equations (5.5) and (5.7) it follows that correlation of S and ζ is negative. If $|\Delta\zeta/\zeta| \ll 1$, we can linearize Equation (5.7) and obtain simple practical formula:

$$\Delta S \approx -\frac{1}{\sqrt{6}} \frac{|q|}{k\theta} U, \quad (5.8)$$

where $U = \Delta\zeta$ is measurable variable potential difference.

All known local impacts, influencing U , namely, temperature, pressure, chemism, electric field, concentration and movement of the electrolyte, illumination and even cosmic ray variations must be excluded.

The detector based on weakly polarized electrodes has been constructed as follows. As the electrodes marine geophysical *C-Mn* ones were chosen in most of experiments (and *Ag-AgCl* in some of them) [77]. The electrodes were positioned in the glass vessel with the *NaCl* subsaturated water solution; separation between contact windows measured 1.5 cm. The vessel was rigidly encapsulated so that evaporation as well as atmospheric pressure variations were fully eliminated. The vessel was positioned in the Dewar, which in turn was into the thick-wall case. For small residual temperature variations control the sensor of temperature (allowing measuring it continuously accurate to 0.001 K) was positioned between internal wall of the Dewar and the electrode vessel. The quantity U was measured continuously (with time resolution 0.1 - 1^m) accurate to 0.5 μ V. In **Figure 5.1** the simplified sketch of the electrode detector is presented. Complicated internal design of the electrodes is not shown here. Detailed description of the electrode detector construction and design is presented in References [18,24].

The special investigation was dedicated to the problem of local temperature influence (which was the only noticeable noise-forming factor not completely suppressed by screening) and its mathematical exclusion [78]. As a whole the design of detector ensures elimination of the all local impacts, except cosmic ray variations. The special investigation [79] had revealed some retarded influence of these variations on detector signal, but it proved to be negligible as compared with nonlocal influence of other sources (to be discussed in Chapter 5).

The theory of the photomultiplier detector is simpler. We start from known formula of the entropy per electron:

$$S = \frac{q\varphi}{kT} + \frac{5}{2}, \quad (5.9)$$

where $q\varphi$ is the work function of the cathode. From Richardson-Dushman equation we have:

$$\frac{q\varphi}{kT} = \ln[A(1-R)] + 2 \ln T - \ln j, \quad (5.10)$$

where $A = mk^2 e/\pi^2 \hbar$, R is reflection coefficient, j is emission current density. Substituting Equation (5.10) into Equation (5.9) we derive the entropy production:

$$\dot{S} = -\frac{\dot{j}}{j} = -\frac{\dot{I}}{I}, \quad (5.11)$$

where I is the dark current. In small amplitude approximation we obtain the working formula relating the measured signal with left-hand side of nonlocality equation:

$$\Delta S = -\frac{\Delta I}{\langle I \rangle}. \quad (5.12)$$

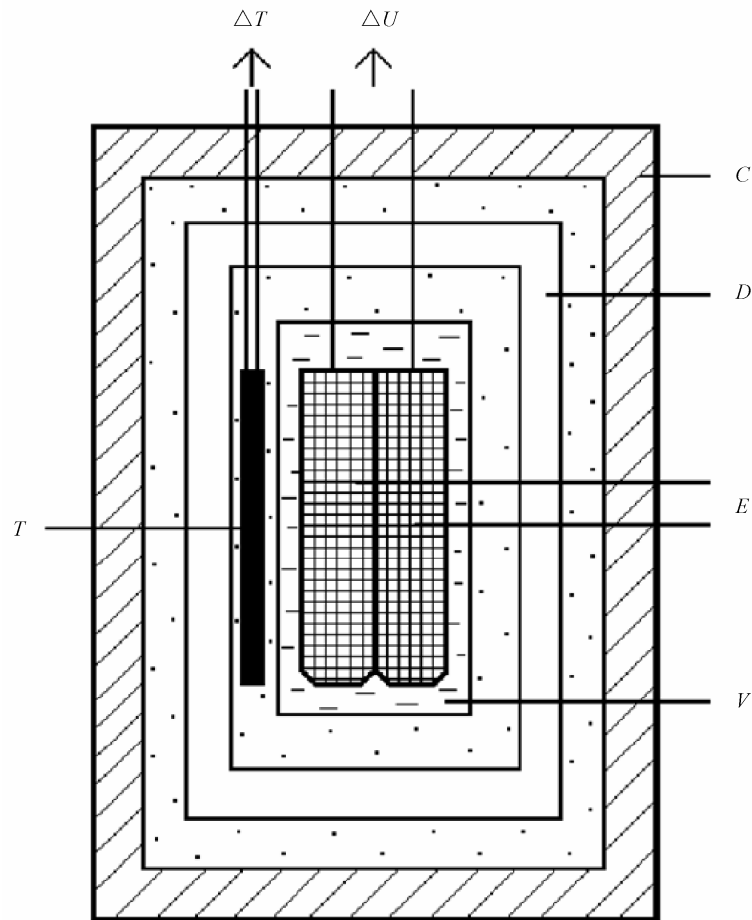


Figure 5.1. Simplified sketch of the electrode detector. *C*, case (thickness of the walls is 20 mm); *D*, Dewar; *V*, vessel with the electrolyte; *E*, electrodes (complicated internal design is not shown); *T*, temperature sensor. Materials: shade, caprolon; doubleshade, ebonite; dots, air; unshaded space, vacuum.

The noise-forming factors (local impacts) influencing on I to be excluded are: temperature, electric and magnetic field, illumination, moisture, feed voltage instability and cosmic ray variations.

The photomultiplier detector is constructed similarly to the electrode one on the base of photomultiplier with the *Cb-Cs* cathode of small area. The photomultiplier was positioned in the similar Dewar with its bleeder of dynode feed voltage and with the temperature sensor (allowing continuous measuring accurate to 0.001 K) and the additional external electric field screen. The simplified sketch of the detector is presented in **Figure 5.2**. The feed voltage was double stabilized accurate to 0.1%. The quantity I was measured continuously (with time resolution 0.1 - 1^m) accurate to 0.05 nA. Detailed description of the photomultiplier detector construction and design is presented in Reference [24].

Analogously to the electrode detector, only noticeable noise-forming factor not completely suppressed by screening was local temperature influence. Its influence has specially been investigated and the algorithm of its mathematical exclusion has been developed in Reference [78]. Next, a possible noise-forming factor could be the magnetic field variations, which therefore were measured by the quantum magnetometer. At last a possible influence of cosmic ray variations has specially been investigated [79] with the similar result as in the case of the electrode detector—this (retarded) influence turned out negligible as compared with nonlocal influence of other sources.

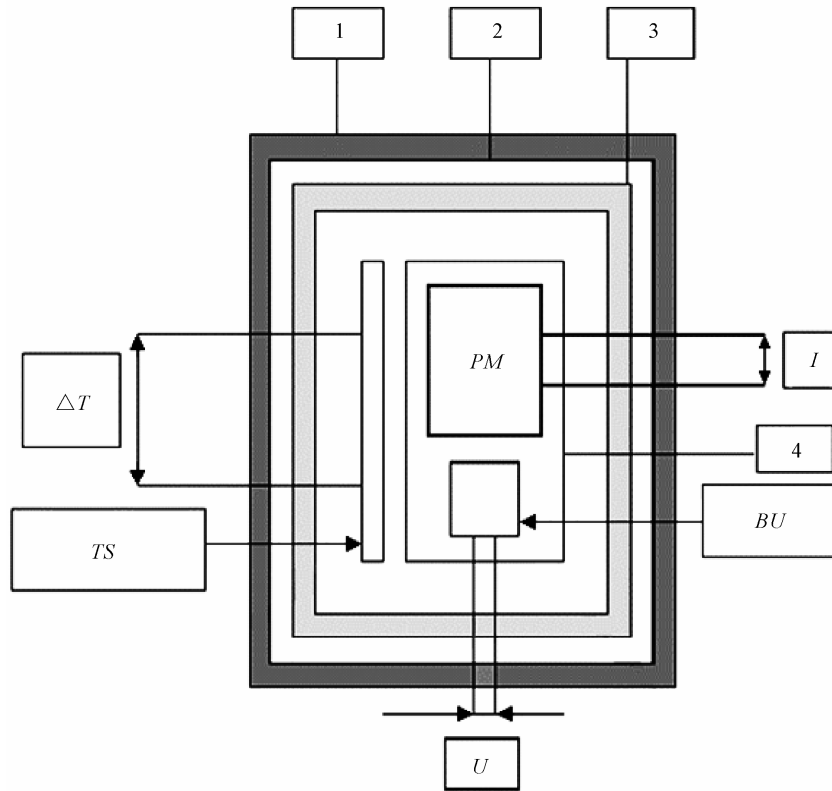


Figure 5.2. Simplified sketch of the photomultiplier detector. *PM*, photomultiplier; *BU*, bleeder of dynode feed voltage *U*; *TS*, temperature sensor; 1, external foam plastic case; 2, light screen; 3, Dewar; 4, electrostatic copper screen.

The theory of ion mobility detector is rather complicated [22], but the final formula is like (5.12):

$$\Delta S = -\frac{\Delta d}{\langle d \rangle}, \quad (5.13)$$

where the signal d in that case is electric current dispersion in the electrolyte cell.

The noise-forming factors influencing on d to be excluded are temperature, pressure, chemism and concentration of the electrolyte, electromagnetic field and feed voltage instability.

The ion mobility detector measures measuring fluctuation of conductivity (corresponding to fluctuation of ions mobility) in the hermetic electrolyte cell with stabilized and precisely measured temperature. These fluctuations were measured as high-frequency (5...15 kHz) voltage fluctuation on the cell under applied stabilized low-frequency (3 Hz) current. The dispersion d was computed over every 1^m time interval. The simplified sketch of this detector is presented in **Figure 5.3**. The steps taken to screening of the detector against the local influences were comparable with those of the electrode and photomultiplier ones. Detailed description of the ion mobility detector construction and design is presented in References [22,24].

Two experimental setups for study of macroscopic nonlocality had been constructed. The Geoelectromagnetic Research Centre (GEMRC) setup consists of the nearby *C-Mn* electrode and photomultiplier detectors, another (*Ag-AgCl*) electrode detector spaced at 300 m, and the apparatus for the local impacts control. The latter includes feed voltage, internal and external (lab) temperature and magnetic field. In addition hourly data on cosmic ray counting rate and atmospheric pressure were taken from spaced at 300 m

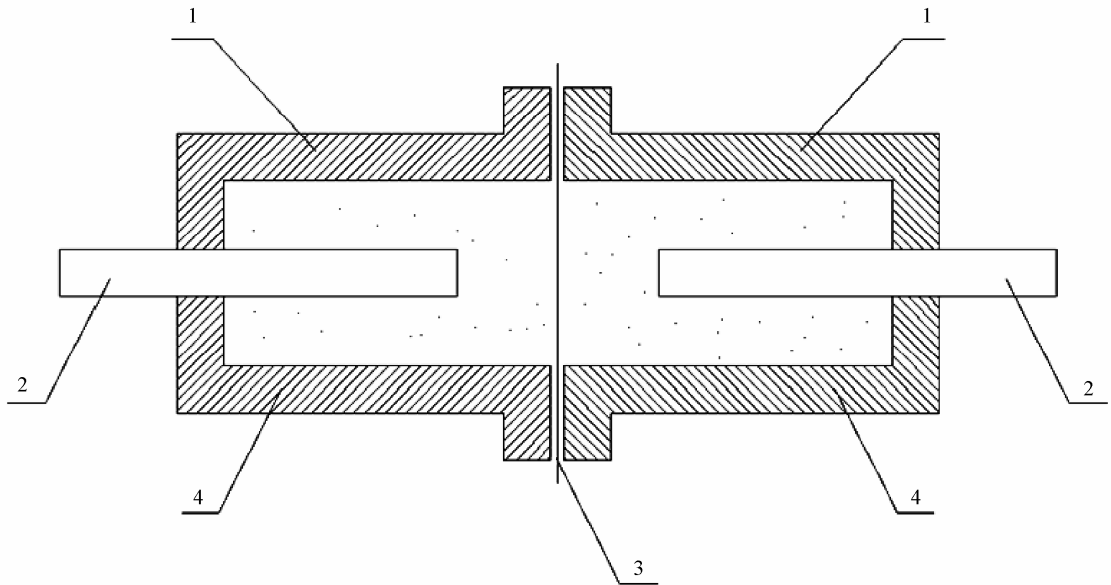


Figure 5.3. Simplified sketch of the ion mobility detector (by Morozov [22]). 1, plastic plug-and-socket case; 2, graphite electrodes; 3, thin film with small orifices; 4, electrolyte.

IZMIRAN neutron monitor. The Bauman Moscow State Technical University (BMSTU) setup created by A.N. Morozov is spaced at 40 km from the GEMRC one and includes two nearby ion mobility detectors and the accompanying apparatus, continuously measuring the lab and outdoor (atmospheric) temperature.

Remember that quantum nonlocality violates strong causality and obeys weak one. It means that if a source process is noncontrolled (random), we can observe both retarded and advanced correlations. But if an observer initiates a source-process, only retarded correlation is possible. That is why the most interesting source processes are random large-scale natural ones. Most of the experiments described in Chapter 6 were devoted to study detectors reaction on various geophysical and astrophysical processes with big random component. The experiments with controlled lab artificial source-processes had also been conducted, though they had, of course, demonstrated only retarded correlation.

Chapter 6

Results of the Experiments

Table of Contents

Nonlocality of the Controlled Dissipative Processes

Nonlocality of the Natural Dissipative Processes

6. Results of the Experiments

The experiments with natural source processes were long-term (with duration of continuous series not less than several months). They were conducted in 1993-1996 with the electrode detector (at this first stage without local impact control); in 1996-1997 with the all 3 detectors of the GEMRC setup (with full local impact control) and in 1997 with BMSTU setup; next after 2001 again with GEMRC and BMSTU setups. Except the detector signals the following parameters were measured: internal detectors temperature (residual variations strongly suppressed by thermostating system) accurate to 0.001 K, external (lab) temperature—0.1 K, outdoor (atmospheric) temperature—0.1 K and geomagnetic field —0.01 nT. Sampling rate was chosen from 1^m to 1^h . In addition hourly data on cosmic ray counting rate (as one more reasonable noise-factor) and atmospheric pressure (as index of nonlocal influence of synoptic activity) were taken from nearby IZMIRAN neutron monitor. Standard international data on the global geomagnetic (the *Dst* indices), ionospheric (the set of disturbance indices), and solar (the radio wave flux at 9 standard frequencies within range 245...154,000 MHz and also X-ray flux from GOES satellite) activity were taken to study the most large-scale processes.

Data were processed by the methods of causal, correlational, regressional and spectral analysis. The main point is calculation of conditional and marginal probability distributions of detector signals (X) and source processes indices (Y) by the time series. The Y series were taken with enough long “tails” before and after the X series ends to provide calculation of the distributions and their entropies in corresponding time shift range. Other processing methods were standard.

The experiments with controlled lab artificial source-processes were conducted in 1999, when we had wide experience of experimentation with natural source-processes. But logically they should be discussed first.

6.1. Nonlocality of the Controlled Dissipative Processes

6.1.1. Statement of the Problem

Although the experiments with artificial sources were conducted before [1,80-83], the level of their rigour was low, and in addition, the problem itself was badly formulated, therefore the entropy production in the source was not controlled. Our experiment aimed replenishment of this gap—measurement of the nonlocality effect of the artificial dissipative processes in the enough rigour setting.

On the basis of experience of the experiments with the natural sources described in the next sections we had selected the most appropriate electrode detector. The detector design excludes practically all the rinds of local impacts except the temperature variations, which can be essentially attenuated, but in principle cannot be eliminated completely. It restricts the source-process energy from above, because all the dissipative processes are accompanied by the temperature effect. On the other hand, this energy is restricted from below by the level of (nonlocal) noise inevitably taking place in the measuring device.

Within those limits nonlocal influence of an artificial source on the probe-process can, however, to be compatible with nonlocal influence of the geophysical processes. The influence of latter's is excluded by the differential scheme of measurement. Two spaced detectors are used; the source-process is placed near one of them at the distance small as compared with the space. The differential signal is measured.

The optimal energy of the source is near the upper bound of above mentioned range. Therefore in addition to thermo-insulation, the precise control of residual internal temperature difference is necessary.

It should be noted the principal limitation of the experiments with the artificial sources: due to principle of strong causality the advanced part of the signal is unobservable. For the random natural sources, as it is described in the reminder of this chapter, the advanced part is observed; moreover, owing to less efficiency of its screening by the intermediate media, it is essentially prevailed over the retarded one. Only for the advanced part the estimation of transaction cross-section has practically been gained. Therefore a

direct quantitative comparison of these two types of experiments for the present is hampered. The main purpose of the experiments with the artificial sources is verification of universality of the mechanism of nonlocal transaction and study of its statistical properties.

6.1.2. Experimental Setup

The setup scheme is presented in **Figure 6.1**. The source-process is sited at the distance $r = 0.5$ m from the detector measuring the difference of self-potentials U_1 , inside of which there is also a sensor of the internal temperature T_1 . The identical detector $U_2(T_2)$ is sited at distance $l = 4$ m. Subsequently the signals pass through the subtraction schemes $U_1 - U_2$, $T_1 - T_2$ and after amplification by the precision amplifiers A feed into the recorder ΔU and ΔT .

The processes of mixing, isobaric heating and phase transition-melting and evaporation were used as the dissipative source-process. The most effective proved to be (as one should have expected by ΔS value) the process of water boiling. There fore in the major series of experiments the following source was used: the glass vessel in which the water with initial volume 2 l was brought from exactly measured initial temperature (approximately equal to air temperature in the laboratory) by 1.2 kW heater to the boiling point. Boiling lasted up to evaporation of 1 l, after that the heater was turned off.

6.1.3. The Performance of the Experiment

The preliminary stage lasted about a year and included study of the inherent noise of the setup, choice of optimal measurement regime and testing of different variants of the sources.

The main stage of the experiment was carried out during three months (August-October 1999). A total of 50 experiments had been carried out. The main information was gained at the many times repeated experiment in the exactly same performance. The source-process was phase transition (water boiling), $r = 0.5$ m. After turning on the heater the water reached boiling-heat in 12 - 14 minutes (Depending on the lab temperature), boiling lasted 40 minutes. The elementary calculation gives the full entropy change in the source $\Delta S = 5.85 \cdot 10^{26}$ nat. Change of the lab temperature 10 K tells only in the third place of this value. The main part of ΔS contributes the entropy change in the phase transition water-vapour ($4.39 \cdot 10^{26}$ nat). Thus ΔS of the source was equal to the mentioned constant value for the all experiments.

In connection with long relaxation time it was possible to conduct correctly not more than one experi-

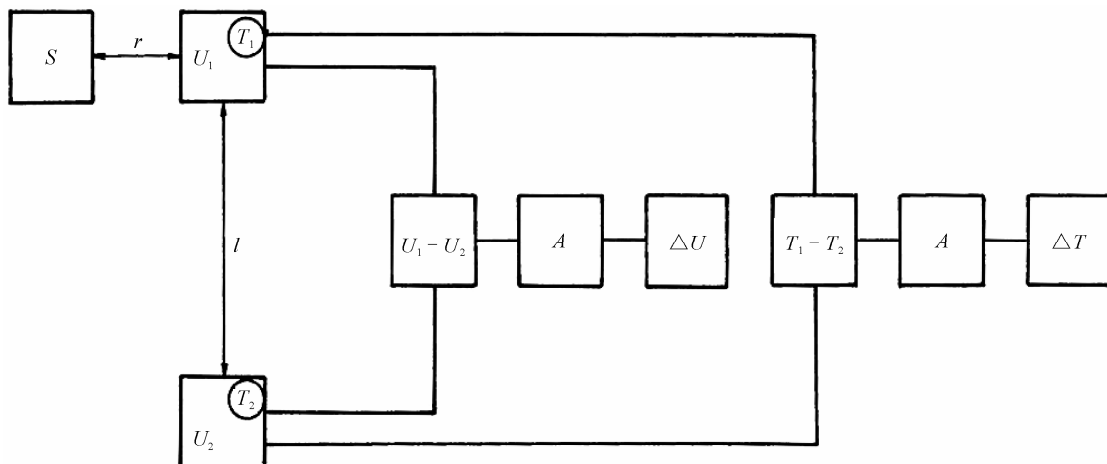


Figure 6.1. Scheme of the experimental setup. S , source-process; U_1 and U_2 , near and distant detectors; T_1 and T_2 , internal temperature sensors; $U_1 - U_2$ and $T_1 - T_2$, subtraction schemes; A , amplifiers; ΔU and ΔT , recorders; $r = 0.5$ m (1 m), distance from the source to the near detector, $l = 4$ m, distance between the detectors.

ment a day. From the beginning to the end of the series the lab temperature smoothly fell from $\sim 30^\circ\text{C}$ (the beginning of August) to $\sim 10^\circ\text{C}$ (the end of October). Space-heating and another heat sources were absent in the laboratory.

47 experiments were conducted at the fixed position of the source relative to both the detectors For 3 experiments the source was transferred to the other detector at $r = 0.5\text{ m}$ to make sure that it changes the sign of differential signal (at the same subtraction scheme).

In the periods between the experiments the measuring device of the setup worked in the continuous regime. It allowed avoid a possible influence of device warming-up at every experiment. In addition, the continuous record of ΔU allowed to be sure in essential exceeding of the effect of artificial process impact above the random noise.

6.1.4. Results and Discussion

According to Equation (4.4) an increase of the entropy in the source implies its increase in the probe-process (varying inversely with the square of the distance). In turn, from Equation (5.8) it corresponds to a decrease of ΔU . Thus from the theory it follows $\Delta S > 0 \Rightarrow \Delta U < 0$.

The main qualitative result of the experiment is that nonlocal response of the detector is reliably recorded and its sign corresponds to the theoretical prediction. The order of ΔU_m magnitude is a millivolt. The local heat impact of the source exists, but it is negligible as compared to the nonlocal one. The internal temperature of the near source detector increases, only of some thousandth of Kelvin. At known temperature coefficient of the electrodes (0.19 mV/K) it would correspond to ΔU change of order a microvolt that is the nonlocal signal stands out above the local one over three orders of magnitude.

Therewith the main surprise turned out very big quantitative scatter of the signal parameters under the strictly same conditions of the impact. The signal magnitude, retardation, time of drop and rise changed from one experiment to other over wide limits and these changes were not related with any changes of the external conditions (meteorological, geomagnetic, etc). The only change in the lab conditions was above mentioned smooth fall of the temperature from the beginning to the end of three-month series of the experiments. However the scatter of subsequently collected results had absolutely chaotic nature, the same at the beginning and at the end of the series. There was only some tendency to the rise of signal mean magnitude from August to October that corresponded Kozyrev result [1]. In spite of chaotic nature, the signal parameters proved to be related by the tolerant statistical regularities.

An example of the experiment registogram is shown in **Figure 6.2**. It is seen that $1^h 10^m$ later after shutdown of the heater the sharp decrease of ΔU occurs ($\Delta U_m = -5.5\text{ mV}$) and subsequently—many-hours relaxation to the starting level. The parallel ΔT record shows that beginning of the detector response approximately coincides with entry of the heat wave, but quantitatively the temperature change is negligible: $\Delta T = 0.008\text{ K}$. It would correspond to the decrease of ΔT owing to the classical local mechanism by 0.0011 mV which is incompatible few as compared to the measured signal. Relaxation time of the temperature disturbance ΔT , as it is seen in **Figure 6.2** is incompatible longer than relaxation time of ΔU . Coincidence of entrance time of thermodiffusion wave and beginning of the nonlocal response conforms to interpretation of Equation (4.4): nonlocal nature of the response is related with the diffusion entanglement swapping. In **Figure 6.2** the subtle detail is also contained, which was observed approximately in a half of the experiments—it is the small wave-like depression of ΔU before the beginning of the main drop. Nature of this precursor is unclear.

The mean, over the all experimental series, parameters of the signal are:

$\langle \Delta U_m \rangle = (-2.46 \pm 1.72)\text{ mV}$; retardation of the effect beginning relative to shutdown of the source
 $\langle \tau_1 \rangle = 97 \pm 36\text{ min}$; retardation of the minimum ΔU_m relative to shutdown of the source
 $\langle \tau_2 \rangle = 149 \pm 47\text{ min}$. Relaxation time constant is about 360 min . Time of the practical end of effect was determined the least exactly. Approximately mean time of redressing (from $\Delta U = \Delta U_m$ till the practical end of effect) proved to be $\langle t_2 \rangle \approx 8 \langle t_1 \rangle$, where t_1 is time of the drop ΔU ($t_1 = \tau_2 - \tau_1$).

Turn to description of the mentioned statistical regularities.

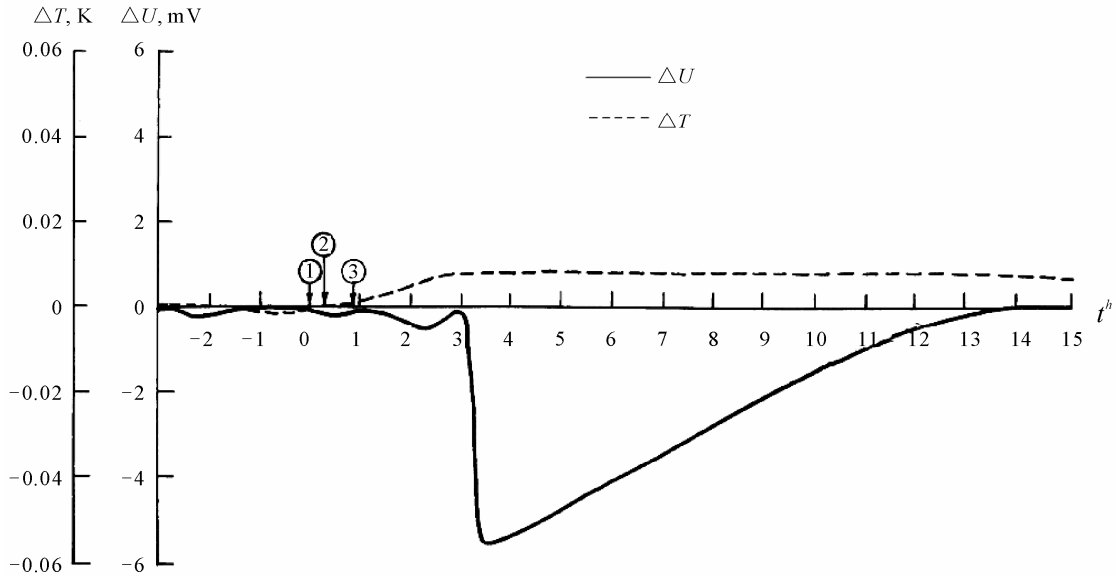


Figure 6.2. Example of the experiment record. ΔU , differential detector signal; ΔT , difference of the internal detector temperatures; t , time in hours; 1) instant of heater turning on; 2) instant of boiling beginning; 3) instant of heater turning off.

First, the curve of ΔU is essentially asymmetric. The equation of regression t_2 on t_1 (in minutes) is:

$$t_2 = 8.76t_1 - 126 \quad (6.1)$$

at correlation coefficient 0.91 ± 0.05 .

Second, this asymmetry is proportional to signal magnitude $|\Delta U_m|$ (in mV):

$$t_1/t_2 = -3.2\Delta U_m + 0.39 \quad (6.2)$$

at the same correlation coefficient.

Third, there is a nonlinear relation of full duration of the effect $t_e = t_1 + t_2$ with the signal magnitude:

$$t_e = t_s [\exp(-\Delta U_m/E) - 1], \quad (6.3)$$

where the empirical estimation $t_s = 40$ min, which is equal to duration of the main process – the phase transition in the source. The empirical estimation of the parameter E has shown that to the second place E is determined by the following combination of the factual detector parameters:

$$E = \frac{\sqrt{6kTg}}{|q|}, \quad (6.4)$$

where $q = 1.6 \cdot 10^{-19}$ A·s (univalent ions of the electrolyte), $T = 293$ K (mean detector temperature), $g = 0.013$ (variation coefficient ($g = \sigma(U)/U$) of given detector). From Equations (6.3), (6.4) and (5.8) it follows that full duration of the effect is determined only by duration of the impact and the double layer entropy:

$$t_e = t_s (\exp \Delta S_\alpha - 1). \quad (6.5)$$

Forth, akin to Equation (6.3), the empirical relation has been established between t_e and τ_2 :

$$t_e = t'_s \left((\exp \tau_2 / \vartheta) - 1 \right), \quad (6.6)$$

where $t'_s = 37$ min, $\vartheta = 49$ min. Comparison of Equations (6.6) and (6.3) shows that increase of the retardation τ_2 corresponds to increase of the magnitude $|\Delta U_m|$. Therefore disturbance of the equilibrium of detector is preceded by some process of the energy accumulation.

The most interesting is empirical relation (6.5). Rewriting it as follows:

$$\Delta S_d = \ln \left(\frac{t_e + t_s}{t_s} \right). \quad (6.7)$$

One can note that at $t_s \ll t_e$ the right-hand side of (6.7) equals $\sup S^1$ —the upper limit of the entropy defined in the first layer of the foliated space of probability operator definition [14]. In other words S^1 is the entropy defined by the normalized curve $\Delta U(t)$ considered as a probability distribution. So the equality

$$\Delta S_d = \sup S^1 \quad (6.8)$$

establishes the direct relation between space and time entropy changes—between redistribution of the charges in the double layer and time distribution of ΔU .

Thus in spite of the large scattering of the signal parameters in the identical experiments, these parameters are related by quite defined and important regularities.

The qualitative results of the experiment on measurement of the nonlocality effect of artificially exited dissipative processes confirm its universal nature and agree with theoretical view upon macroscopic entanglement.

6.2. Nonlocality of the Natural Dissipative Processes

6.2.1. Correlation of the Different Detector Signals

So in our experiments with natural source processes we had long-term measurements with 5 detectors of 3 types. Their signals proved to be rather high and synchronous correlated. For any pairs maximum of correlation function r achieves 0.7 - 0.8 at time shift $\tau = 0$.

Above all it had a meaning to compare our measurements of U (the main C-Mn electrode detector of GEMRC setup) with ones on the remote at 300 m U_r (additional Ag-AgCl electrode detector). It immediately allowed establishing, whether or not the variations of these quantities were merely the internal noises. The correlation coefficient turned out equal to 0.68 ± 0.01 . It is possible only one common trivial cause—the internal temperature. The partial correlation coefficient by eliminating influence of the internal temperature T_U of the detector U turned out equal to 0.74 ± 0.01 . Causality function γ proved to be exactly 1 that is the signals are formed by some common causes. But mathematical exclusion of the single possible common local impact not completely suppressed by screening, namely internal temperature, leads to correlation increase. Therefore local influence of the temperature is not a common cause of the correlated potential variations. Other non-suppressed local factors—the magnetic field and cosmic rays proved to be not influencing on the detectors within their sensitivity at all.

Level of correlation proved to be independent on type of detectors and on their separation within 40 km. In **Figure 6.3**, for example, the correlation function of the most spaced photomultiplier and ion mobility detectors is presented. Maximum of correlation corresponds exactly to zero time shift.

A fragment of synchronous 250-days signal records of the photomultiplier detector I , and ion mobility one d is shown in **Figure 6.4**. Again causality function proved to be exactly 1.

Such correlations can be explained by some large-scale common causes (geophysical or astrophysical processes), but their influence cannot be local. The correlations can be explained only in Cramer's spirit [16,62]: by exchange of the detectors and some large-scale common sources (geophysical or astrophysi-

Chapter 6. Results of the Experiments

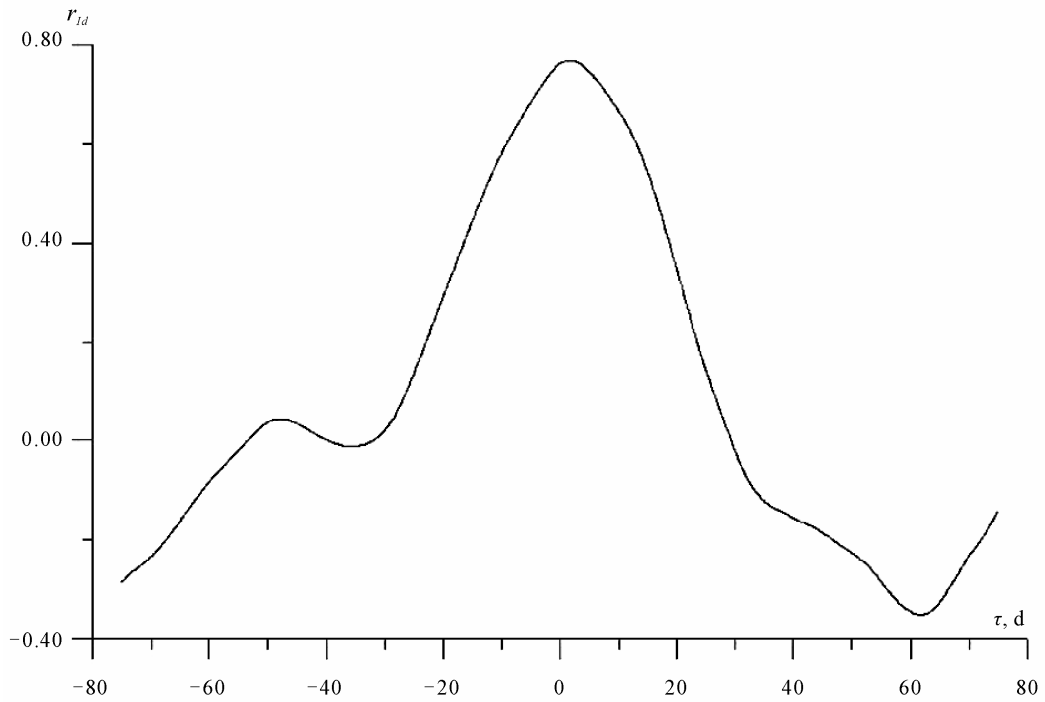


Figure 6.3. Correlation function of photomultiplier detector signal I and ion mobility one d . The τ is time shift in days. Maximum of correlation corresponds exactly τ . Data are low-pass filtered ($T > 20$ days).

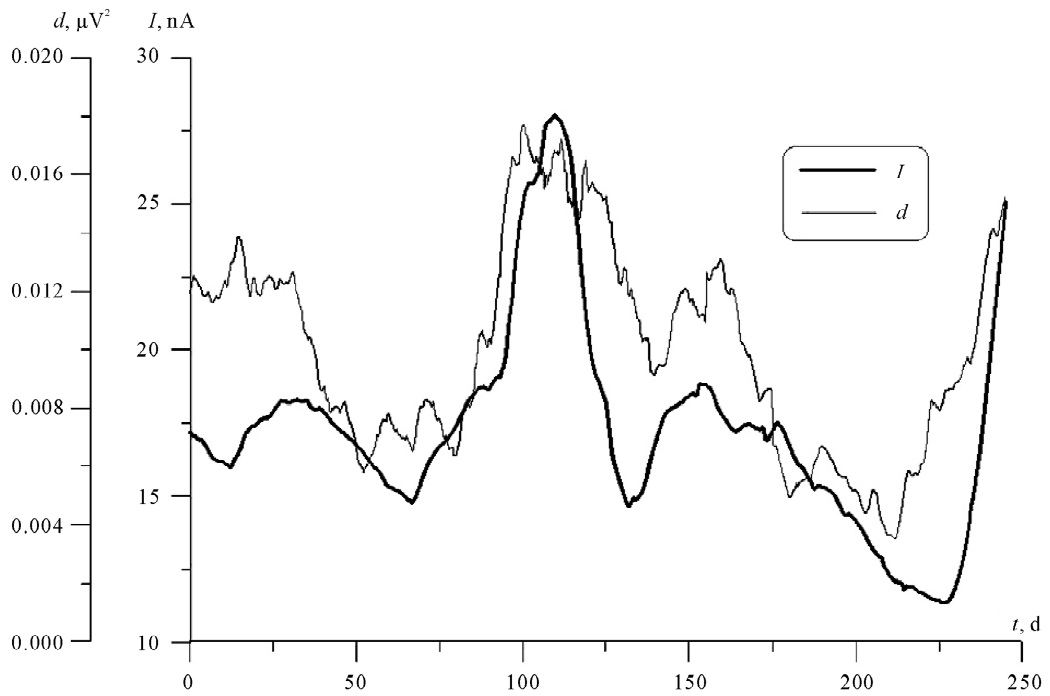


Figure 6.4. Synchronous time variations of photomultiplier detector signal I and ion mobility one d . The t is time in days.

cal processes) by the pairs of retarded and advanced signals, that is to be nonlocal.

6.2.2. Relation of the Detector Signals with the Internal and External Temperature

First of all, temperature variations of the environment lead to its entropy changes. The problem is complicated by trivial local influence of small residual variations of the internal temperature on the probe process. In **Figure 6.5** an example of correlation function of the electrode detector signal and its internal temperature is shown. Negative time shift τ corresponds to retardation of the signal relative to temperature, positive one – to advancement. Due to passive thermostating, dispersion of the internal temperature T_U in the Dewar of the detector U is very small (it is decreased on two orders relative to one of the external lab temperature T_e). Indeed, there is small retarded ($\tau = -20.4^h$) correlation peak $r_{UT_U} = -0.33 \pm 0.02$ (corresponding to the normal negative temperature coefficient of the electrodes $-(141 \pm 9) \text{ V/K}$ [77]). So, there is a small retarded correlation of trivial origin. But in positive τ domain, where correlation must be classically damped out, there is unusual big correlation maximum $r_{UT_U} = 0.87 \pm 0.01$ (anomaly positive sign) at advancement $\tau = 11.8^h$.

In **Figure 6.6** the same example in terms of the independence functions is shown. Just at the same time shifts there are two minima of the independence functions. The advanced minimum is deeper. More exactly $i_{U|T_U} = 0.50^{+0.02}_{-0.01}$ at $\tau = -20.4^h$ and $i_{U|T_U} = 0.43^{+0.01}_{-0.00}$ at $\tau = 12.8^h$ (the deviations of γ from 1 turned out insignificant).

For the short disturbances of U their advancement relative to T_U one can note without any processing, directly in the records (**Figure 6.7**).

Turn to connection between the detector signal and the random variations of external lab temperature (**Figure 6.8**). The independence functions have 3 minima at the shifts 0.0 and ± 27.0 hours. The advanced minimum is deepest and therefore can not be explained by any periodic effect. This picture corresponds to theoretical prediction: we observe symmetrical retardation and advancement, the advanced signal is stronger due to the less absorption by the intermediate medium. Availability of apparent synchronous minimum can be explained interference of the retarded and advanced signals. But is the connection nonlocal?

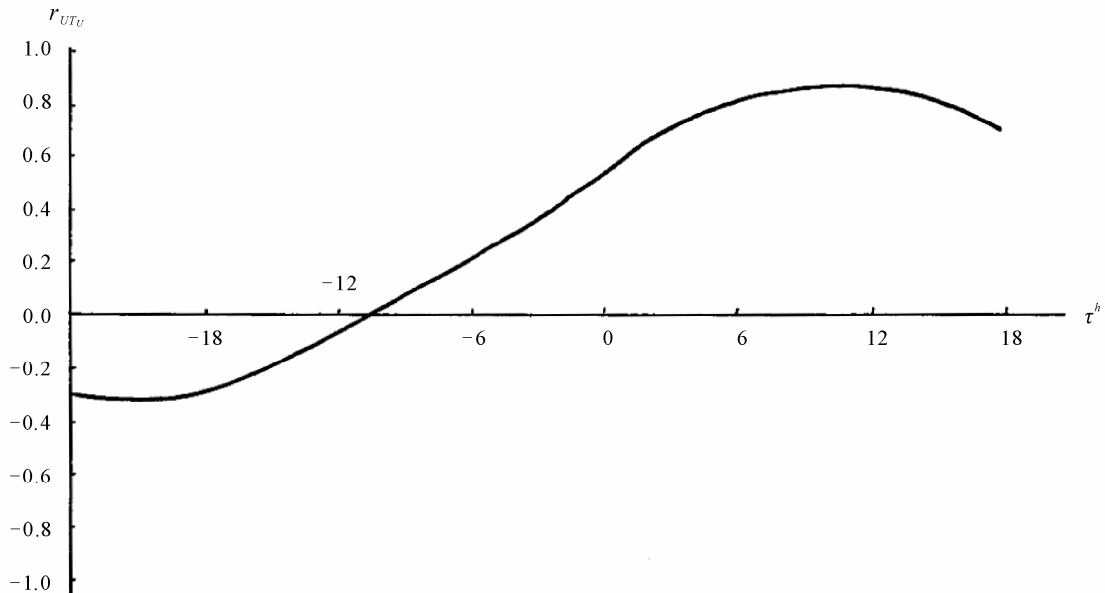


Figure 6.5. Correlation function of detector signal U and internal temperature T_U . τ Is time shift of T_U relative to U in hours.

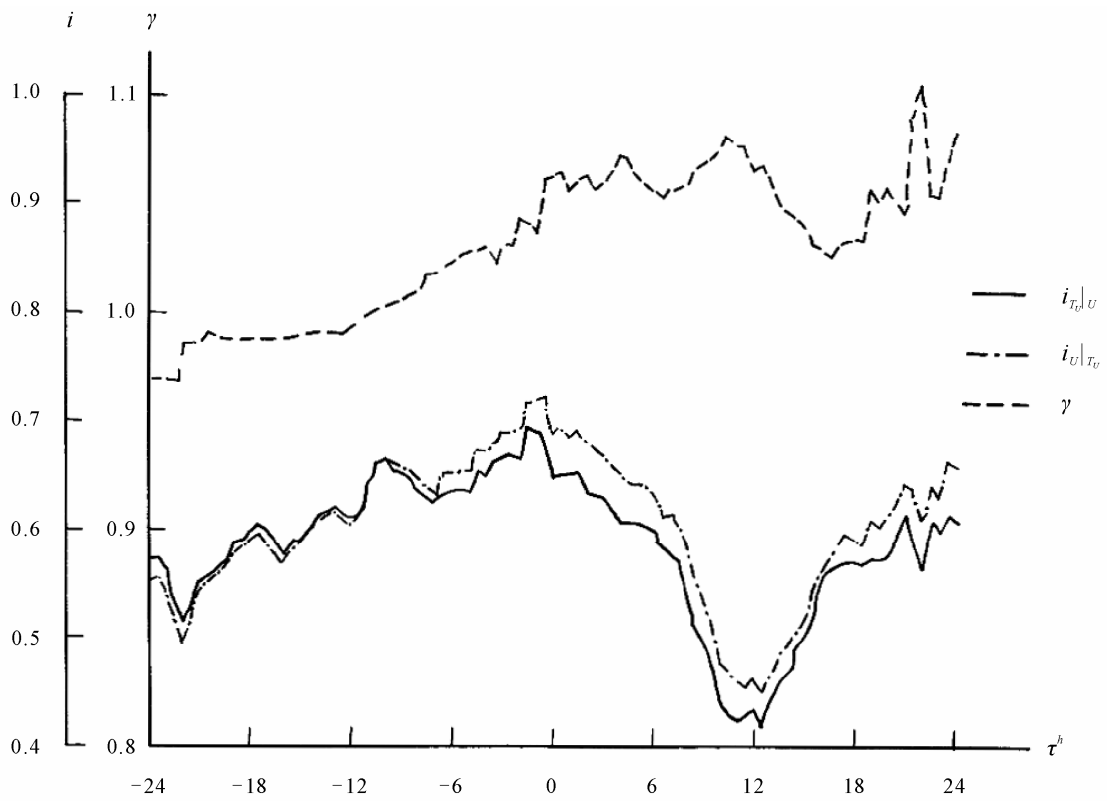


Figure 6.6. Independence functions of detector signal U and internal temperature T_U .

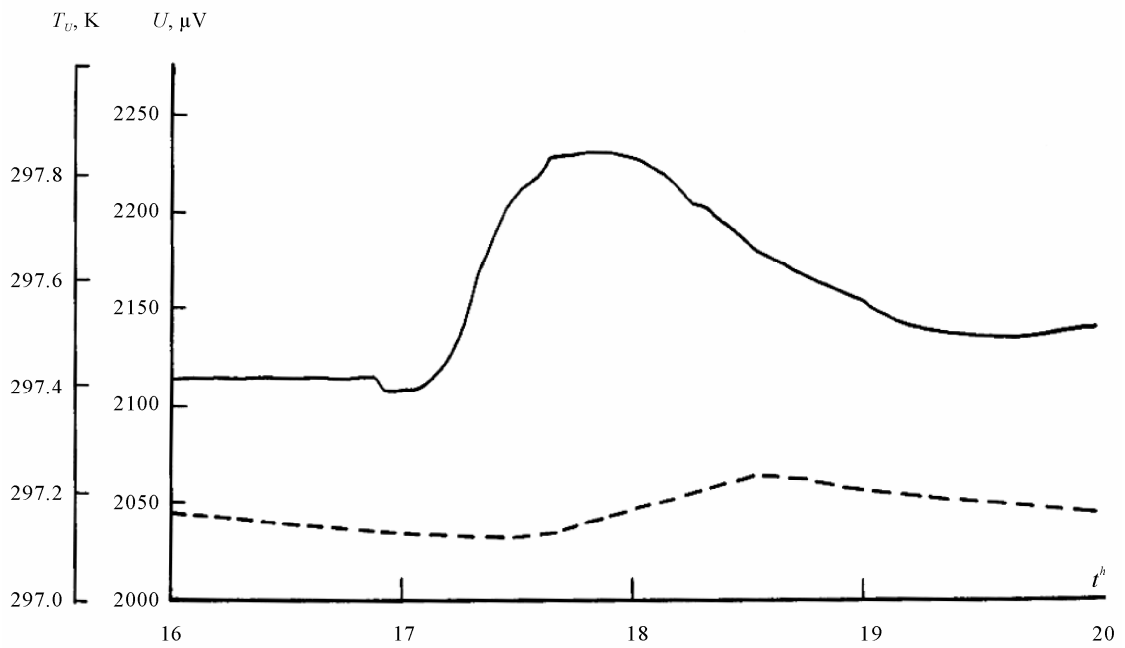


Figure 6.7. An example of synchronous records of the detector signal U and T_U .

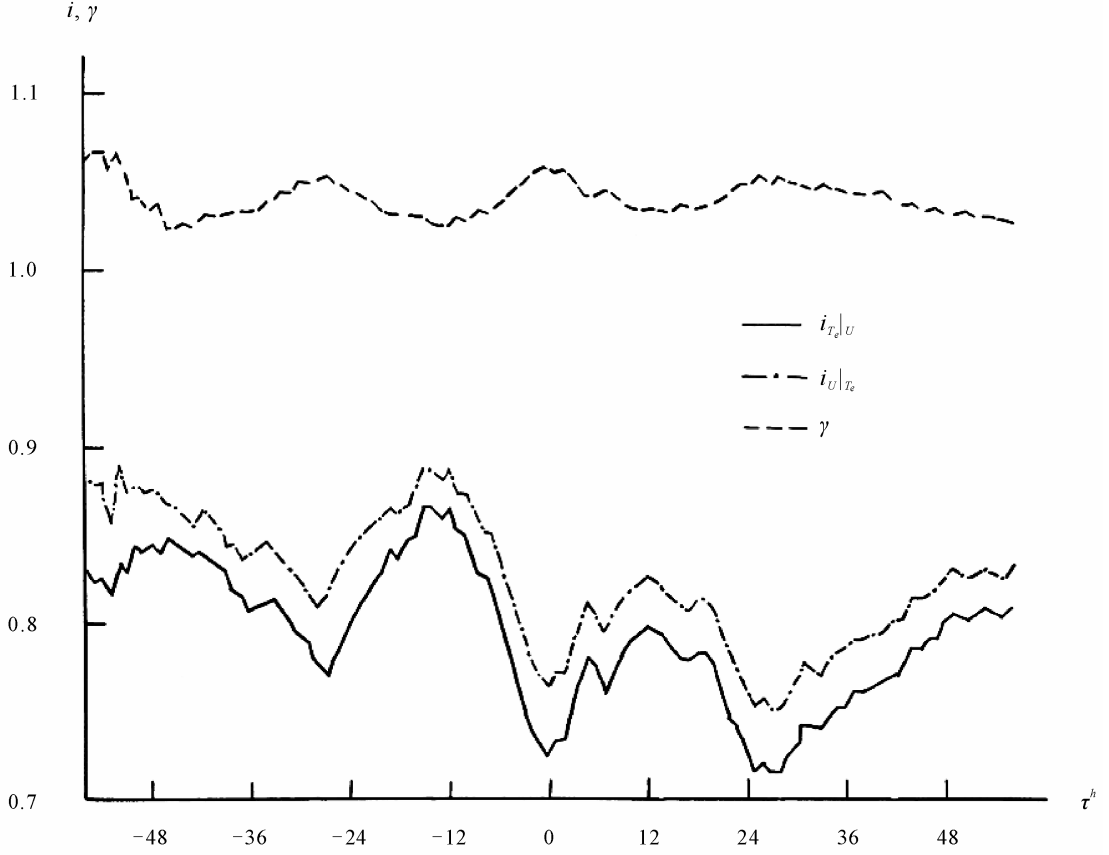


Figure 6.8. Independence functions of detector signal U and external lab temperature T_e .

The experimental values of independence functions are: at $\tau = -27.0^h$ $i_{U|T_e} = 0.81_{-0.00}^{+0.07}$, $i_{T_e|U} = 0.77_{-0.00}^{+0.10}$; at $\tau = 0.0^h$ $i_{U|T_e} = 0.77_{-0.00}^{+0.10}$, $i_{T_e|U} = 0.72_{-0.00}^{+0.13}$; at $\tau = 27.0^h$ $i_{U|T_e} = 0.75_{-0.00}^{+0.11}$, $i_{T_e|U} = 0.71_{-0.00}^{+0.12}$. Therewith independences of T_U and T_e have only single normal minimum: at $\tau = -11.5^h$ $i_{T_U|T_e} = 0.77_{-0.00}^{+0.03}$, $i_{T_e|T_U} = 0.84_{-0.00}^{+0.05}$, i.e. $T_e \rightarrow T_U$.

As there is no any heat source inside the detector, local connection of its signal with temperature works along the causal chain: $T_e \rightarrow T_U \rightarrow U$. According to Equation (4.16) sufficient condition of nonlocality is violation of such Bell-like inequalities:

$$i_{U|T_e} \geq \max(i_{T_U|T_e}, i_{U|T_U}), \quad i_{T_e|U} \geq \max(i_{T_e|T_U}, i_{T_U|U}), \quad (6.9)$$

Substituting the experimental values of independence functions, we conclude that there are two channels of connection between the external temperature and signal: classical local retarded channel and unusual nonlocal advanced channel. For the former at $\tau < 0$ left in Equation (6.9) is fulfilled, for the last at $\tau > 0$ right in Equation (6.9) is reliably violated.

But symmetry by τ for T_e, U with asymmetry for T_U, U calls for analysis. The space-time diagram of transaction of T_e, T_U, U is schematized in **Figure 6.9** τ^{ret} and τ^{adv} denote times of information passage along the retarded and advanced channel respectively, other notations are clear from the figure. T_e and T_U both are connected with U by pairs of the symmetrical retarded and advanced channels, while T_e is connected with T_U only by retarded one, it follows from geometry of this scheme that

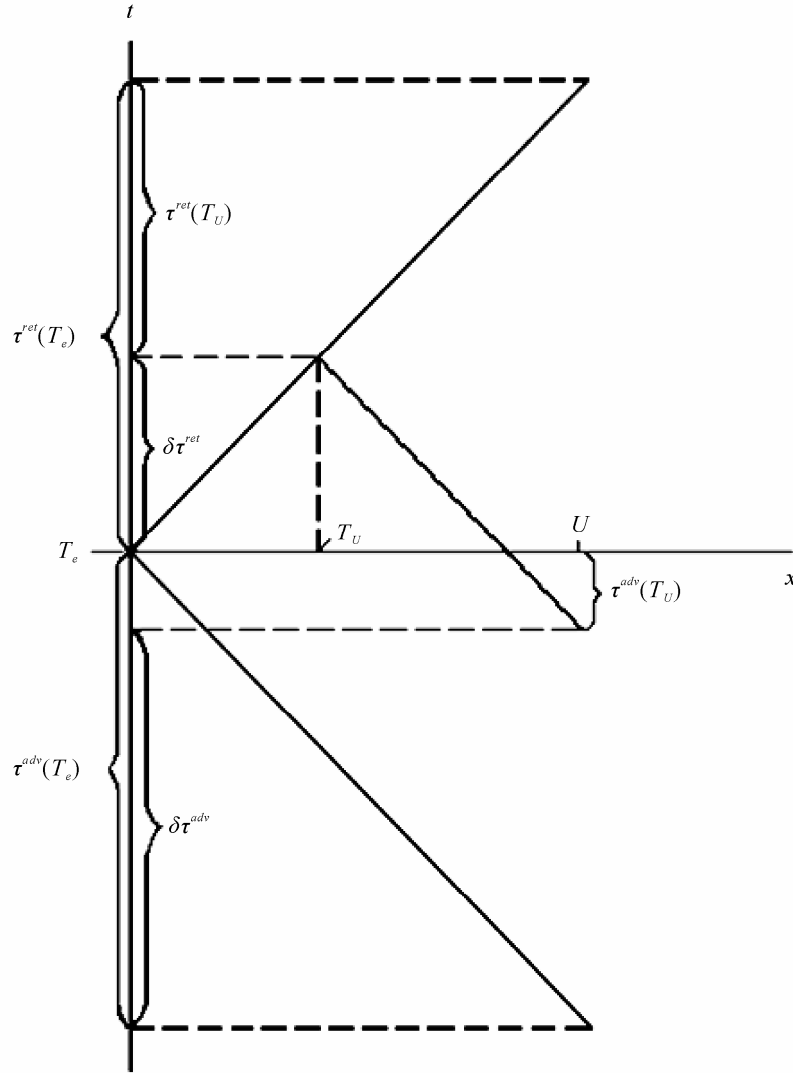


Figure 6.9. Diagram of transaction of the external (lab) temperature T_e , internal temperature T_U and self potential difference of the electrodes U . Scales of distance x and time t are arbitrary. The τ^{ret} and τ^{adv} are respectively retardation and advancement of the temperatures (T_U or T_e) relative to U . The $\delta\tau^{ret}$ and $\delta\tau^{adv}$ are differences of respective τ^{ret} and τ^{adv} .

$$\delta\tau^{adv} = \tau^{adv}(U|T_e) - \tau^{adv}(U|T_U) = \tau^{adv}(U|T_e) - [\tau^{ret}(U|T_U) - \tau^{ret}(T_U|T_e)]. \quad (6.10)$$

But $\tau^{ret}(T_U|T_e) = \tau^{ret}(U|T_e) - \tau^{ret}(U|T_U) = 2\delta\tau^{ret}$. Therefore $\delta\tau^{adv} = 2\delta\tau^{ret}$. Substituting mentioned above values of τ , one can be content with $\delta\tau^{adv} = 2\delta\tau^{ret}$ accurate to 7%. Therefore the diagram of **Figure 6.9** quantitatively explains the positions of all the peaks of independence functions.

Since there is some influence of T_e on the detector signal, and as mentioned in Section 6.2.1 the signals of different detectors are synchronously correlated, we should verify a possibility that that the lab temperature variations T_e is the trivial common cause of electrode U and photomultiplier I detector signal variations. The set of partial correlations: $r_{U|T_e} = 0.78 \pm 0.01$, $r_{U|T_e|I} = 0.24 \pm 0.02$, $r_{T_e|U} = 0.09 \pm 0.02$, in comparison with simple pair correlations: $r_{UI} = 0.75 \pm 0.01$, $r_{U|T_e} = 0.49 \pm 0.02$, $r_{T_e} = 0.45 \pm 0.02$,

clearly shows that T_e is not such a common cause. Another evidence is demonstrated in Reference [24] good similarity of the amplitude spectra of I and U , while the spectrum of T_e is quite different.

6.2.3. Relation of the Detector Signals with the Synoptic Activity

Consider now the variations of the atmospheric temperature T_a as an index of the synoptic activity. Taking into account passive thermostating, the local causal connection $T_a \rightarrow T_e \rightarrow T_U \rightarrow U$ must lead to weak correlation U with T_a at very long (many-days) retardation. Following usual geophysical practice of study of the large-scale processes, for exception of a possible influence of the small-scale inhomogeneities, compare measurements of U and T_a at the remote sites. Under a typical horizontal temperature scale (a few hundred km), distance between the GEMRC and BMSTU setups (40 km) is quite optimal. That is why the measurements of T_a near BMSTU setup have been taken for comparison with U .

The most important feature of U, T_a dependence proved to be a dramatic exceeding of correlation at advancement of U relatively T_a ($\tau > 0$) above weak (less than 0.4) retarded correlation ($\tau < 0$), as it is shown in **Figure 6.10**. Next there are five maxima r_{UT_a} at τ equal to $-25, -13, 0, 13, 28$ days. Symmetry relatively $\tau = 0$ is exactly analogously described above relation U with T_e . The greatest correlation is at $\tau = 13^d$: $r_{UT_a} = 0.725 \pm 0.005$. The causal analysis has shown corresponding minima of the independence function (at $\tau = 13^d$ $i_{U|T_a} = 0.72 \pm 0.01$, $\gamma = i_{T_a|U} / i_{U|T_a} = 1.02_{-0.00}^{+0.02}$, that is $T_a \rightarrow U$). Thus there is statistical reliable advanced connection of U with T_a .

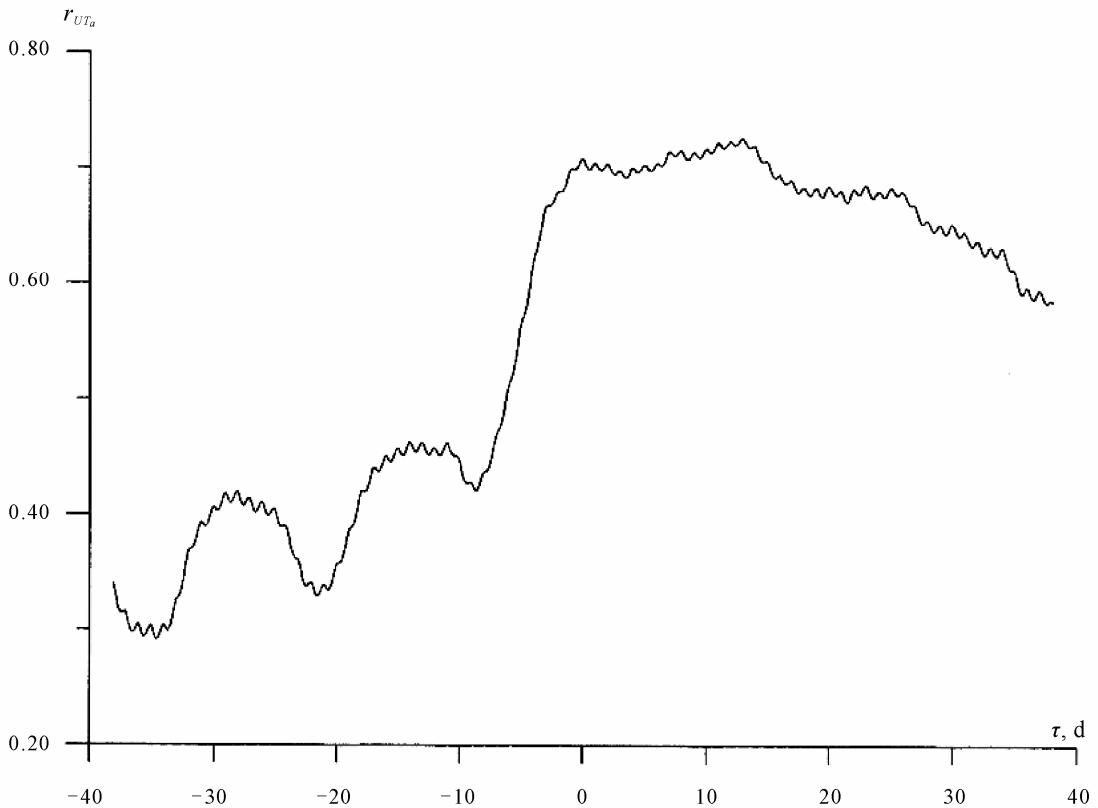


Figure 6.10. Correlation function of the detector signal U and atmospheric temperature T_a . The τ is time shift of T_a relative to U in days (negative τ corresponds to retardation of U relative to T_a , positive τ —to advancement).

Typical space scale of the temperature is a few hundred km. More appropriate synoptic activity index is the atmospheric pressure, which scale a few thousand km. In **Figure 6.11** an example of causal analysis of the electrode detector signal and pressure is shown. At advancement 69 days ($r_{UP} = -0.78 \pm 0.02$) there is the deepest independence function minimum and the highest causality function peak ($i_{U|P} \approx 0.30$, $\gamma = i_{P|U} / i_{U|P} \approx 2.3$). The synoptic activity is a cause of the detector signal, but they progress in reverse time!

For comparison the correlation function by the same data is presented in **Figure 6.12**. It is seen that on most part of the τ interval correlation is insignificant ($|r_{UP}| < 0.4$). There is a peak $r_{UP} = -0.78 \pm 0.02$ exactly at the same $\tau = 69^d$ as in **Figure 6.11**.

That result is independent on type of detector. In **Figure 6.13** the same example with the photomultiplier detector is shown. The picture is alike and advancement is almost the same, it equals 73 days. Corresponding correlation peak is $r_{UP} = -0.86 \pm 0.01$.

It is even possible to give the simplest forecast. In **Figure 6.14** fore the same example time variation of pressure (passing a cyclone) and preceding on 73 days variation of the dark current are shown.

6.2.4. Relation of the Detector Signals with the Geomagnetic Activity

It is beyond reason to consider electrode detector signal U depended on magnetic field B by any way. Therefore detection of relation of the potential with the Earth magnetic field variations would be a good test for the hypothesis (4.4), as these variations could be easy related with electric current dissipation in the source (magnetosphere). Special experiments on influence on the detector of U by the artificial magnetic field (up to $10^{-3} T$) in the frequency range from 0 to 1 Hz had confirmed absence of any response of U within sensitivity of the apparatus.

Analysis of the first long time series with the setup quantum modulus magnetometer (1996-1997) have shown existence of stable correlation $r_{UB} = -0.56 \pm 0.01$ with great advancement U relative to B

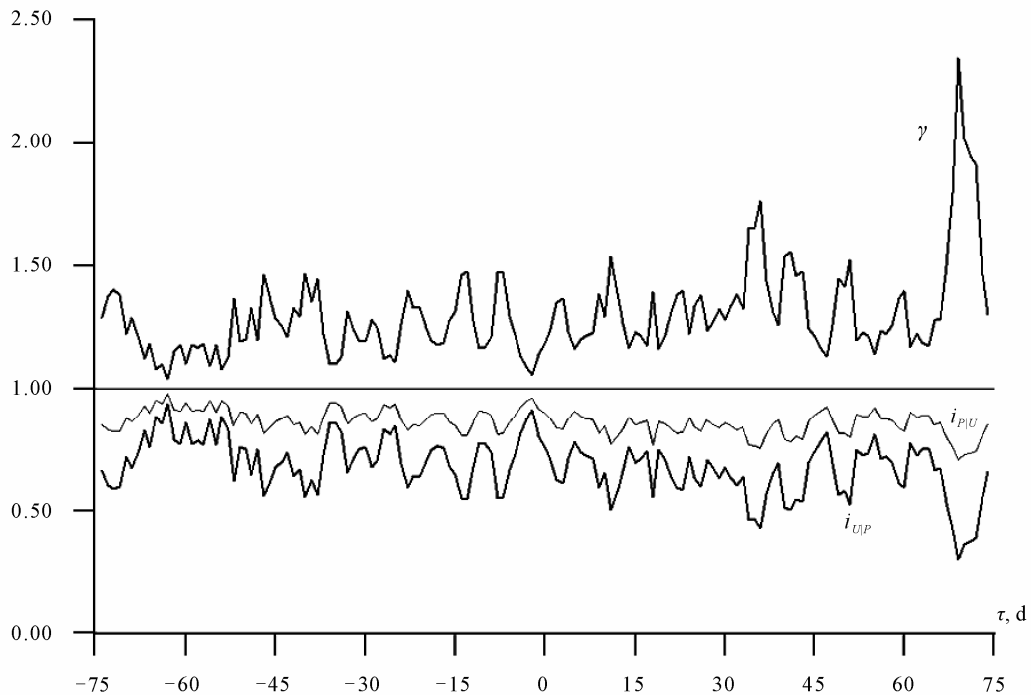


Figure 6.11. Independence i and causality γ functions of the electrode detector signal U (March-April, 1997) and the atmospheric pressure P . The τ is time shift of P relative to U in days.

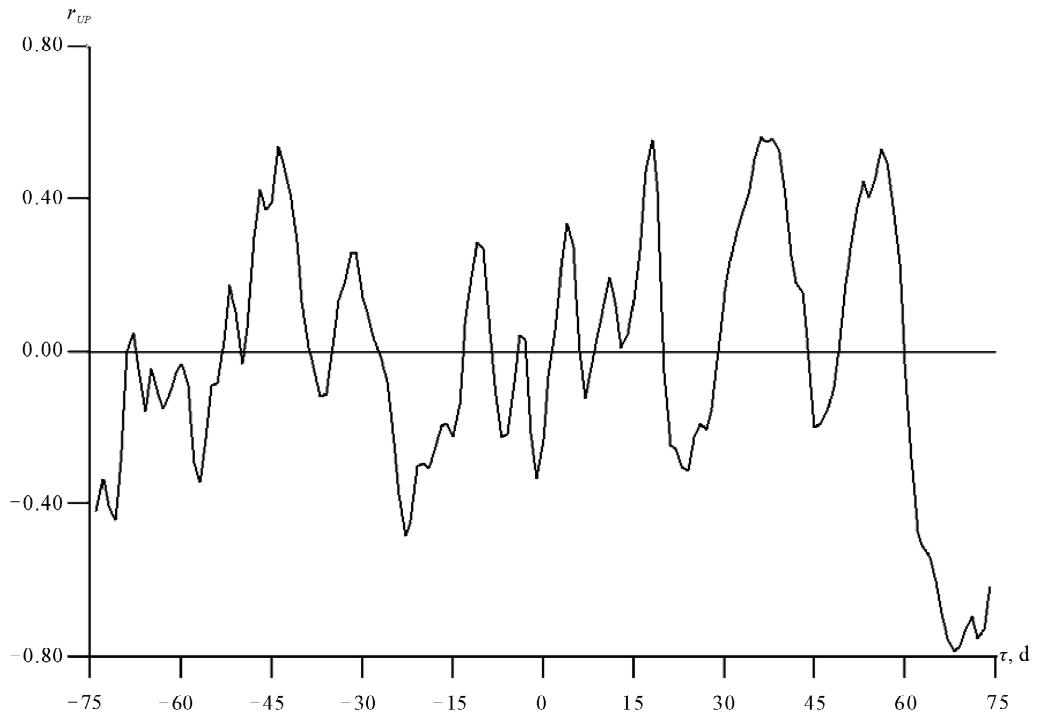


Figure 6.12. Correlation function corresponding to Figure 6.11.

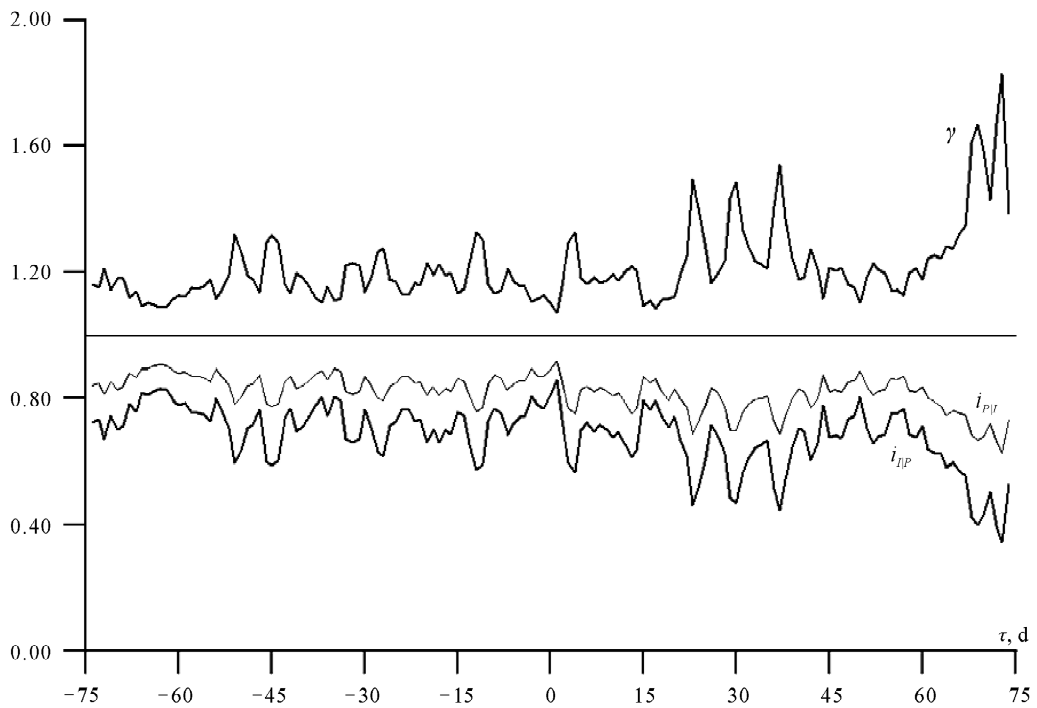


Figure 6.13. Independence i and causality γ functions of the photomultiplier detector signal I (March-April, 1997) and the atmospheric pressure P . The τ is time shift of P relative to I in days.

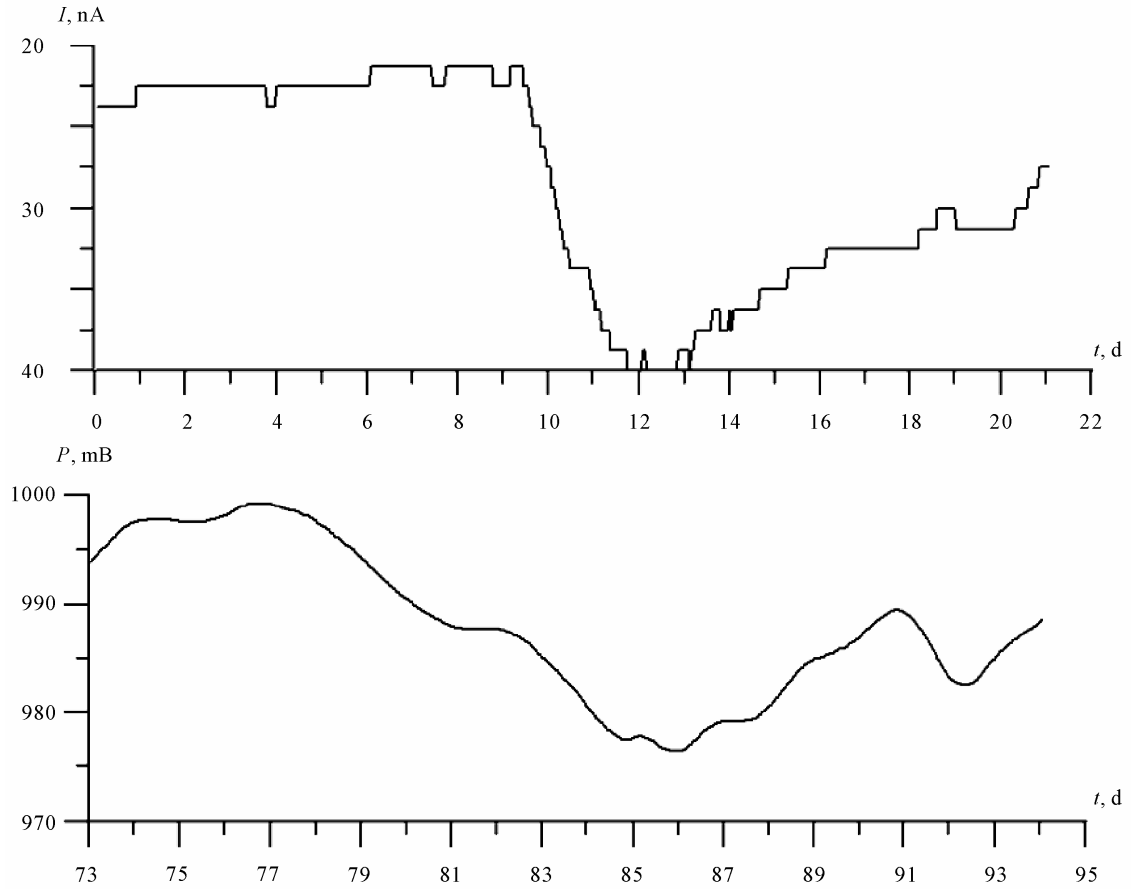


Figure 6.14. The variation of the detector signal I forecasting variation of atmospheric pressure P with advancement 73 days. The origin of time corresponds to March 24, 1997.

($\tau = 48.5^h$) (**Figure 6.15**). In the causal analysis at this τ there is minimum $i_{B|U} = 0.79_{-0.01}^{+0.02}$, γ differs from 1 insignificantly. Thus relation U and B is statistically reliable, but both from prior reasons and from advancement U relative to B it can not be result of a local influence B on U . Therefore B is an indicator of some process interacting with U .

The obtained two-day advancement is close to time of the solar wind propagation and therefore this could suggest that self-potentials correlate more likely with the wave component of the solar activity than with the geomagnetic variations. But in the next I shall demonstrate that advancement of correlation with the solar activity is far more.

In the synchronous amplitude spectra of U and B (described in detail in References [17,18]) there is a good similarity, in particular, positions of the main long-period peaks are almost coincided (80^h), positions of pikes at periods 32.0^h , 15.0^h , 12.0^h , 6.15^h and 5.33^h are exactly coincided. In The period (T) dependence of amplitude ratio U/B is approximated by formula $U/B, m^2/s \approx 19\sqrt{T}$.

We could take the magnetic field measured by setup's high quality quantum magnetometer, but it turned out that correlation of the detector signal was bigger and had more advancement with Dst -index of global geomagnetic activity, reflecting the most large-scale dissipative processes in the magnetosphere.

The process of geomagnetic activity is weaker as compared with synoptic one described above, and especially solar one described below, but the most convenient for interpretation. The fact is that our detectors are insensitive to the variable magnetic field, but this field can easily be related with the entropy

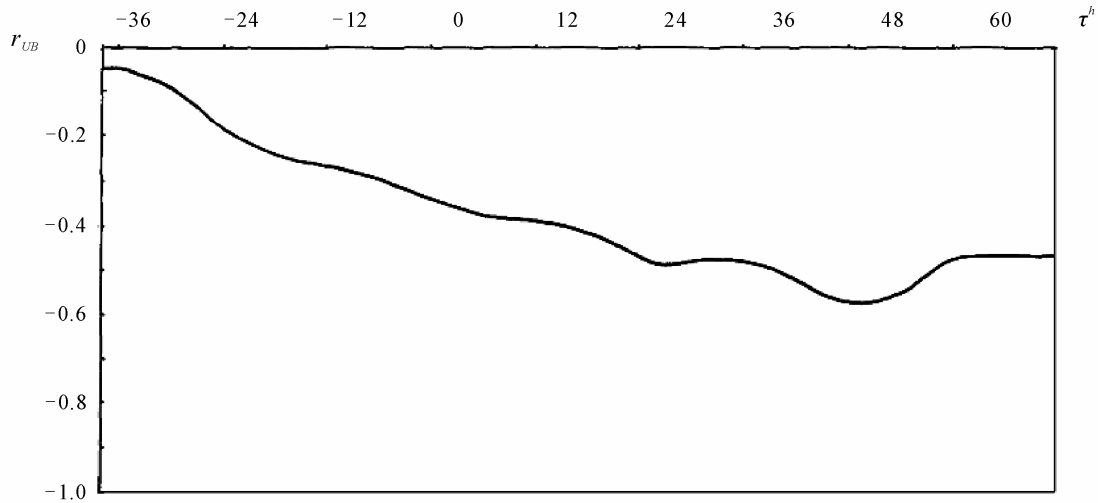


Figure 6.15. Correlation function of the detector signal U and magnetic field B .

production in the magnetosphere. Certainly, as to detector signal is formed by the different sources, data must be appropriately filtered so as to suppress other contributions. The problem of signal separation is quite standard and I shall not describe it in detail. The separation of contributions from the solar and geomagnetic activity is rather sophisticated because the former is clear cause for the latter, and the former is strongest among other sources (Section 6.2.5). Similarity and distinction of contributions from synoptic and geomagnetic activity are demonstrated in **Figures 6.16** and **6.17**.

For this example the series length 7.3 months provides high resolution $2 \cdot 10^{-4} h^{-1}$, but for convenience **Figure 6.16** is plotted with less resolution. There is a good similarity of U and Dst : the 67 spectral peaks coincide. Similarity of U and P is worse (the 25 peaks coincide). The number of U peaks coinciding either with Dst or with P equals 85. So the spectral structure of P and Dst is different and separation of their contribution is possible.

In **Figure 6.17** the same spectra are shown with maximal resolution in the low-frequency domain. The greatest peaks correspond to the periods 27 and 13.5 days (U and Dst), and 90 and 46 days (U and P). The first couple is obviously related with the solar rotation (and corresponding variability in the geomagnetic activity), the second one is related with synoptic activity.

For the analysis of the anticipatory effects the periodic components were suppressed by filtration and we consider further only the random component. The matter of fact is advanced correlation is the property only of random processes. If deterministic, *i.e.* in the given case, periodic component of variation is not suppressed, then anticipatory effect might be amplified by autocorrelation. It would be useful in practice, but here we are going to study namely advanced crosscorrelation and therefore we have to suppress that component. The main periodicity in the geomagnetic activity related with solar rotation synodic period (about 27 days) and its harmonics, and corresponding maxima are pronounced in the detector signals. We have to suppress periods equal and less than solar synodic period. Indeed due to nonlinearity, related Dst spectral lines have periods some more the synodic one (up to 32 days). Investigation of Dst , U , I and d spectra by our experimental data allowed to select optimal low-pass filtration as $T > 28^d \dots 31.8^d$. But in the long period domain there is correlated nonlocal interference from the solar activity. Moreover, direct influence of solar activity is prevailed over geomagnetic one [26-29]. Although for possible future practical application of nonlocal correlations for direct forecast of geomagnetic activity such interference is even useful (because geomagnetic activity is caused by solar one and all existing methods of long-term forecast of the former are indirect, based on forecast of the latter), we tried as far as possible to attenuate it. The matter of fact, due to nonlinear effects of generation of the geomagnetic activity in response to the

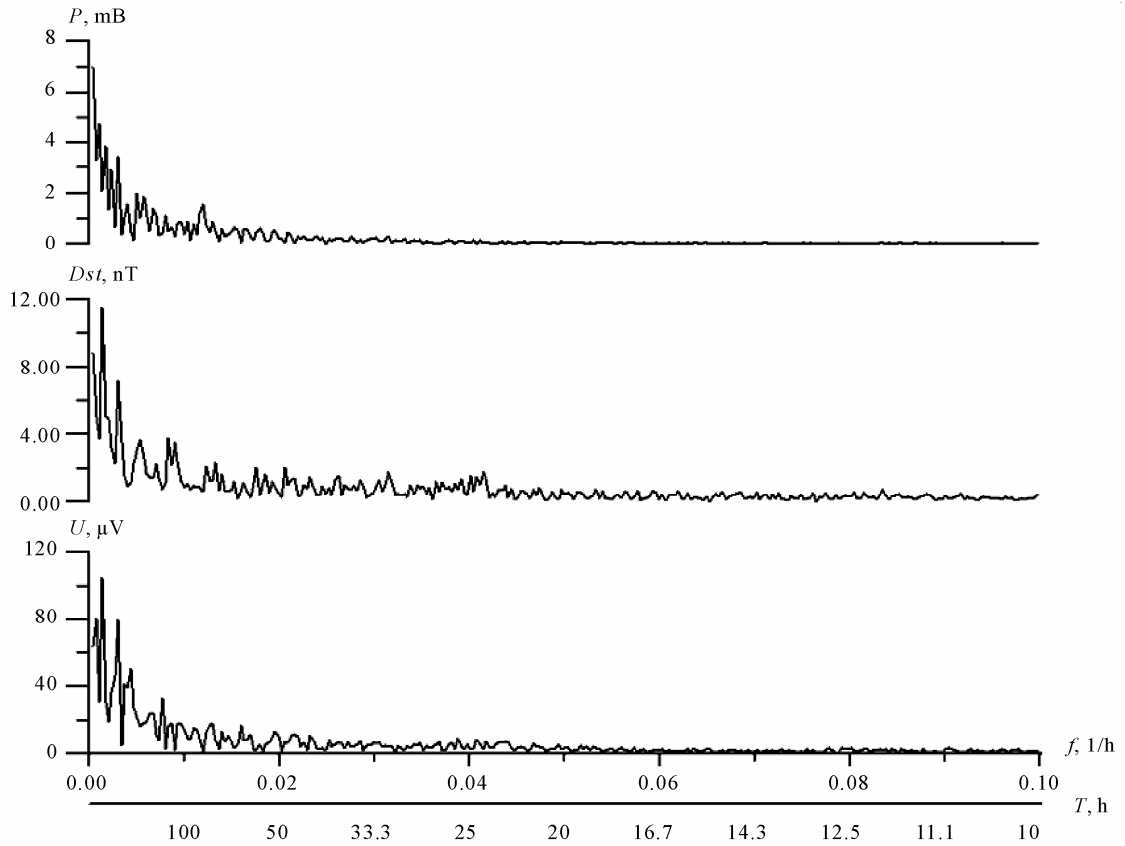


Figure 6.16. Amplitude spectra of U , Dst and P in the period range from 10 hours to 111 days, September 1993-April 1994 (the T is period in hours, f is frequency in inverse hours).

solar one there are (random) long period spectral maxima of Dst , while amplitudes of any index of solar activity increase to long periods, at least to year, almost monotonously (there are not definite spectral lines in the mentioned range). Therefore we can attenuate influence of solar activity by high-pass filtration $T_m > T$, where T_m is selected individually for each time series as period shorter than which Dst spectrum has significant own random maxima. Due to annual period of geomagnetic activity T_m usually was equal to the first or the second annual harmonic period. This procedure also provided suppression of the annual meteorological contribution to the detector signals. Thus the data were processed by wide-band filtration. There was only one time series, for which there was not a need the high-pass filtration to detect Dst contribution.

The qualitative results are the same as in Section 6.2.3: advanced correlations exceed retarded ones and level of correlation increases along source space scale.

Thus for magnetic field measured by setup's magnetometer advancement equals 2 days, while for Dst -index of global geomagnetic activity, reflecting the most large-scale magnetosphere current systems it equals about month (it is not stable value; for different realizations and for different period range position τ of the main peak of γ , i or r may be from 8^d to 140^d [19,20,25-27]). Value of maximal, *i.e.* advanced, γ does not exceed 1.15 (expectation errors of i and γ are about 1%). The level of advanced correlation with Dst after appropriate filtration, increasing signal/noise ratio (the noise includes direct influence of the Sun on the detector signal), can achieve 0.70 - 0.95. Herewith correlation time asymmetry (defined as $\max |r^{adv}| / \max |r^{ret}|$ in the shift τ range $\pm 371^d$ are within from 1.10 ± 0.01 to

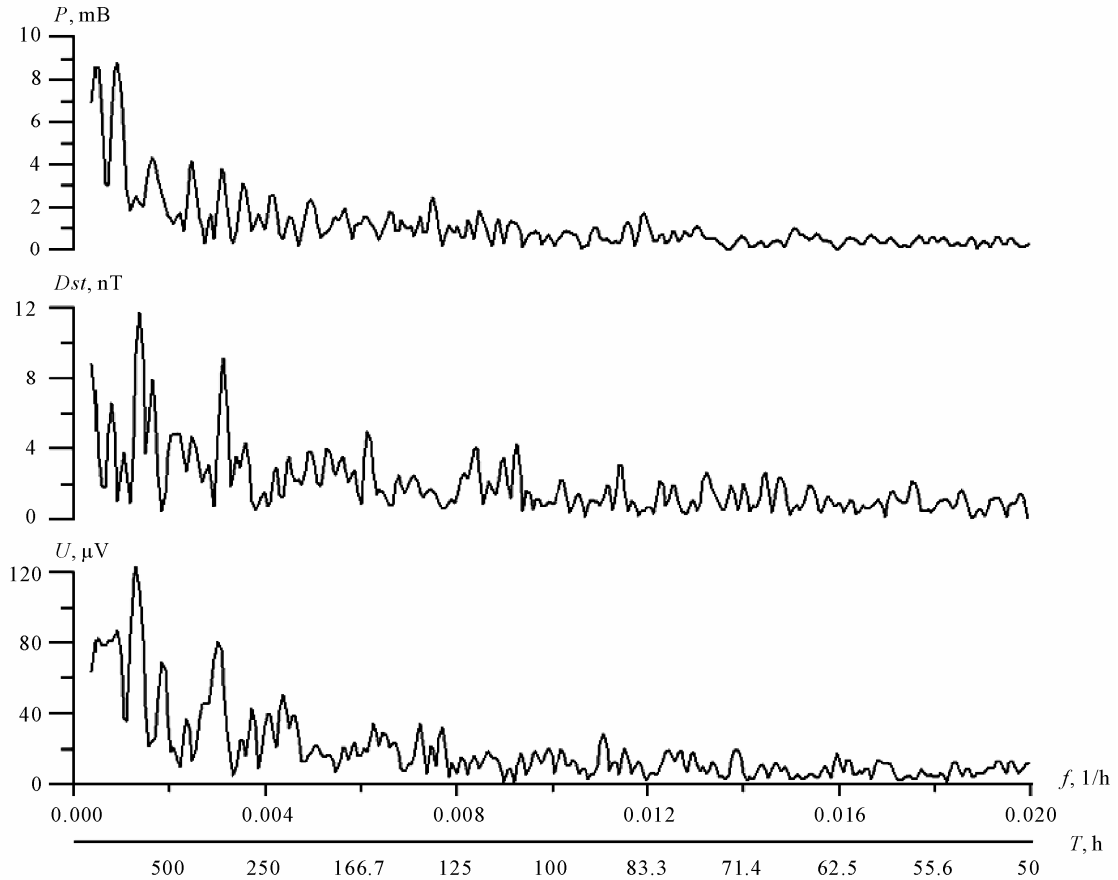


Figure 6.17. The same as in **Figure 6.16** with maximal resolution in the period range from 2.1 to 111 days.

2.64 ± 0.01 [20,26]. The typical example of correlation function showing advanced detector response, $\max r_{UDst} = 0.70 \pm 0.02$ at $\tau = 42^d$, is presented in **Figure 6.18**. This example has been computed by the longest available series: the electrode detector signal U one with duration 2 years and 9 months (10/26 1994-07/24/1997); the Dst series was taken from 1 year before to 1 year latter relatively to ends of U one.

The obvious forecasting applications will be developed in the last section. For the present we will confine ourselves by wittingly primitive simplest demonstration of the forecast possibility by shift the optimal filtered time series on corresponding to **Figure 6.18** $\tau = 42$ days (**Figure 6.19**).

Mentioned 42 days is rather typical value of the main correlation maximum advancement. Another typical value also turned out 130^d . But for the different time series it may vary considerably. For example, in **Figure 6.20** is the case when it equals 60 days. But always the level of advanced correlation is quite high (here 0.72 ± 0.01). And correlation asymmetry that is ratio of maxima of advanced to retarded correlation is always more than 1. For this example it equals 2.64 ± 0.01 .

Turn to the quantitative interpretation. Taking into account complexity and, as a rule, poor knowledge of large-scale natural source-processes parameters, it is extremely difficult to verify theoretically values of time shifts by the detector signal and standard geophysical data. But it is possible to hope on order estimation of σ in Equation (4.4), *i.e.* on verification of effect magnitude. The process of geomagnetic activity is the most convenient, because it admits to use in the right-hand site of Equation (4.4) the simplest model for the source entropy production density:

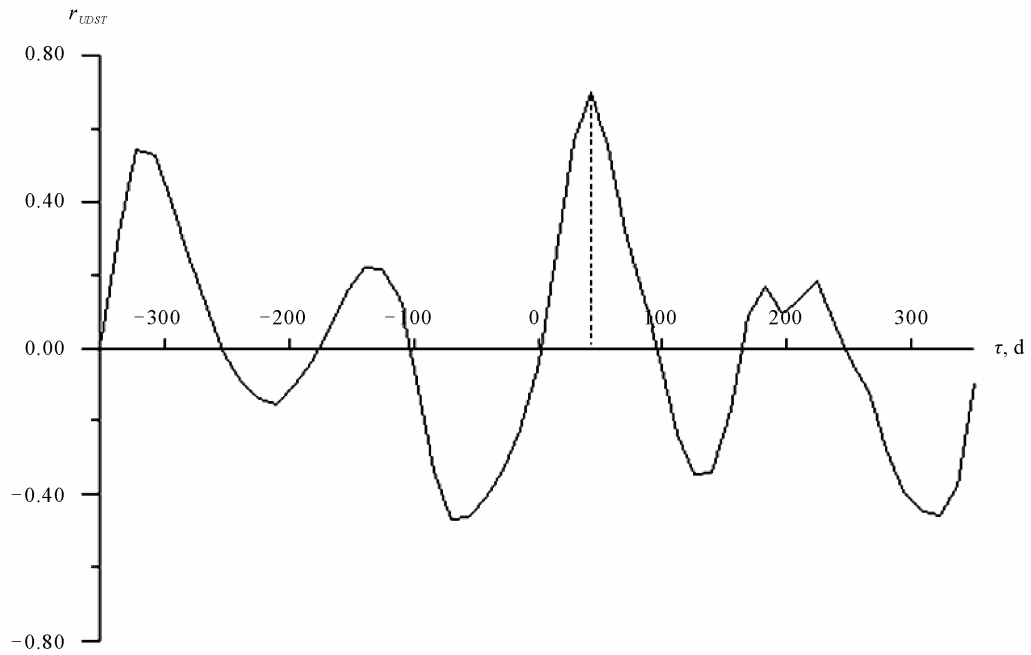


Figure 6.18. Correlation function of the detector signal U and geomagnetic activity Dst ($364 > T > 28$ days).

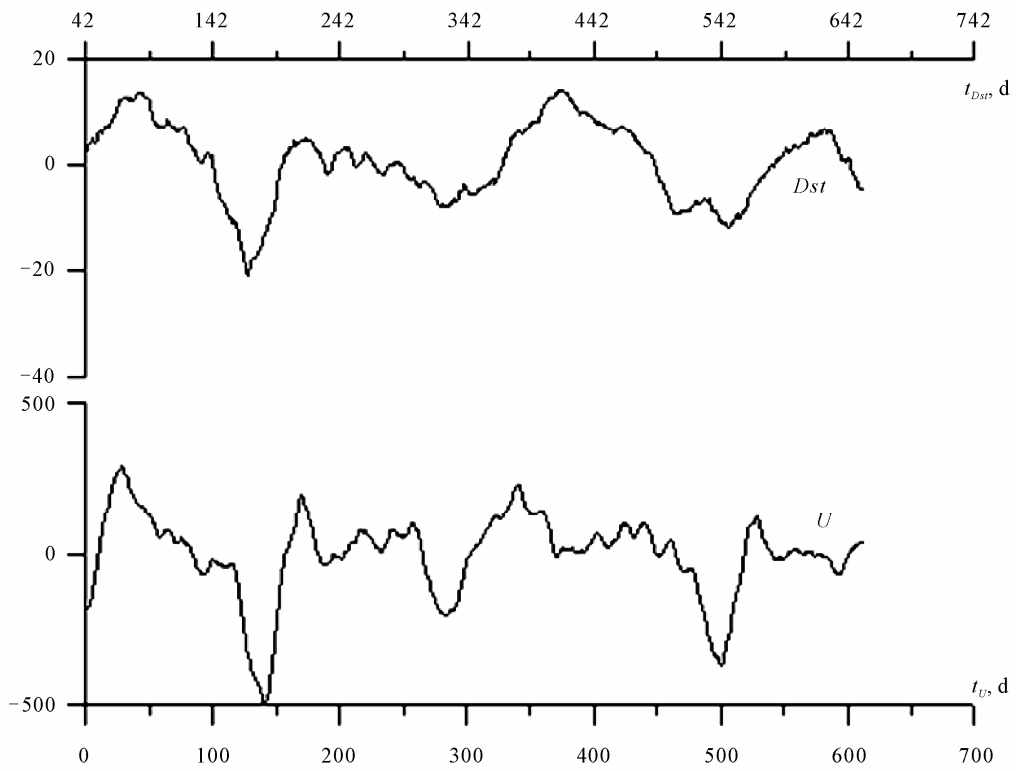


Figure 6.19. The detector signal U (μV) forecasts the random component of geomagnetic activity Dst (nT) with advancement 42 days. The origin of time count corresponds 5/10/1995.

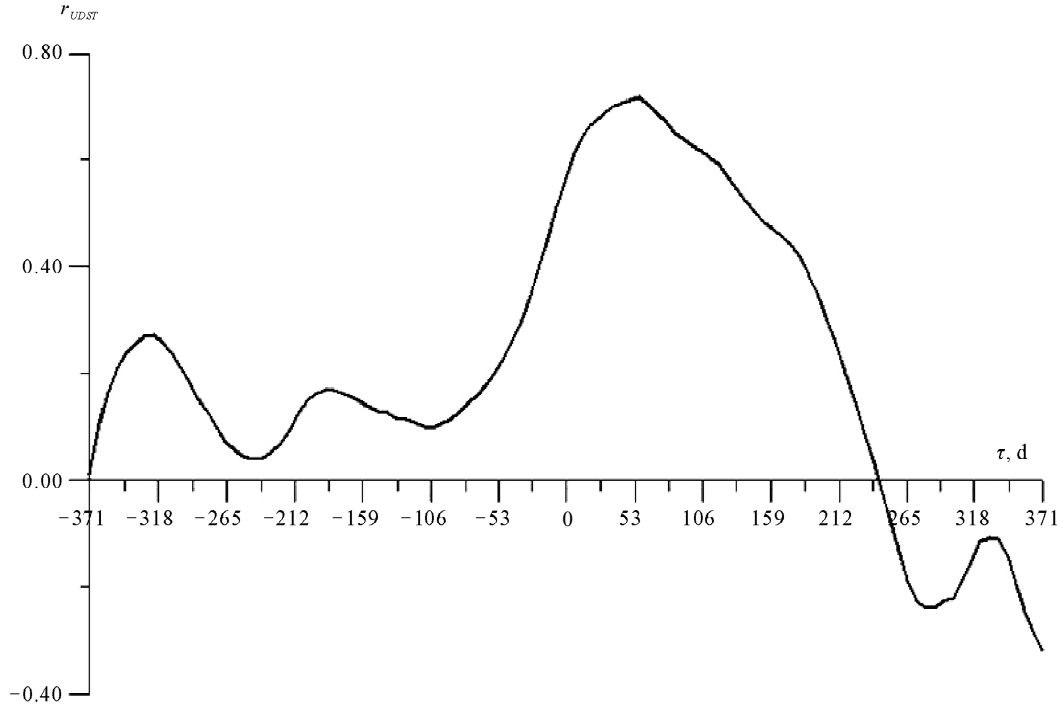


Figure 6.20. Correlation function of the detector signal U and geomagnetic activity Dst ($T > 31.8$ days).

$$\dot{s} = \frac{\langle E^2(f) \rangle}{\rho k T_s} = \frac{|Z(f)|^2 \langle F^2(f) \rangle}{\rho k T_s}, \quad (6.11)$$

where E is electric field, f is frequency, ρ is source medium resistivity, T_s is source medium temperature, Z is impedance, F is magnetic field (hereafter it is more convenient to use $F = B/\mu_0$). The Z and ρ we may consider for simplicity as scalars. By substituting Equation (6.11) into Equation (4.4) further simplification is possible, using the known properties of the electromagnetic field of the magnetospheric source. First, the field F is well approximated by plane wave, therefore it is possible to factor out the \dot{s} from the integral, and, restricting our consideration to the spectral amplitudes, we reduces this integral simply to thickness of dynamo-layer. Second, use quasi-steady-state approximation of the plane wave impedance of homogenous medium: $|Z(f)|^2 = 2\pi f \mu_0 \rho$. Dependence on ρ disappears, and for spectral amplitudes it is easily to show, taking into account Equations (5.8), (5.12) and (5.13) [17-19,24] that following ratio is frequency-independent:

$$\frac{U(f)}{F^2(f)} = const \quad (6.12)$$

and analogously for $I(f)$ and $d(f)$. Equations type of (6.12), of course, are approximated, because above simplest expression for $|Z(f)|^2$ is rather rough approximation.

But the geomagnetic activity, as a separate source process, has a flaw—it is close correlated with solar activity especially at long periods $T > 27$ days. On the other hand, short periods (and correspondingly small space scales) $T < 1$ day do not cause enough strong detector reaction. It holds significance also choice of an index of geomagnetic activity. The Dst -index due to procedure of its calculation is most representative at $T > 2$ days. For these reasons the spectral window $20^d > T > 2^d$ was selected for analysis.

However in that window nonlocal interference from the synoptic activity is just possible. Therefore it is a need to select for analysis enough long time segment with quiet weather condition. That is why in the all previous studies we succeeded in estimation of σ only in one case [17]. It was estimation by electrode detector and setup's quantum magnetometer data: $\sigma \approx 2 \cdot 10^{-21} \text{ m}^2$. The last reference also indicates the desirability to estimate σ by data of different detectors, because every of them may be noised in different manner.

Close examination of more recent data has shown that the most appropriate data segment turns out series 07/14/2003-10/27/2003. Amplitude spectra of I and Dst are rather similar (**Figure 6.21**): many of individual peaks coincide (at periods 450, 371, 321, 135, 92.2, 79.9, 72.9, 61.8, 59.4, 55.8 and 49.5 hours). Peak-to-peak variation coefficient (ratio of the standard deviation to the mean) for I/Dst^2 equals 0.12, while for I/Dst it equals 0.31, that confirms approximate validity of equation type of Equation (6.12).

For σ estimation we combine Equation (4.4) in plane wave approximation, (5.12) and (6.11). In this approximation the source is characterized by two parameters: thickness of dynamo-layer h and temperature T_s , for which we take the well known $h \approx 1.3 \cdot 10^6 \text{ m}$ and $T_s \approx 1.3 \cdot 10^3 \text{ K}$. Then for realization I we obtain the average estimation $\sigma \approx 5 \cdot 10^{-20} \text{ m}^2$.

The realization of U synchronous to I proved to be noisier, that probably shifted the estimation up. But using Equation (5.8) instead of (5.12) we obtained in the same spectral window close average estimation $\sigma \approx 8 \cdot 10^{-20} \text{ m}^2$.

The realization segment of d synchronous to I was shorter, might be because of that, using Equation (5.13) instead of (5.12) we obtained in the same spectral window bigger average estimation $\sigma \approx 6 \cdot 10^{-19} \text{ m}^2$.

In view of the fact that accepted model of the complex source of the variable geomagnetic field is extremely approximated and separation of the useful signal from interference is poor, coincidence of above estimations with theoretical one (about 10^{-20} m^2 by $\sigma \approx \hbar^4 / m_e^2 e^4$ in Equation (4.4)) may be thought as

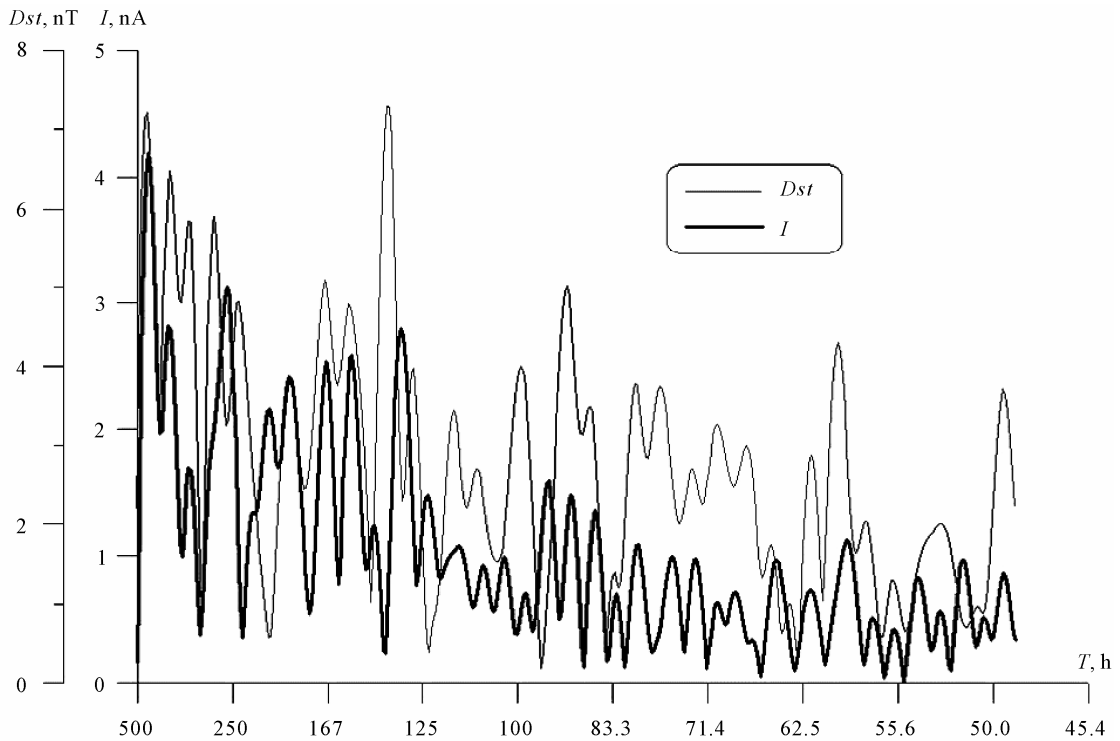


Figure 6.21. Amplitude spectra of the detector signal I and geomagnetic activity Dst .

satisfactory. Thus transaction cross-section is of order of an atom one.

6.2.5. Relation of the Detector Signals with the Ionospheric Activity

It was disclosed an interesting manifestation of the ionospheric activity in U variations. It has been turned out that probability of the sudden ionospheric disturbances during phase of an increase of U substantially exceeds this probability during phase of a decrease. Probabilities ratio is 4.5. If only the sudden enhancements of the atmospherics were selected such probability ratio became to 7.1.

It may be suggested following qualitative interpretation of these facts. The sudden ionospheric disturbances are the sharp increase of ionisation of the lower ionosphere. That corresponds to the decrease of the entropy resulting, according Equations (4.4) and (5.8), to the increase of the potentials. In the case of the sudden enhancements of the atmospheric there is an additional effect related with the thunderstorm activity.

6.2.6. Relation of the Detector Signals with the Solar Activity

The solar activity proved to be the most powerful dissipative process acting on detectors. It is well known that solar activity is the cause of the geomagnetic and ionospheric ones; the retardation of the latter's ranges from 8 minutes to 2 days. As index of the solar activity we used solar radio wave flux R . It should be stressed that detectors are insensitive to the solar radio waves; their flux is only index of the source entropy production.

In **Figure 6.22** an example of the synchronous independence function U on the solar radio wave flux

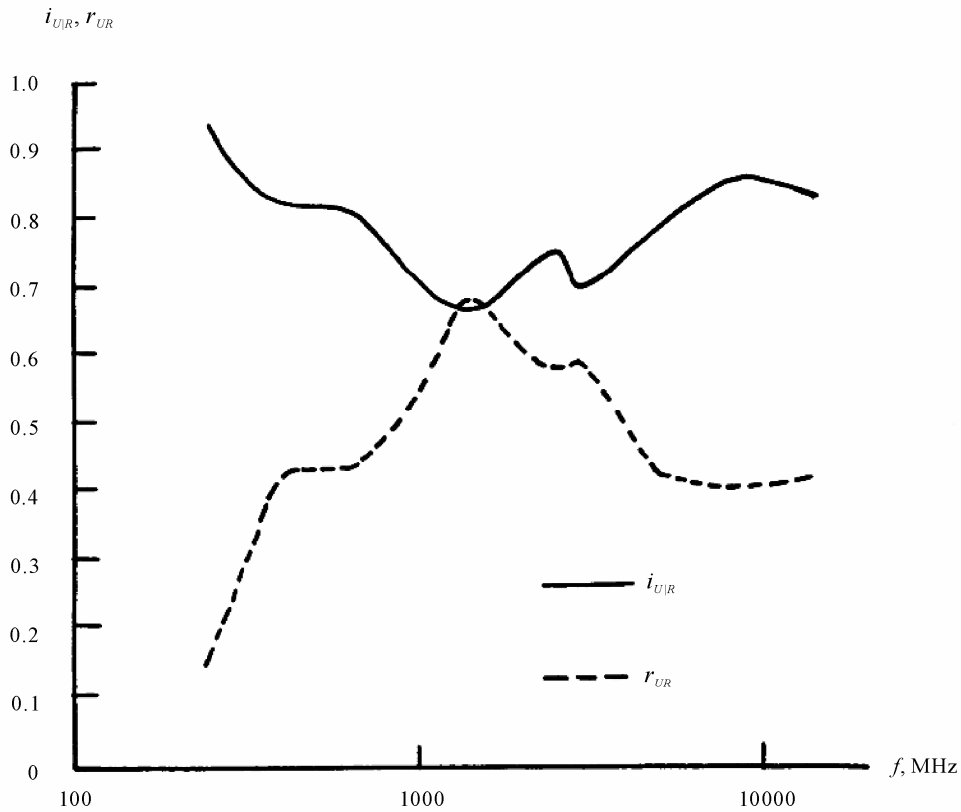


Figure 6.22. Independence of U on solar radio wave flux R $i_{U|R}$ and their correlation r_{UR} as functions of frequency f of R .

R (in the standard range 245...15,400 MHz) and their correlation function, computed by daily averaged series 12/10/1996-12/11/1997 are shown. Both curves point out the optimal frequency 1415 MHz, corresponding to the radiation from the level of the lower corona-upper chromosphere, where the most intensive dissipative processes take place. At this frequency $i_{U|R} = 0.66^{+0.02}_{-0.00}$ ($\gamma = i_{R|U}/i_{U|R} = 1.23 \pm 0.01$), $r_{UR} = 0.68 \pm 0.02$. In all these series R were taken reduced to 1 $A.U.$ One can expect that use an observable series R instead of reduced one has to increase correlation slightly. Indeed at the frequency 2800 MHz for which both the series of R are presented in the “Solar-Geophysical Data”, it turns out that for reduced R : $r_{UR} = 0.59 \pm 0.02$, while for observable R : $r_{UR} = 0.62 \pm 0.02$.

One can suggest the cosmic ray flux as a possible local mechanism of influence of the solar activity on the detector. We have tested it by data of the IZMIRAN neutron monitor, situated near (100 m) our setup. Correlation of U with the cosmic ray counting rate turned out much less of above and below mentioned correlation U with R : -0.30 ± 0.03 at daily averaging and not significant at monthly averaging. Therefore cosmic rays are not carriers of the interaction.

Consideration of all the available time series that the optimal frequency varies from year to year, but always remains within the range 610 - 2800 MHz, really corresponding to emission from the upper chromosphere—lower corona level that is just from the level of maximal dissipation the magneto-sound waves energy.

Examples of synchronous amplitude spectra of solar radio wave flux R at three frequencies, Dst index and detector signal U are shown in **Figures 6.23** and **6.24**. All the spectra exhibit two principal maxima: at Sun’s rotation period and its second harmonic. The spectrum of Dst is more complex, since the Dst -variation arises due to multifactorial and nonlinear influence of the Sun on the current inducing the magnetic field (due to source emf and via plasma conductivity variations). In the realization showed in **Figure 6.23** the spectrum of U is most closer to the spectrum of R_{610} in the spectral maxima width and the general spectrum shape, including the rise in the region of the longest periods. The ratio of the amplitudes of the first and second harmonics of the Sun’s rotation period is 0.95 (for U), 0.69 (Dst), 0.99 (R_{610}), 0.87 (R_{1415}), and 0.69 (R_{2800}). Thus in this parameter U is also closest to R_{610} . In the realization showed in Fig. 6.24 that ratio is 1.2 for U , 0.74 for Dst , and 1.1 for all R , that is, the first harmonic in U and R is large than the second one and vice versa in Dst . In this case U is most similar to R_{2800} in the principal maxima width and general spectrum shape. At last **Figure 6.24** approximately corresponds to a minimum of 11-year cycle of solar activity, and, accordingly, all the spectra in **Figure 6.24**, including U have less amplitude as compared to **Figure 6.23**.

Thus spectral analysis points out the certainly closer relation of the detector signal directly with the solar activity than with its effect—geomagnetic activity. However optimal frequency of the solar radio wave flux, reflecting level of the source-processes in the solar atmosphere, may change in time.

In **Figure 6.25** the correlation function r_{UR} of the detector signal U and solar activity R (by the longest U realization 10/26/1994-02/11/1996, at the optimal $f = 610$ MHz and with low-pass filtration $T > 28$ days) is shown. The R series was taken from 1 year before to 1 year latter relatively to ends of the U series. Thus **Figure 6.25** is computed by data corresponding to **Figures 6.18** and **6.23**. The main maximum in **Figure 6.25** $r_{UR} = 0.51 \pm 0.02$ is observed at advancement $\tau = 42$ days. The position of this and also the other two advanced maxima also corresponds to the results of causal analysis considered below. Retarded correlation is insignificant.

But the solar activity excites much more close (to the detector) the process of geomagnetic activity and it is legitimately to speculate that latter is direct cause of U variation. Although correlation of U with the geomagnetic activity in **Figure 6.18** is bigger than with the solar one in **Figure 6.25**, it results from the optimal band filtration in the former case. At the same low-pass ($T > 28$ days) filtration correlation of the detector signal with geomagnetic activity is almost the same: $\max r_{UDst} = 0.50 \pm 0.02$ at the same $\tau = 42$ days. The same value of τ is explained by small response time of Dst on R (1 - 2 days) as compared with low-pass filter parameter $T = 28$ days. Correlation of Dst with R seems practically synchronous at given time resolution ($r_{Dsr} = 0.30 \pm 0.02$ at $\tau = 0$).

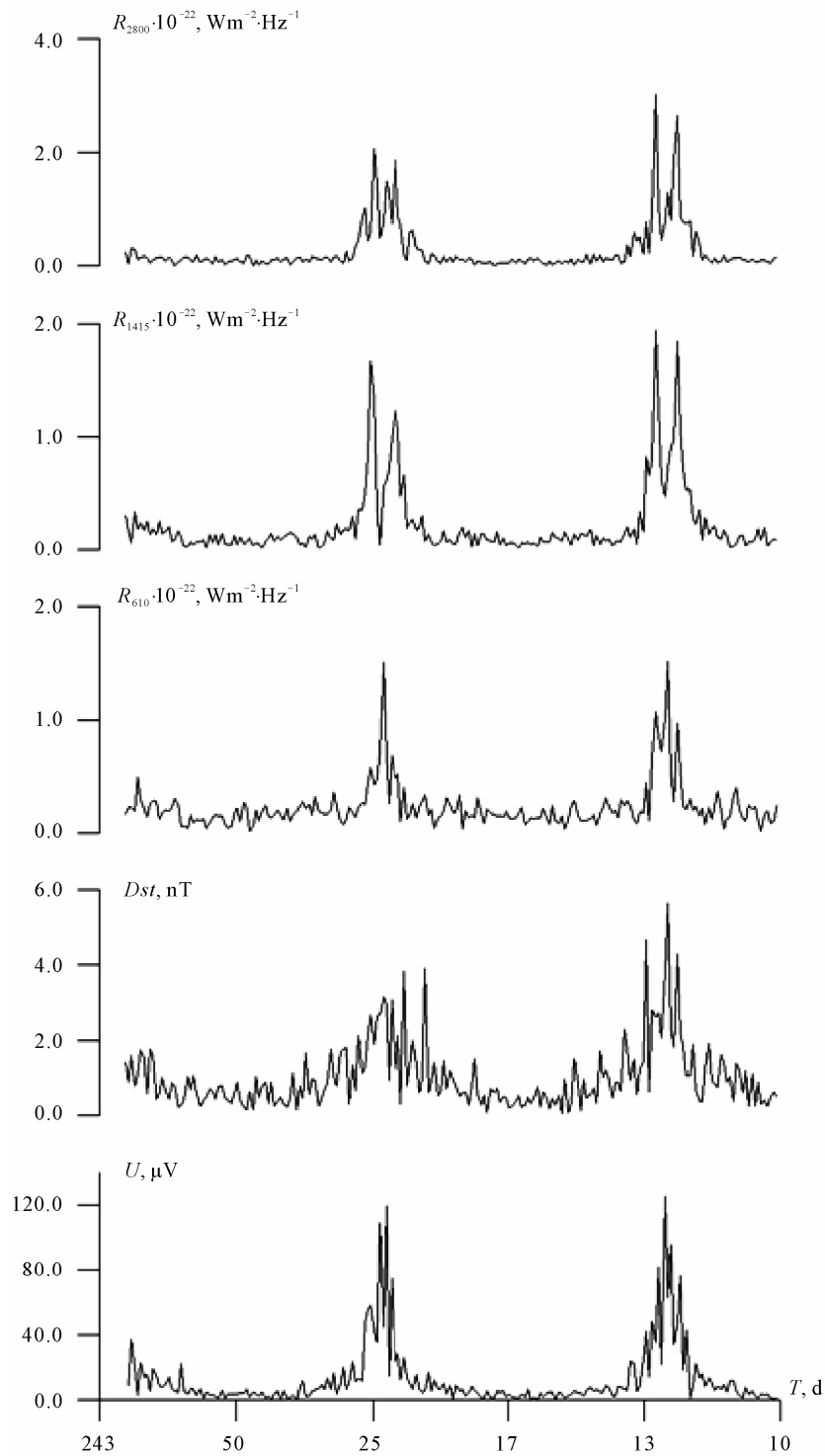


Figure 6.23. Amplitude spectra of the solar radio wave flux at frequencies 2800 MHz R_{2800} , 1415 MHz R_{1415} and 610 MHz R_{610} , the geomagnetic activity index Dst and detector signal U in the period range T from 10 days to 243 days. Realization 10/26/1994-02/11/1996.

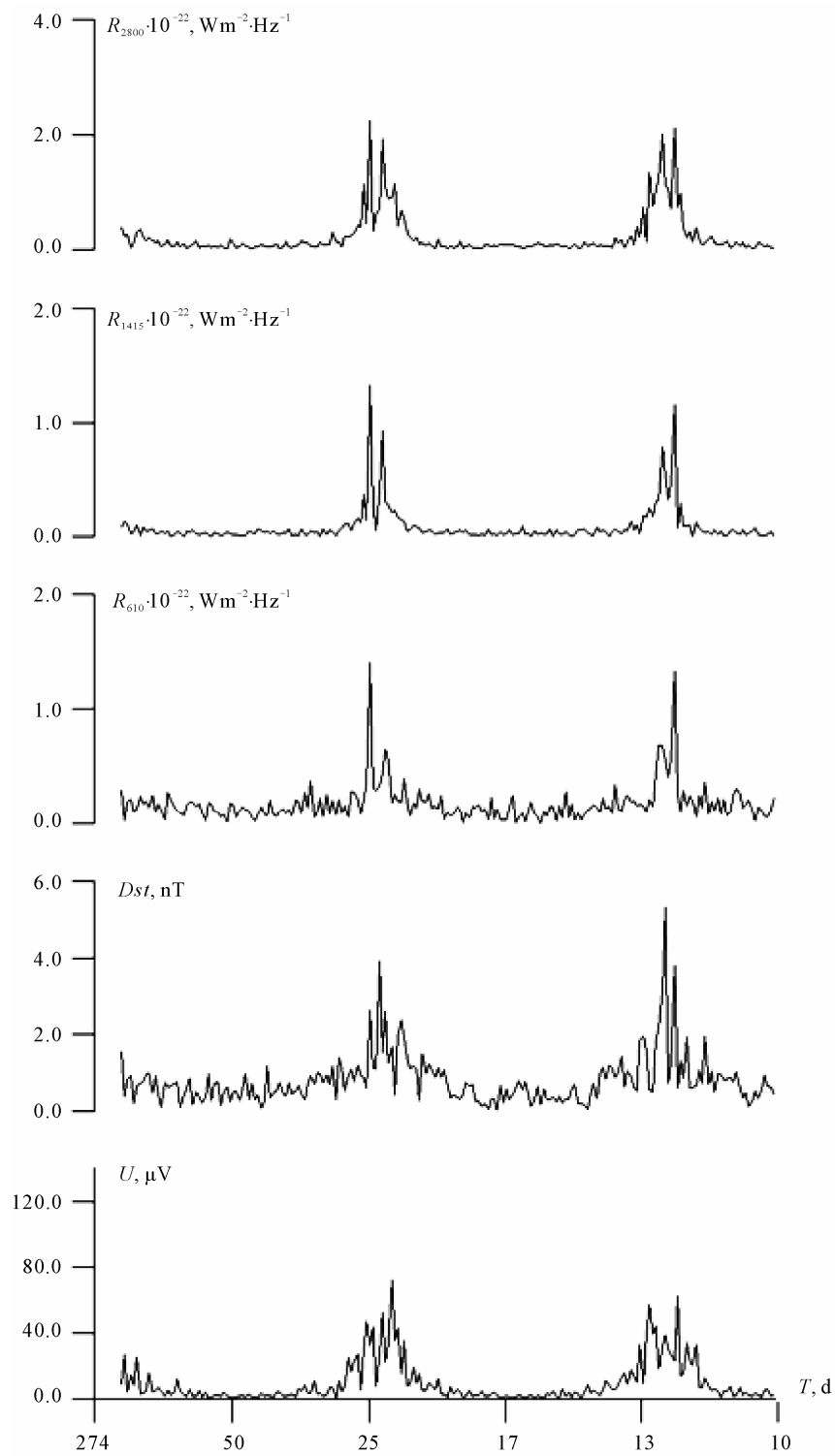


Figure 6.24. Amplitude spectra of R_{2800} , R_{1415} , R_{610} , Dst and U in the period range T from 10 days to 274 days. Realization 03/16/1996-07/23/1997.

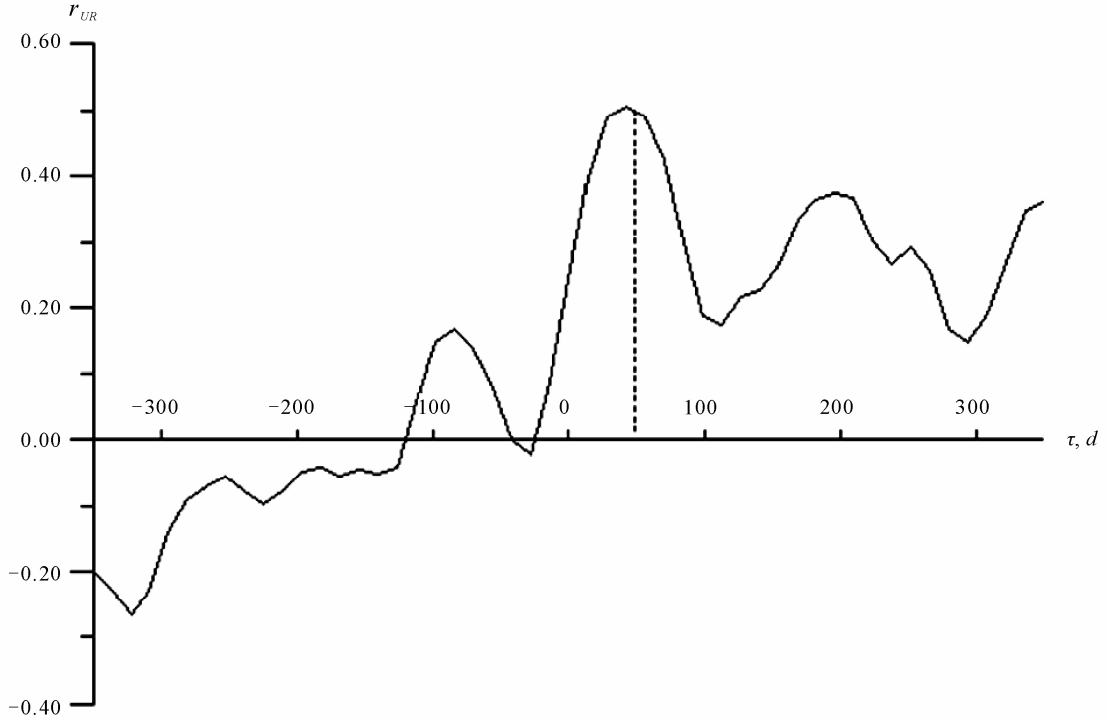


Figure 6.25. Correlation function of the detector signal U and solar activity R ($T > 28$ days).

Hence we observe probably a direct influence of the solar activity on the detector signal that is typical property of nonlocality. For proof consider Bell-type inequality (4.16) for this case:

$$i_{U|R} \geq \max(i_{U|Dst}, i_{Dst|R}), \quad (6.13)$$

The fulfillment of In Equation (6.13) is sufficient condition for locality of connection along the causal chain $R \rightarrow Dst \rightarrow U$ (since any local solar influence on the detector can not come avoiding the magnetosphere that is source of Dst variations). The experimental values are: $i_{U|R} = 0.807^{+0.010}_{-0.009}$, $i_{U|Dst} = 0.836^{+0.000}_{-0.002}$, $i_{Dst|R} = 0.832^{+0.008}_{-0.000}$. In Equation (6.13) is violated, therefore connection $R \rightarrow U$ is nonlocal.

Availability of signaling in reverse time allowed developing the method of the statistical background forecasts (Section 6.2.7). But a natural question is: what about forecasting of the individual events? Our experience had shown that detectors responded only to the most powerful of them, such as solar flares of X -class. Visible detector signal is very smooth usually. But sometimes, for instance, at the beginning 2003 several extremely sharp splashes (with duration of order of an hour) and with big magnitude, from 4 to 134 μV were observed in the electrode detector signal on January 1, 9, 14, 15, and February 3, 11, 13, 14. The biggest splash presented in **Figure 6.26** was on February 3. And just 42 days after, the famous flare on March 17 happened (**Figure 6.27**). It was a seldom gigantic flare of X -class.

In such a manner this powerful solar event caused advanced response of the electrode detector with several time shifts and with the main predictor at $\tau = 42$ days. Moreover splash shapes of the self-potentials (**Figure 6.26**) and solar X-rays one (**Figure 6.27**) are similar. In spite of the greatest magnitude this solar flare was not geoactive, it did not cause of a magnetic storm, because of its inappropriate position on the Sun. Therefore this solar event impact on the detector was direct, *i.e.* nonlocal.

Return to statistics. The results of causal and correlation analysis of the detector signals and solar activity R have shown that in the advanced domain ($\tau > 0$) values of the independence function are

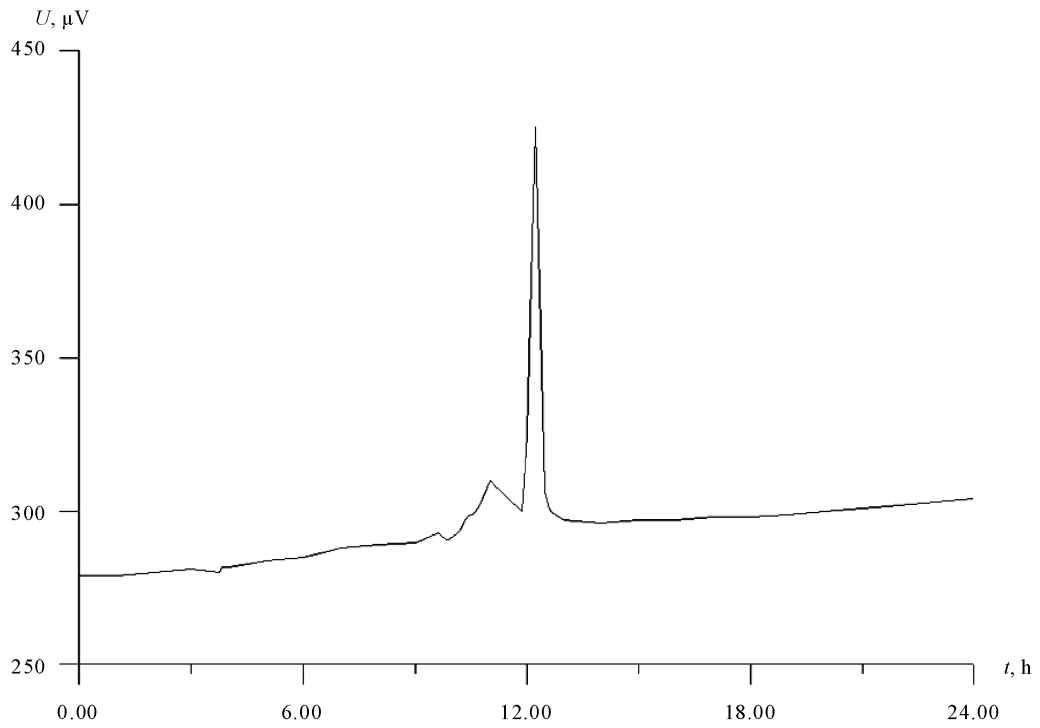


Figure 6.26. Unusual splash of the detector signal U on February 3, 2003.

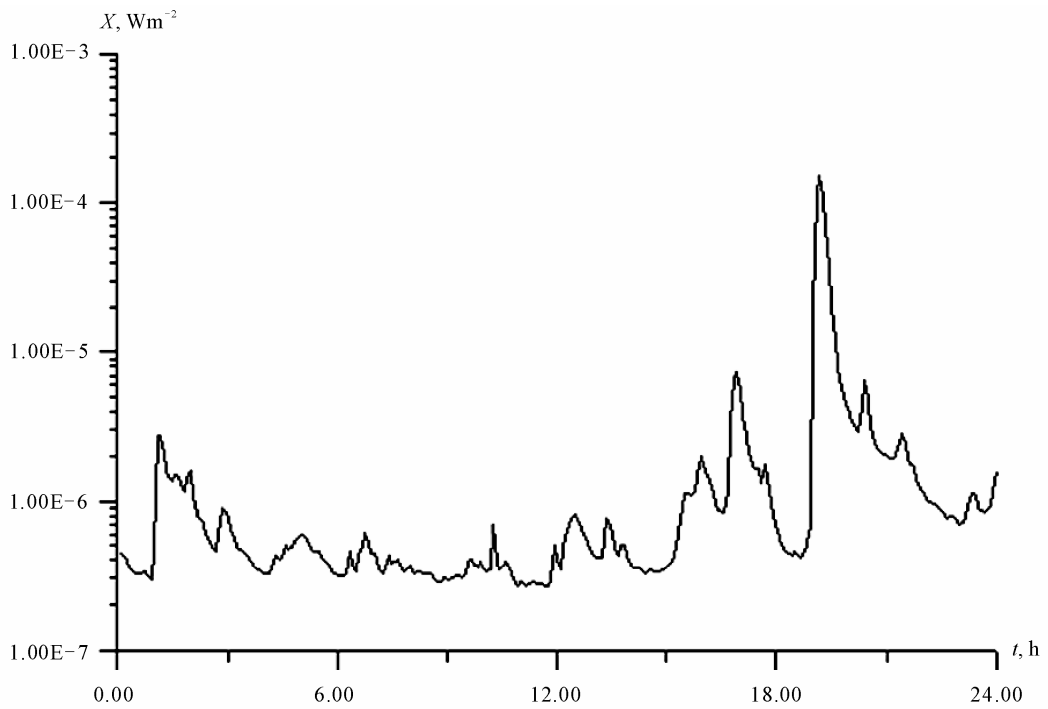


Figure 6.27. Gigantic solar flare (X-ray flux) on March 17, 2003, *i.e.* 42 days after the event recorded by detector, which is shown in **Figure 6.26**.

much less and ones of causality function are much more than in the retarded domain ($\tau < 0$), position τ of the main peak of γ , i or r may be from 42^d to 280^d . Value of maximal, *i.e.* advanced, γ amounts up to 1.58, while r ranges into 0.50 - 0.92 (and relation with R is explicitly nonlinear). Big τ interval corresponding to significant $\gamma > 1$ is explained by big volume of the solar atmosphere occupied by the source processes with diffusion propagation.

Consider in greater detail the results by a annual series 10/19/2002-10/18/2003 when correlation turned out particularly big. As solar activity data we took daily solar radio flux R at optimal for the given case frequency 1415 MHz and two adjacent ones: 610 and 2800 MHz. Time series was taken for about 3 years (beginning 371 days before and finishing 371 days after the ends of U series). As geomagnetic activity data we took international hourly Dst -index for the same time as R . To suppress the periodic components (the synodic solar rotation period in the R , Dst and U , and the annual period, including its second harmonic, in the Dst and U) data were wide-band filtered in the period range $183^d > T > 28^d$. (For Dst because of splitting of the spectral line corresponding to the solar rotation period, optimal lower bound of the wide-band filtration was more: 32^d).

After this filtration the correlation function r_{UR} has been calculated in the time shift range $\tau = \pm 371^d$. Correlation time asymmetry is $\max |r_{UR}^{adv}| / \max |r_{UR}^{ret}| = 1.18 \pm 0.06$ that is quite reliable. Maximal correlation $r_{UR}^{adv} = 0.92 \pm 0.03$ is at advancement $\tau = 130^d$. **Figure 6.28** demonstrates a possibility of the solar long-term forecast by the shift of corresponding annual segment of R series (at 1415 MHz) forward relative to U one by $\tau = 130^d$. The forecasting effect is evident quite clearly. The peculiarity of this forecasting picture is that U curve is smoother than R one (with the same filtration). Therefore U responses mainly on long term and, correspondingly, large-scale disturbances of R . It should be empha-

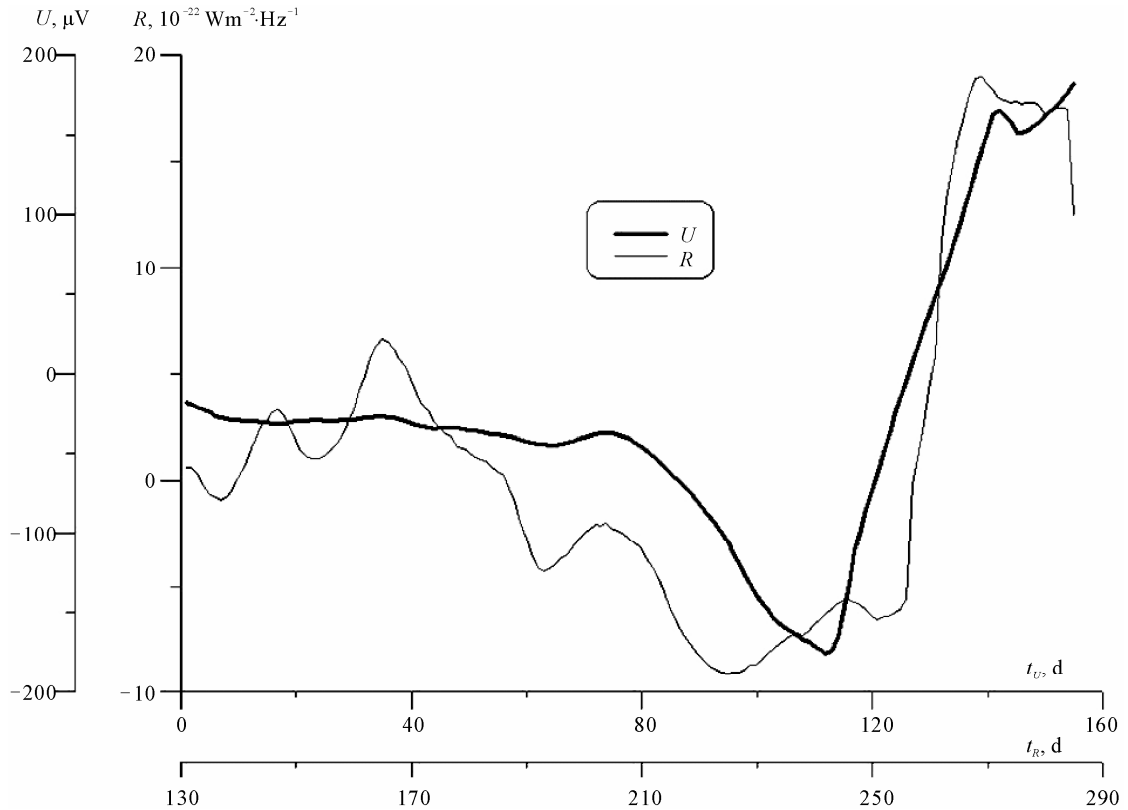


Figure 6.28. The detector signal U forecasts the solar radio wave flux R with advancement 130 days. Origin of time axis corresponds to 01/07/2003.

sized that U forecasts namely random component of R , which is eluded forecasting by any classical methods.

At the adjacent frequencies the main maximum is also at $\tau = 130^d$, but level of correlation is slightly less: for 610 MHz $r_{UR}^{adv} = 0.88 \pm 0.04$ and for 2800 MHz $r_{UR}^{adv} = 0.90 \pm 0.03$. That is the frequency 1415 MHz is optimal.

The main extremum of correlation r_{UDst} is almost at the same time shift (about 10^d more), but it is weaker: $r_{UDst}^{adv} = -0.87 \pm 0.04$. Correlation time asymmetry is also weaker: $\max |r_{UDst}^{adv}| / \max |r_{UDst}^{ret}| = 1.11 \pm 0.06$. On the other hand, though the Dst -variation is excited just by solar activity, due to complexity of their relation, their correlation is rather weak. For given series Dst and R at 1415 MHz the main extremum $r_{DstR} = -0.38 \pm 0.07$ is observed at $\tau = -10^d$ (Dst is retarded relative to R).

Thus we have $r_{UR} = 0.92 \pm 0.03$, $r_{UDst} = -0.87 \pm 0.04$ (both advanced) and $r_{DstR} = -0.38 \pm 0.07$ (retarded). Such relationship suggests that connection of U and R is direct, i.e. nonlocal. But all three links might be nonlinear. Indeed nonlocality of (classical local) $R - Dst$ link is well known, as well as $Dst - U$ (Equation (6.12)) and (as it is demonstrated below) $R - U$.

But independence functions are equally fit for linear or any nonlinear type of dependence. All three independence functions of In Equation (6.13) were calculated with mentioned above time shifts. The results are: $i_{U|R} = 0.46_{-0.02}^{+0.01}$, $i_{U|Dst} = 0.51_{-0.02}^{+0.00}$, $i_{Dst|R} = 0.83_{-0.02}^{+0.00}$. In Equation (6.13) is reliably violated, therefore connection $R \rightarrow U$ is nonlocal. Even choice of optimal frequency of R 1415 MHz is not crucial: for 610 MHz $i_{U|R} = 0.50_{=0.01}^{+0.03}$, for 2800 MHz $i_{U|R} = 0.49_{-0.01}^{+0.02}$, In Equation (6.12) is violated, though slightly less.

Turn now to the causal analysis of data, which explicitly demonstrate irreversibility in irreversible time—the causal connection in reverse time. In addition is capable to reveal the interesting features of the source. Consider it on example of the year corresponding to the onset of a cycle of solar activity (12/10/1996-12/11/1997). Since this series covered the minimum of solar activity we selected the less restrictive low-pass data filtration: $T > 7^d$. It is seen in **Figures 6.29-6.31** how much strong detector re-

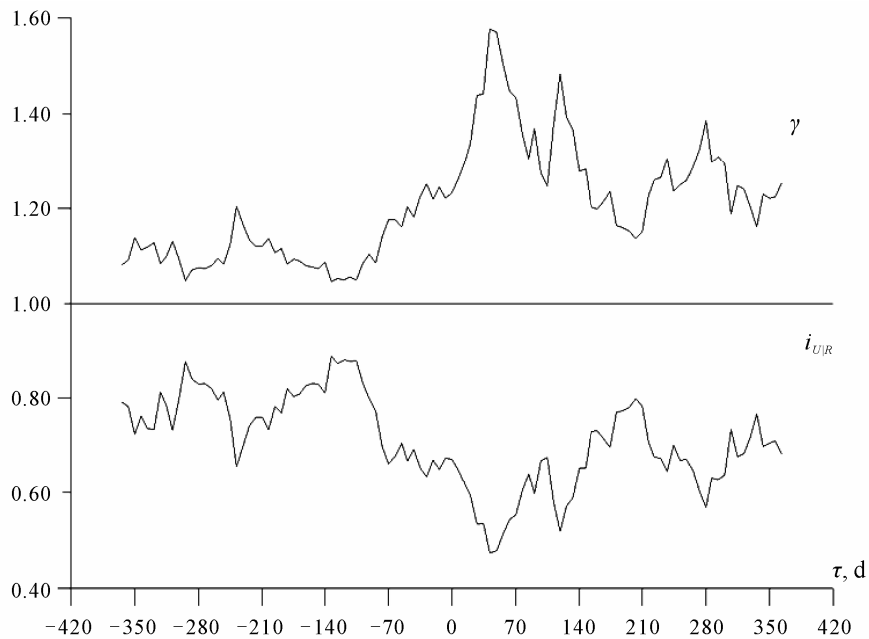


Figure 6.29. Independence and causality functions of the detector signal U and solar radio flux R at frequency 2800 MHz. Realization U 12/11/1996-12/10/1997 (realization R_{2800} begins 1 year before and finishes 1 year after U one).

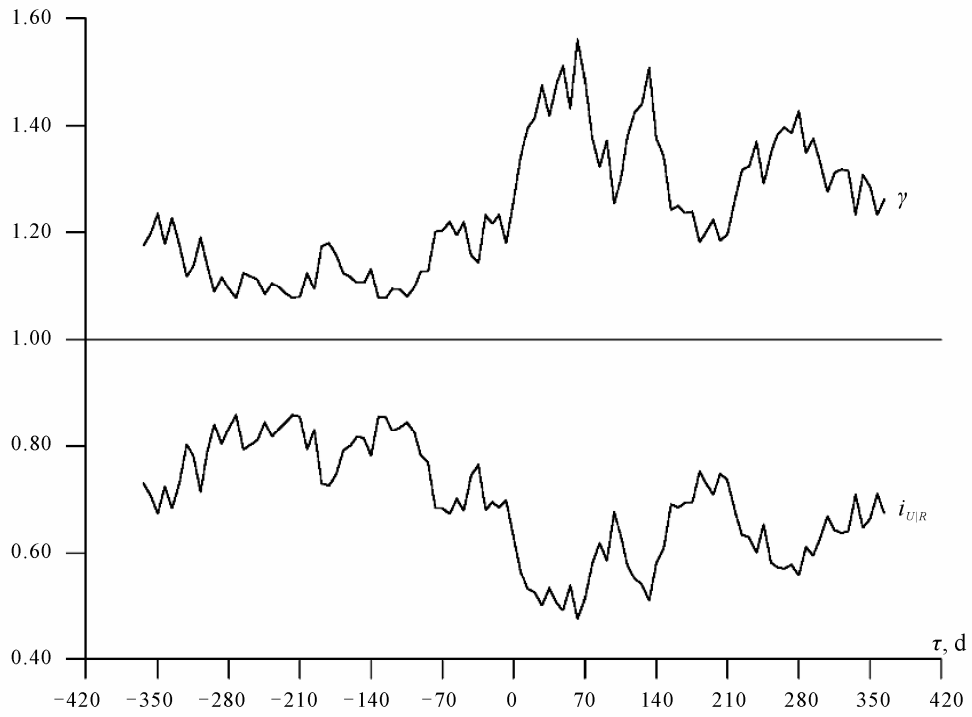


Figure 6.30. The same as in Figure 6.29 for R frequency 1415 MHz.

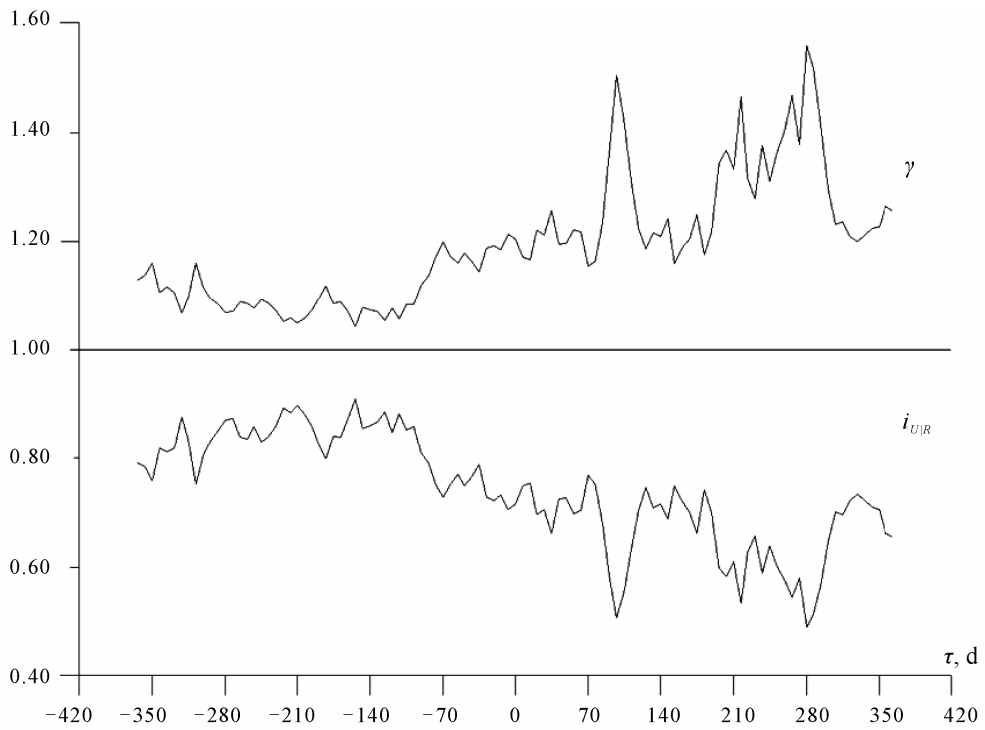


Figure 6.31. The same as in Figure 6.29 for R frequency 610 MHz.

sponse to the processes of solar activity. In the advanced domain ($\tau > 0$) values of the independence function of the detector signal U on R at the all three frequencies is much lower than in the retarded domain, and the causality function is much more than 1. The absolute minimum $i_{U|R} = 0.47$ and the absolute maximum $\gamma \approx 1.58$ are observed for R_{2800} at $\tau = 42^d$.

The wide τ interval corresponding to significant $\gamma > 1$ is explained by a large volume of the solar atmosphere filled with the source-processes during diffusive propagation. The common feature of the advanced correlation of the detector signal advanced connection of the detector signal and the radio emission is existence of three γ peaks (see **Figure 6.29-6.31**). For the frequency of 2800 MHz these peaks correspond to advancement: 42, 119 and 280 days; for 1415 MHz: 63, 133 and 280 days; for 610 MHz: 98, 217 and 280 days. The third peak, $\tau = 280^d$ is common for all three levels of radio emission generation, hence corresponds to a process of the greatest spatial scale.

A comparison the results of causal and correlation analysis have shown the nonlinear $U(R)$. The primary maxima of correlation function coincide with the minima of $i_{U|R}$ (maxima of γ); however they differ in height. At the frequency of 2800 MHz the correlation r maximum is observed, corresponding to the highest γ peak: $r = 0.50 \pm 0.03$ at $\tau = 42$ days (the correlation is significant with reliability no less than 0.999 [24]); the highest maximum corresponds to the third γ peak: $r = 0.72 \pm 0.02$ at $\tau = 280$ days.

If the data reduced AU published in “Solar-Geophysical Data” are taken instead of observed radio emission data, the dependence of U on R slightly decrease. So for the frequency 2800 MHz at $\tau = 42$ days the γ and r peaks decrease by factor 1.03 and 1.11, respectively ($i_{U|R}$ increases at the significance limit: by factor 1.01). Thus, the weak effect of the Earth orbit ellipticity also manifests itself in the detector response.

Figures 6.29-6.31 show that the first and second γ peaks shift towards longer τ as the frequency decreases (source level rises). Further, one can see that large values of γ shift towards large τ as the frequency decreases, with a small decrease in the extreme deviations of γ and $i_{U|R}$: $\gamma = 1.58$, $i_{U|R} = 0.47$ ($\tau = 42$ days) for R_{2800} ; $\gamma = 1.56$, $i_{U|R} = 0.48$ ($\tau = 63$ days) for R_{1415} ; $\gamma = 1.56$, $i_{U|R} = 0.49$ ($\tau = 280$ days) for R_{610} . These features show that processes at overlying levels are activated latter than at underlying ones (the solar activity diffuses upwards). Thus notwithstanding the unusual method of solar activity measurement (by the advance response of an isolated laboratory probing process), the result appears to be quite evident.

6.2.7. Application of Reversibility in Irreversible Time—Forecasting of the Random Large-Scale Processes

Availability of the advanced correlation allowed demonstrating the possibility of the forecast of random component of the solar and geomagnetic activity by the detector signal by means of shift of the realizations. But for the real forecast in such a simplest approach fails, since, first, the processes are far from δ -correlated ones, therefore big errors are unavoidable and, second, position of the main correlation maximum is instable because of non-stationarity of the processes and one can use it only for a *posteriori* demonstration.

To solve the real forecast problem we have elaborated a method based on the convolution of impulse transfer characteristic with multitude of the preceding detector signal values. On the “training” interval $[t_1, t_2]$ we compute the impulse transfer characteristic $g(\tau)$, which relates the detector signal X and the forecasted parameter Y , by solving the following equation:

$$Y(t) = \int_{t_1}^{t_2} g(\tau) X(t - \tau) d\tau . \quad (6.14)$$

The solution of Equation (6.14) in the discrete form is reduced to the system of linear equations $\{Y = XK\}$. The components of K vector are equivalent to coefficients of plural cross-regression (for the case of eigendistribution). The number of equations n equals to the advancement of the forecast.

X is the square matrix $n \times n$, the rows are formed from values of the detector signal on the training interval. The first row consists of the values with time index from 1 to n , the second—from 2 to $n+1$, etc. The sequential values of the Y are corresponding to the each row of matrix. The system is solved with the Gauss method. The stability of the results is achieved by an optimal regularization. Practically the advancement is chosen to be equal to the expected average position of the maximum correlation. The total training interval for Y ends by the last observed value, while for X —preceding on Δt .

The transfer characteristic computed in such a way is then used for the calculation of the only value of the forecasted parameter Y with the advancement Δt . For this purpose the direct problem (6.14) is solved by X interval ended by the last observed value. On the next step (day) the training interval moved forward and the next value Y is forecasted. Such procedure allows minimizing influence of non-stationarity. To suppress the residual instability the received sequence goes through an optimal low-pass postfiltration.

This method is more preferential then those often employed in the analogous situation (of uncertainty of the cross-correlation function maximum) the plural regression method on correlation matrix calculation, since the suggested one does not require any additional hypothesis about the probability distribution. It is essential, for the reason that distribution very seldom is the eigendistribution. But the latter is needed for uniqueness of the regression problem traditional solution. In addition the distribution is not nearly always Gaussian, what is needed for correspondence of this solution to the maximal likelihood criterion.

Note that Equation (6.14) is rather universal and convenient for solving of the anticipatory problem in question, but it could apply to an ordinary deterministic forecast. But physically there is difference of principle in directionality of causal connection: in our method $Y \rightarrow X$, while in any customary ones $Y \rightarrow X$. Namely time reversal allows forecasting the random processes.

The described algorithm has been tested on data previously collected in our experiments, but we have done it, simulating the forecast in real time. We have employed all obtained detector signal hourly time series of sufficient length – not less than one year for the solar radio flux R and two years for the geomagnetic activity Dst (because of shortcoming of the series length, especially valuable with wide-band prefiltration necessary for Dst). Only the data of the electrode detector U (which proved to be the most technically reliable) have satisfied this requirement.

Results of day by day forecasting were compared with factual evolution of R or Dst . Quality of the forecast was assessed by standard deviation of the forecasting and factual curves ε (absolute error in corresponding units, *i.e.* $10^{-22} \text{ Wm}^{-2} \cdot \text{Hz}^{-1}$ for R and nT for Dst). Certainly, both the curves were taken after the same prefiltration.

According to the algorithm, every point of forecasted curves presented below is the result of a computation by selected observed data, the minimal volume of which is determined by the forecast advancement (determining duration of the training interval) and by the filter parameters. It should be stressed that we have restricted ourselves to the forecasts of only the long-period random component that is the background forecasts, although the macroscopic correlation effect in itself admits the forecast of individual powerful events.

In **Figure 6.32** the solar forecast (R at 610 MHz) by the longest available time series is shown. Prefiltration in this case was $T > 28$ days, postfiltration $-T' > 14$ days. Thus data are taken by the same data and with the same prefiltration as for **Figure 6.25**. Resulting advancement $\Delta t = 35$ days, error $\varepsilon = 0.88$, while without postfiltration $\Delta t = 42$ days, $\varepsilon = 1.16$. In this case there is a clear utility of postfiltration.

In **Figure 6.33** the geomagnetic forecast (Dst -index) by the same detector data (that is by the longest experimentally obtained time series) and with the same postfiltration as for **Figure 6.32** (but with another prefiltration $28 < T < 364$ days to suppress the specific deterministic component of geomagnetic activity) is shown. Thus data are taken by the same data and with the same prefiltration as for **Figure 6.18**. Resulting advancement of the forecast $\Delta t = 35$ days, error $\varepsilon = 1.7$. Without postfiltration $\Delta t = 42$ days, but $\varepsilon = 2.4$.

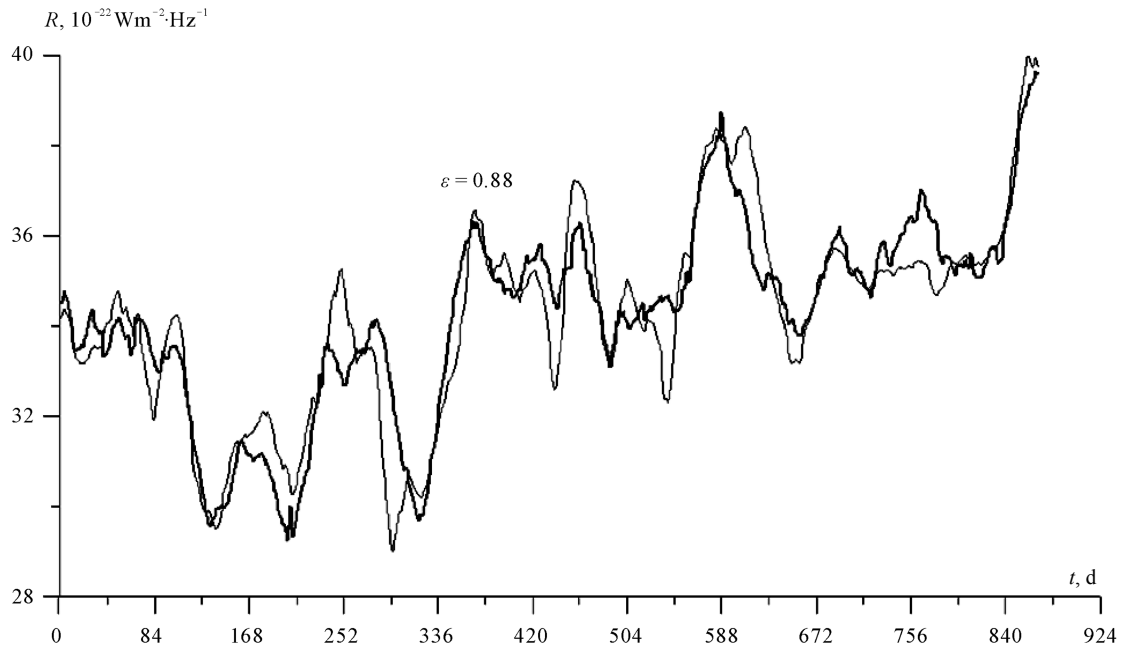


Figure 6.32. The forecast of solar activity with advancement 35 days (fine line) compared to the factual curve (thick line). The origin of time count (days) corresponds to 3/20/1995.

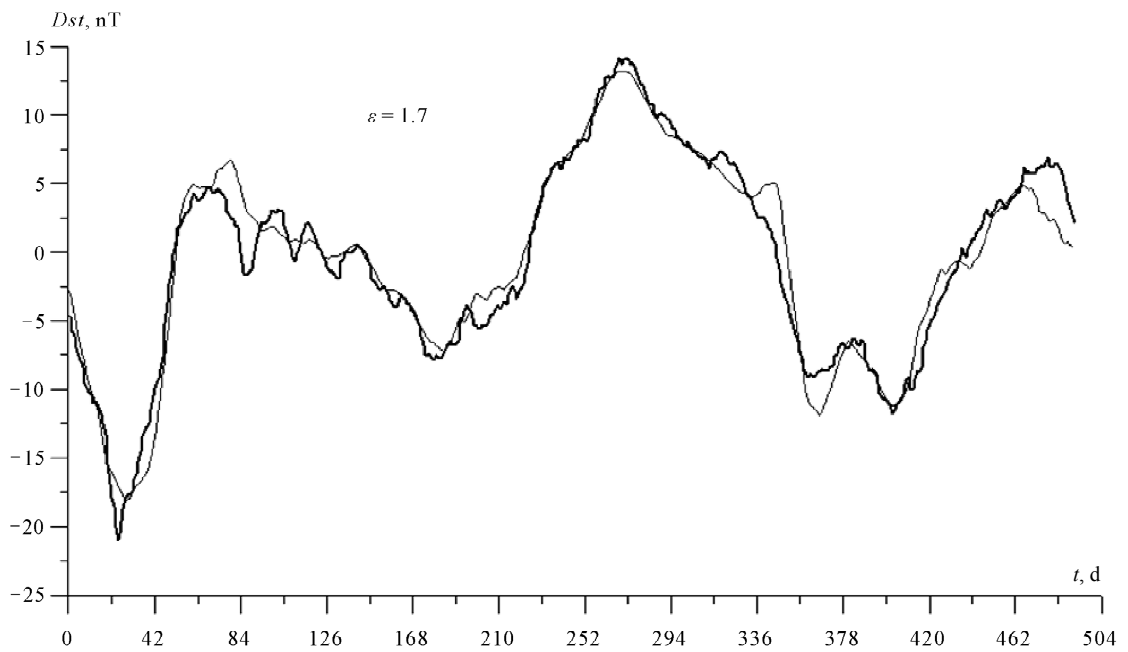


Figure 6.33. The forecast of geomagnetic activity with advancement 35 days (fine line) compared to the factual curve (thick line). The origin of time count (days) corresponds to 9/19/1995.

In **Figure 6.34** the solar forecast (R at 2800 MHz) with the same data and with the same prefiltration ($T > 7$ days) as for **Figure 6.29** is shown. This is time (1997) of beginning of the next in turn solar cycle.

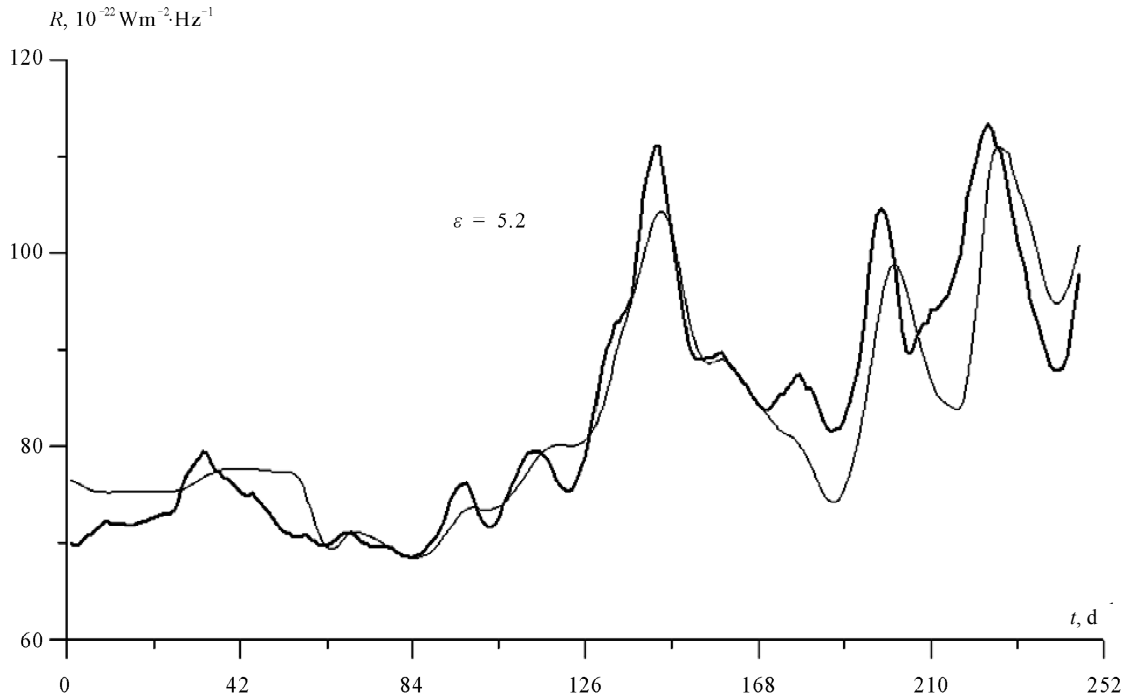


Figure 6.34. The forecast of solar activity with advancement 39 days (fine line) compared to the factual curve (thick line). The origin of time count (days) corresponds to 3/21/1997.

As it is well known, 11 years is only a mean value of the cycle period, the moment of a cycle beginning (*i.e.* the increase after a minimum) is a random event. It is interesting to test the capability of the method around this time. Namely for this reason prefiltration for this case is only $T > 7$ days. The forecasting curve was postfiltered also with $T' > 7$ days. Resulting advancement $\Delta t = 39$ days and error $\varepsilon = 5.2$ are only slightly less than without postfiltration: $\Delta t = 42$ days, $\varepsilon = 5.4$. It can be seen that the cycle beginning (the sharp increase of R at 125^d) is well predicted.

In **Figure 6.35** the solar forecast (R at 1415 MHz) by data of the more recent (2001-2003) experiment provided the most advancement is shown. Prefiltration was $28 < T < 183$ days, postfiltration $-T' > 14$ days. Resulting $\Delta t = 123$ days, $\varepsilon = 2.0$. Without postfiltration $\Delta t = 130$ days, $\varepsilon = 2.4$.

In **Figure 6.36** the geomagnetic forecast (Dst -index) by the same data and with the same pre- and postfiltration as for **Figure 6.35** is shown. Resulting $\Delta t = 123$ days, $\varepsilon = 2.9$, while without postfiltration $\Delta t = 130$ days, $\varepsilon = 3.5$.

As is seen from **Figures 6.32-6.36** the forecast quality is wholly satisfactory, the error ε is small as compared with corresponding typical values of R or Dst .

A few examples, of course, do not allow a certain concluding about statistical dependence of the error ε on the advancement Δt . But it is clear that some minimum $\varepsilon(\Delta t)$ must exist, corresponding to a mean position of maximum $\gamma(\Delta t)$, *i.e.* an optimal advancement must be for such a forecast.

It is well known that geomagnetic activity is a direct effect of solar one. The retardation of geomagnetic activity relative to solar one equals about 1 day (maximum 2 days) that is insignificant in our time scale. Therefore the advancement of correlation of the both processes with the detector signal is practically equal. Hence the optimal advancement for the solar and geomagnetic forecasts by the same time series of the detector signal turns out the same (the pairs shown in **Figures 6.32** and **6.33**, and in **Figures 6.35** and **6.36**).

It is well known also that, in spite of the clear causal connection, the correlation coefficient of solar

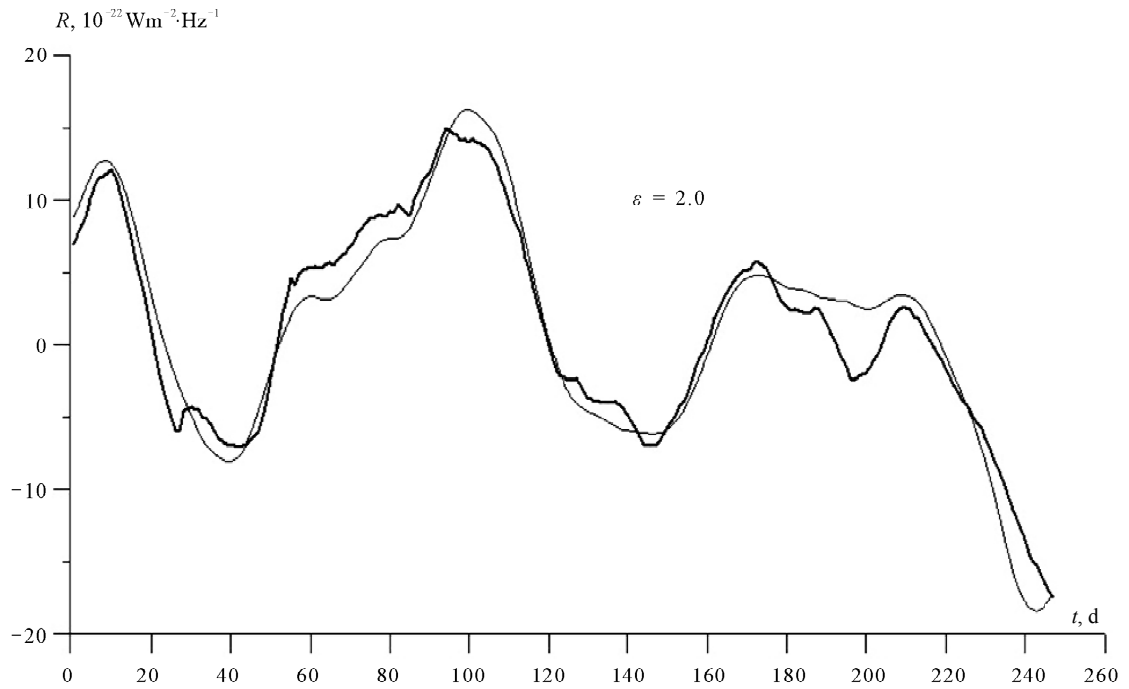


Figure 6.35. The forecast of solar activity with advancement 123 days (fine line) compared to the factual curve (thick line). The origin of time count corresponds to 2/20/2003.

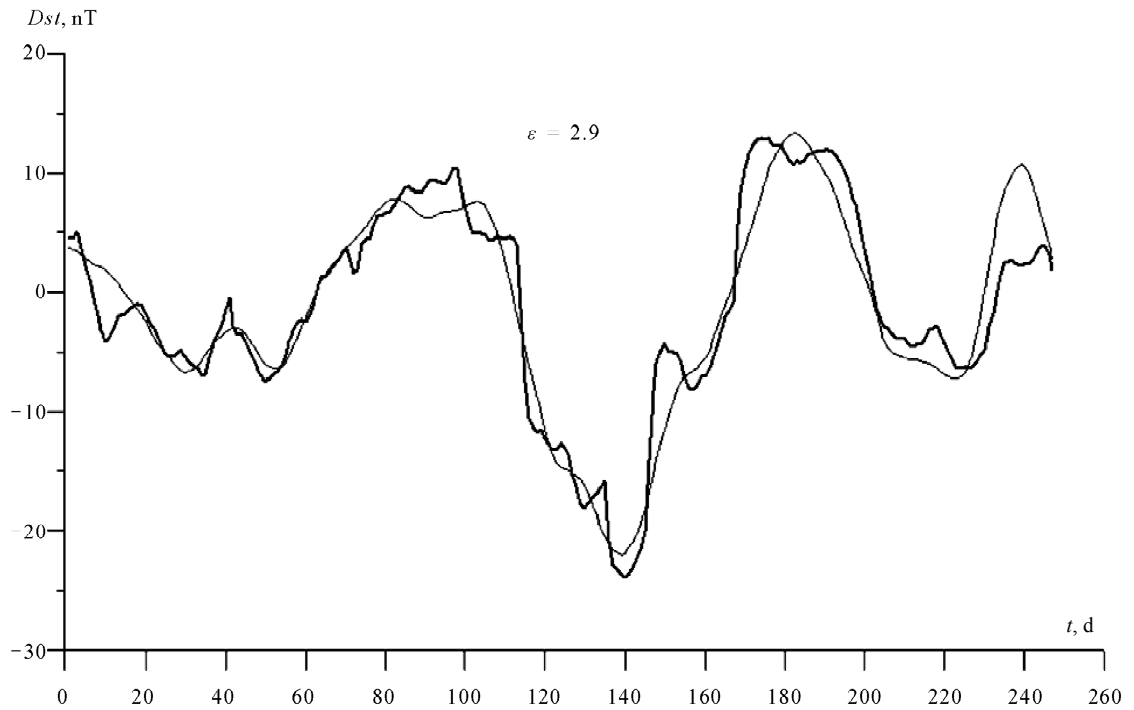


Figure 6.36. The forecast of geomagnetic activity with advancement 123 days (fine line) compared to the factual curve (thick line). The origin of time count corresponds to 2/20/2003.

and geomagnetic activities is rather small (of order—0.3 in terms of R and Dst). Under this condition, an equal success of the solar and geomagnetic forecasts (their accuracy is acceptable for all the practical purposes) means that the detector signal contains direct information about the both activities. Probably it is a consequence of bipartite nature of the macroscopic entanglement of three biseparable states.

Thus employment of nonlocal correlation allows realizing the background long-term forecast of solar and geomagnetic activity with acceptable for all the practical purposes accuracy. Probably this idea may be also implemented for the forecasts of the dissipative processes with big random component in other geospheres, e.g. for the seismic activity.

Conclusion and Discussion

In this small book we started from Kozyrev idea on fundamental time irreversibility and its classical application and finished with surprising manifestation of reversibility in this irreversible time—the possibility of observation of the random future as an existing reality. The key to these questions lies with quantum causality.

The causality is one of the universal physical principles. It plays the twofold role. On the one hand, in the problems brought to the enough theoretical level, this principle allows selecting of the physically realizable solutions among a plethora of the mathematically admissible ones. It is just the case of relativity theory. On the other hand, the establishment of causal-effect connections in analysis of the complicated systems is the first step to the construction of a phenomena model.

In references to the causality principle, usually it does not bear in mind anything except retardation of the effect relative to the cause. With indefinite terms the “cause” and “effect” in the theoretical problems it may lead to the confusions. In the complicated phenomena investigation the rather serious mistakes are possible. It is particularly important for the quantum entangled states. Usually the question about possible reversal of time ordering at quantum correlation through a spacelike interval is avoided presupposing quantum correlation to be causeless. But it is in conflict with the possibility of quantum information transfer. Although practically the conflict is damped by the fact that for the communication purposes one should use an ancillary classical subluminal channel, recently the problem became relevant in connection with macroscopic entanglement, quantum wormholes, etc.

The necessity of formal taking into account of really existing causal connections was felt by many researchers. Moreover Kozyrev’s deeper insight into causality problem had been led him to the interesting theoretical and experimental consequences, partly developed by us in Chapter 1. In answer to this challenge the formal method of classical causal analysis described in Chapter 2 was suggested. This method had been successfully applied before to the various theoretical and experimental problems of classical electrodynamics, magnetohydrodynamics and geophysics. Recently it is also applied to the experiments on macroscopic entanglement. But the classical approach to that quantum phenomenon is rather limited.

Having developed and tested the quantum causal analysis in Chapter 3, we discovered, in particular, that there are the entangled states with both positive independence functions. For such states the classical measure of causality γ is valid. It gave a support of correctness of the γ use in our experimental study of macroscopic entanglement (in addition to the fact of the use of measuring device classical output). Nevertheless in these experiments we deal with quantum causality. In Chapter 3 it has easily been proven that quantum causality, unlike the classical one, can exist only in the open systems. Another interesting property of the mixed entangled states is that they obey the weak causality, for which reverse time is allowed. It is the most important point for understanding of the observed anticipatory effects (advanced correlations).

Of course, our theoretical approach to macroscopic entanglement developed in Chapter 4 is essentially heuristic. There is an obvious theoretical gap between Chapters 3 and 4 in spite of the discussed arguments for the basic equation (4.4), including formal ones expressed by Equations (4.1)-(4.3) and Equations (4.5)-(4.8). The strongest argument for validity of Equation (4.4) is: it describes factual Kozyrev’s results (at least qualitatively) as well as our results (quantitatively!). But since it has not been derived from the first principles, I am far from considering of Equation (4.4) to be more than a heuristic equation and it may turn out a naive approximation of reality. Therefore development of a consistent theory at the crossing point of quantum information, action-a-distance electrodynamics and causal mechanics is burning.

The experiments were performed with three types of detectors. In their construction the main attention was paid to exclusion of all possible local impacts (temperature, and the like). The design of the experimental setups and their parameters (Chapter 4) are described in detail enough for reproducing by other

Conclusion and Discussion

researchers. Technically the most reliable turned out the electrode detectors; that is why most of results presented in Chapter 6 were obtained by their data.

The experiments with controlled (deterministic) lab source-processes (phase transition, etc.) demonstrated, of course, only retarded correlations.

The main effort was directed to detection of correlations with the spontaneous (random) source-processes in the environment: the meteorological, ionospheric, geomagnetic and solar activity in the long-term experiments in 1993-2003. The main results are:

1) Signals of all 5 detectors of 3 types spaced up to 40 km turned out synchronously correlated and this correlation can not be explained by a local impact of any common factors. Level of correlation achieves 0.7 - 0.8 and it is independent of type of detectors and their separation within 40 km.

2) Magnitudes of the detector signals are satisfactory corresponded to predictions of Equation (4.4). Thus Equation (4.4) has been verified quantitatively.

3) The most prominent fact is reliable detection of the advanced response of the probe-processes to the all above source ones. Both inequalities (4.11) and (4.16) are violated. For relatively small space scales advancement and retardation times are symmetrical and in such cases the synchronous response is added. For relatively large space scales retardation time is more than advanced one. Maxima of the correlation functions of the detector signals and the indices of source-activity are observed at advancement of order 10 hours - 100 days and its magnitude is as much as 0.50 - 0.95. Both the advancement and correlation magnitudes increase with the source spatial scale. Advanced correlation always more than retarded, their ratio is 1.1 - 2.6.

The advanced/retarded correlation asymmetry is a consequence of absorption asymmetry. The latter was theoretically predicted (at the qualitative level) by Hoyle and Narlikar [65]. In Chapter 6 I have cast doubt only on their cosmological interpretation of this theoretical statement. Our experiments have confirmed the predicted advanced/retarded asymmetry. But doubt about its cosmological nature became stronger.

Indeed perfect absorption of the retarded direct particle field and imperfect absorption of the advanced one is decisive statement for Steady-state and Quasi-steady-state cosmology. The question to an experiment is that to verify whether advanced/retarded efficiencies ratio observed in nonlocal transaction is independent of the matter screening properties? If yes, it is strong evidence for Steady-state and Quasi-steady-state cosmology. If no, it is evidence of T-noninvariantness in more broad sense. Our experimental results point to the latter answer. The advanced/retarded ratio proved to be variable. The scatter of the ratio from 1.1 to 2.6 is too large to accept the former answer. However since the ratio tends to increase as the space scale increase, may be at scales larger than solar one the ratio becomes asymptotically constant. Then the cosmological hypothesis has a chance. It is a question to the future experiments.

But regardless of the interpretation, the level of advanced correlation proved to be enough for the employment of macroscopic entanglement for solar and geomagnetic activity forecast.

All employed at present methods of the forecast of natural processes, in particular solar and geomagnetic activity operate with its components determined its own evolution and by the external factors (even if the statistical approaches are used). However a random (spontaneous) component is rather essential. It is associated with that forecasted system is complicated in a synergetic sense, the typical feature of which is instability caused by the trajectory divergence in the phase space. In the case of geomagnetic activity it is not very important for the short-term geomagnetic forecast, because the external factors, *i.e.* the solar activity and interplanetary medium state are given by the observations yet. Therefore unpredictability many of the solar activity manifestations, *e.g.* the flares, is not of importance. But for the long-term geomagnetic forecasts which are explicitly or implicitly based on the solar activity forecast, the random component is comparable with the determined one (and exceeds it for the catastrophic events). Thus impossibility of taking into account the random component degrades accessible accuracy and advancement of the forecast.

The only phenomenon of macroscopic entanglement gives a basic possibility of the random component

forecast. In Chapter 6 the availability of fairly strong advanced correlations with large value of advancement enables us to put and solve the problem of forecasting of random large-scale natural processes on the macroscopic nonlocal correlations effect. We have considered this problem as applied to the solar and geomagnetic activities. The pragmatic forecasting algorithm on the macroscopic correlations has been developed. Its efficiency has been proved on all data of the long-term experiments in regime of the real forecast with advancement up to four months. The accuracy of the obtained solar and geomagnetic forecasts is acceptable for all the practical purposes.

It should be stressed that the suggested method is unique namely by the possibility of forecasting of the spontaneous (random) component of variations. Repeat, all existing approaches to the forecasting problem are deterministic (in spite of employment of statistical cross- or auto-regression algorithms), the random component is an unavoidable error for them. Indeed a true random process can not be forecasted by any classical way. Namely quantum nature of the macroscopic nonlocal correlations effect has allowed forecasting such processes. Therefore the suggested method is essentially complementary to the customary ones.

Thus employment of nonlocal correlation allows realizing the background long-term forecast of solar and geomagnetic activity with acceptable for all the practical purposes accuracy. Probably this idea may be also implemented for the forecasts of the dissipative processes with big random component in other geospheres, e.g. for the seismic activity.

In summary it may be said that I have presented a theoretical and an experimental approach to the anticipatory effect of nonlocal correlations. The former is rather heuristic at macroscopic level, while the latter is quite rigorous. It stands to reason that the development of the theory of macroscopic entanglement, especially in the action-at-a-distance electrodynamics spirit, has a fundamental importance. Perhaps our theoretical approach is too rough. But at the contemporary rigour of level, the experiments have confirmed Kozyrev results about surprising manifestation of reversibility in irreversible time—the possibility of observation of the future random states (undetermined by the previous evolution).

I would be happy if this book inspires the readers on development of a consistent theory as well as on performance of the wider experiments.

References

- [1] N. A. Kozyrev, "On the possibility of experimental investigation of the properties of time," In: J. Zeman, Ed., *Time is Science and Philosophy*, Academia, Prague, 1971, pp. 111-132.
- [2] M. L. Arushanov and S. M. Korotaev, "Geophysical effects of causal mechanics," In: A. P. Levich, Ed., *On the Way to Understanding the Time Phenomenon. Part 2*, World Scientific, Singapore, 1996, pp. 101-108.
- [3] M. L. Arushanov and A. M. Goryachev, "To a problem on necessity of the registration of effects of causal mechanics on an example of simple barotropic model of the atmosphere," *Meteorology and Atmospheric Physics*, Vol. 85, No. 3, March 2004, pp. 10-18.
- [4] S. M. Korotaev, "Formal definition of causality and Kozyrev's axioms," *Galilean Electrodynamics*, Vol. 4, No. 5, October 1993, pp. 86-89.
- [5] S. M. Korotaev, "On the possibility of causal analysis of the geophysical processes," *Geomagnetism and Aeronomy*, Vol. 32, No. 1, February 1992, pp. 27-33.
- [6] S. M. Korotaev, O. A. Hachay and S. V. Shabelyansky, "Application of causal analysis to the vertical diffusion process of magnetic field in the ocean," *Geomagnetism and Aeronomy*, Vol. 32, No. 1, February 1992, pp. 48-53.
- [7] S. M. Korotaev and O. A. Hachay, "Causal analysis and its application to study of the electromagnetic processes in the sea," *Izvestia Physics of the Solid Earth*, Vol. 28, No. 4, April 1992, pp. 52-61.
- [8] S. M. Korotaev, O. A. Hachay and L. K. Low, "Results of causal analysis application to observations of the variable magnetic field in the sea," *Izvestia Physics of the Solid Earth*, Vol. 28, No. 5, May 1992, pp. 35-44.
- [9] S. M. Korotaev, S. V. Shabelyansky and V. O. Serdyuk, "Generalized causal analysis and its employment for study of electromagnetic field in the ocean," *Izvestia Physics of the Solid Earth*, Vol. 28, No. 6, June 1992, pp. 77-86.
- [10] O. A. Hachay, S. M. Korotaev and A. K. Troyanov, "Results of application of the causal analysis to seismoacoustic and electromagnetic emission borehole data processing," *Volcalonogy and Seismology*, Vol. 14, No. 3, March 1992, pp. 92-100.
- [11] S. M. Korotaev and O. A. Hachay, "Role of retardation in the causal analysis of the geophysical processes," *Geomagnetism and Aeronomy*, Vol. 32, No. 4, August 1992, pp. 119-121.
- [12] S. M. Korotaev, O. A. Hachay and S. V. Shabelyansky, "Causal analysis of the process of horizontal informational diffusion of electromagnetic field in the ocean," *Geomagnetism and Aeronomy*, Vol. 33, No. 2, April 1993, pp. 128-133.
- [13] M. L. Arushanov and S. M. Korotaev, "Causal analysis and its employment for study of physical processes in the atmosphere," *Meteorology and Hydrology*, No. 6, June 1994, pp. 15-22.
- [14] S. M. Korotaev, "Role of different definitions of the entropy in the causal analysis," *Geomagnetism and Aeronomy*, Vol. 35, No. 3, June 1995, pp. 387-393.
- [15] S. M. Korotaev and E. O. Kiktenko, "Causal analysis of the quantum states," *AIC Conference Proceedings*, Vol. 1316, No. 1, 2010, pp. 3295-329.
- [16] J. G. Cramer, "Generalized absorber theory and Einstein-Podolsky-Rosen paradox," *Physical Review D*, Vol. 22, No. 2, January 1980, pp. 362-376.
- [17] S. M. Korotaev, V. O. Serdyuk, M. O. Sorokin and J. M. Abramov, "Geophysical manifestation of interaction of the processes through the active properties of time," *Physics and Chemistry of the Earth (A)*, Vol. 24, No. 8, August 1999, pp. 735-740.
- [18] S. M. Korotaev, V. O. Serdyuk and M. O. Sorokin, "Effect of macroscopic nonlocality on geomagnetic and solar-ionospheric processes," *Geomagnetism and Aeronomy*, Vol. 40, No. 3, June 2000, pp. 323-330.
- [19] S. M. Korotaev, A. N. Morozov, V. O. Serdyuk and J. V. Gorohov, "Experimental evidence of nonlocal transaction in reverse time," In: M. C. Duffy, Ed., *Physical Interpretation of Relativity Theory*, BMSTU Press, Moscow, 2003, pp. 200-212.
- [20] S. M. Korotaev, A. N. Morozov, V. O. Serdyuk, J. V. Gorohov and V. A. Machinin, "Experimental study of macroscopic nonlocality of large-scale geomagnetic dissipative processes," *NeuroQuantology*, Vol. 3, No. 4, August 2005, pp. 275-294.
- [21] S. M. Korotaev S.M. "Experimental study of advanced correlation of some geophysical and astrophysical processes," *International Journal of Computing Anticipatory Systems*, Vol. 17, 2006, pp. 61-76.
- [22] A. N. Morozov, "Irreversible Processes and Brownian Motion," BMSTU Press, Moscow, 1997 (in Russian).
- [23] S. M. Korotaev, V. O. Serdyuk, M. O. Sorokin and V. A. Machinin, "Experimental study of nonlocality of the controlled dissipative processes," *Physical Thought of Russia*, No. 3, March 2000, pp. 20-26 (in Russian).
- [24] S. M. Korotaev, A. N. Morozov, V. O. Serdyuk and M. O. Sorokin, "Manifestation of macroscopic nonlocality in some natural dissipative processes," *Russian Physics Journal*, Vol. 45, No. 5, May 2002, pp. 3-14.

References

- [25] S. M. Korotaev, V. O. Serdyuk, V. I. Nalivaiko, A. V. Novysh, S. P. Gaidash, Yu. V. Gorokhov, S. A. Pulinets and Kh. D. Kanonidi, "Experimental estimation of macroscopic nonlocality effect in solar and geomagnetic activity," *Physics of Wave Phenomena*, Vol. 11, No. 1, February 2003, pp. 46-55.
- [26] S. M. Korotaev, V. O. Serdyuk, J. V. Gorohov, S. A. Pulinets and V. A. Machinin, "Forecasting effect of macroscopic nonlocality," *Frontier Perspectives*, Vol. 13, No. 1, February 2004, pp. 41-45.
- [27] S. M. Korotaev, A. N. Morozov, V. O. Serdyuk, V. I. Nalivaiko, A. V. Novysh, S. P. Gaidash, Yu. V. Gorokhov, S. A. Pulinets and Kh. D. Kanonidi, "Manifestation of macroscopic nonlocality in the processes of solar and geomagnetic activity," *Vestnik Journal of Bauman Moscow State Technical University*, Special Issue, Moscow, 2005, pp. 173-185.
- [28] S. M. Korotaev, A. N. Morozov, V. O. Serdyuk, J. V. Gorohov and V. A. Machinin, "Experimental study of advanced nonlocal correlation of large scale dissipative processes," In: P. Rowlands, Ed., *Physical Interpretation of Relativity Theory*, BMSTU PH, Moscow, 2005, pp. 209-231.
- [29] S. M. Korotaev, A. N. Morozov, V. O. Serdyuk, J. V. Gorohov, V. A. Machinin and B. P. Filippov, "Experimental study of advanced nonlocal correlations of the process of solar activity," *Russian Physics Journal*, Vol. 50, No. 4, April 2007, pp. 333-341.
- [30] S. M. Korotaev, V. O. Serdyuk and J.V. Gorohov, "Forecast of solar and geomagnetic activity on the macroscopic nonlocality effect," *Hadronic Journal*, Vol. 30, No. 1, February 2007, pp. 39-56.
- [31] S. M. Korotaev, V. O. Serdyuk and J. V. Gorohov, "Signals in reverse time from heliogeophysical random processes and their employment for the long-term forecast," In: P. Rowlands, Ed., *Physical Interpretation of Relativity Theory*, BMSTU PH, Moscow, 2007, pp. 222-230.
- [32] S. M. Korotaev, V. O. Serdyuk and J. V. Gorohov, "Forecast of solar and geomagnetic activity on the nonlocal correlations," *Doklady Earth Sciences*, Vol. 415A, No. 6, October 2007, pp. 975-978.
- [33] S. M. Korotaev and V. O. Serdyuk, "The forecast of fluctuating large-scale natural processes and macroscopic correlations effect," *International Journal of Computing Anticipatory Systems*, Vol. 20, 2008, pp. 31-46.
- [34] N. A. Kozyrev and V. V. Nasonov, "New method of determination of trigonometric parallaxes on the base of difference between actual and visible position of the stars," In: A. A. Efimov, Ed., *Astrometry and Heavenly Mechanics*, VAGO Press, Moscow, 1978, pp. 168-179 (in Russian).
- [35] N. A. Kozyrev and V. V. Nasonov, "On some properties of time revealed by astronomy observations," In: A. A. Efimov, Ed., *Manifestation of Cosmic Factors on the Earth and Stars*, VAGO Press, Moscow, 1980, pp. 76-84 (in Russian).
- [36] N. A. Kozyrev, "Astronomical proofs of reality of 4D minkowski geometry," In: A. A. Efimov, Ed., *Manifestation of Cosmic Factors on the Earth and Stars*, VAGO Press, Moscow, 1980, pp. 85-93 (in Russian).
- [37] S. M. Korotaev, "Logic of causal mechanics: Observations-theory-experiments," In: A. P. Levich, Ed., *On the Way to Understanding the Time Phenomenon. Part 2*, World Scientific, Singapore, 1996, pp. 60-74.
- [38] C. E. Shannon and W. Weaver, "The mathematical theory of communication," University of Illinois Press, Champaign, 1949.
- [39] N. J. Cerf and C. Adami, "Quantum extension of conditional probability," *Physical Review A*, Vol. 60, No. 2, August 1999, pp. 863-897.
- [40] N. J. Cerf, "Entropic bounds on coding for noisy quantum channels," *Physical Review A*, Vol. 57, No. 5, May 1998, pp. 3330-3347.
- [41] S. Mukohyama, "Comments on entanglement entropy," *Physical Review D*, Vol. 58, No. 10, November 1998, Article ID: 104023.
- [42] A. Borrás, A. R. Plastino, M. Casas and A. Plastino, "Quantum brachistochrone evolution of systems of two identical particles: The role of entanglement," *Physical Review A*, Vol. 78, No. 5, November 2008, Article ID: 052104.
- [43] W. K. Wootters, "Entanglement of formation of an arbitrary states of two qubits," *Physics Review Letters*, Vol. 80, No. 10, March 1998, pp. 2245-2248.
- [44] W. Dür, "Multipartite entanglement that is robust against disposal of the particles," *Physical Review A*, Vol. 63, No. 2, February 2001, p. 020303.
- [45] S. S. Jang, Y. W. Cheong, J. Kim and H. W. Lee, "Robustness of multiparty nonlocality to local decoherence," *Physical Review A*, Vol. 74, No. 6, December 2006, Article ID: 062112.
- [46] W. Song and Z.-B. Chen, "Invariant information and complementarity in high-dimensional states," *Physical Review A*, Vol. 76, No. 1, July 2007, Article ID: 014307.
- [47] M. B. Plenio, S. F. Huelga, A. Beige and P. L. Knight, "Cavity-loss-induced generation of entangled atoms," *Physical Review A*, Vol. 59, No. 3, March 1999, pp. 2468-2475.
- [48] A. M. Basharov, "Decoherence and entanglement by radiation decay of two-atom system," *Journal of Experimental and Theoretical Physics*, Vol. 121, No. 6, June 2002, pp 1249-1260.
- [49] M. B. Plenio and S. F. Huelga, "Entangled light from white noise," *Physics Review Letters*, Vol. 88, No. 19, May 2002, Article ID: 197901.

- [50] M. S. Kim, J. Lee, D. Ahn and P. L. Knight, "Entanglement induced by a single-mode heat environment," *Physical Review A*, Vol. 65, No. 4, April 2002, Article ID: 040101.
- [51] D. Braun, "Creation of entanglement by interaction with a common heat bath," *Physics Review Letters*, Vol. 89, No. 27, December 2002, Article ID: 277901.
- [52] L. Jakobczyk, "Entangling two qubits by dissipation," *Journal of Physics A*, Vol. 35, No. 7, July 2002, pp. 6383-6392.
- [53] F. Benatti, R. Floreanini and M. Piani, "Environment induced entanglement in Markovian dissipative dynamics," *Physics Review Letters*, Vol. 91, No. 7, August, 2003, Article ID: 070402.
- [54] T. Choi and H. J. Lee, "Quantum entanglement induced by dissipation," *Physical Review A*, Vol. 76, No. 1, July 2007, Article ID: 012308.
- [55] W. J. Munro, D. F. V. James, A. G. White and P.G. Kwiat, "Maximizing the entanglement of two mixing qubits," *Physical Review A*, Vol. 64, No. 3, September 2001, Article ID: 030302.
- [56] V. Coffman, J. Kundu and W. K. Wootters, "Distributed entanglement," *Physical Review A*, Vol. 61, No. 5, May 2000, Article ID: 052306.
- [57] A. K. Rajagopal and R. W. Rendell, "Robust and fragile entanglement of three qubits: Relation to permutation symmetry," *Physical Review A*, Vol. 65, No. 3, March 2002, Article ID: 032328.
- [58] A. K. Rajagopal and R. W. Rendell, "Separability and correlation in composite states based on entropy methods," *Physical Review A*, Vol. 66, No. 2, August 2002, Article ID: 022104.
- [59] K. Życzkowski, P. Horodecki, M. Horodecki and R. Horodecki, "Dynamics of quantum entanglement," *Physical Review A*, Vol. 65, No. 1, January 2002, Article ID: 012101.
- [60] Y. Sun, Y. Chen and H. Chen, "Thermal entanglement in the two-qubit Heisenberg XY model under a nonuniform external magnetic field," *Physical Review A*, Vol. 68, No. 4, October 2003, Article ID: 044301.
- [61] X. Wang and Z. D. Wang, "Thermal entanglement in ferromagnetic chains," *Physical Review A*, Vol. 73, No. 6, June 2006, Article ID: 064302.
- [62] J. G. Cramer, "The transactional interpretation of quantum mechanics," *Reviews of Modern Physics*, Vol. 58, No. 3, September 1986, pp. 647-688.
- [63] A. S. Elitzur and S. Dolev, "Is there more to T?" In: R. Buccery, M. Saniga and W. M. Stuckey, Eds., *The Nature of Time: Geometry, Physics and Perception*, Kluwer Academic Publishers, Norwell, 2003, pp. 297-306.
- [64] M. Laforest, J. Baugh and R. Laflamme, "Time-reversal formalism applied to bipartite entanglement: Theoretical and experimental exploration," *Physical Review A*, Vol. 73, No. 3, March 2006, Article ID: 032323.
- [65] F. Hoyle and J. V. Narlikar, "Cosmology and action-at-a-distance electrodynamics," *Reviews of Modern Physics*, Vol. 67, No. 1, March 1995, pp. 113-156.
- [66] D. Home and A. S. Majumdar, "Incompatibility between quantum mechanics and classical realism in the strong macroscopic limit," *Physical Review A*, Vol. 52, No. 6, December 1995, pp. 4959-4962.
- [67] C. Simon and J. Kempe, "Robustness of multiparty entanglement," *Physical Review A*, Vol. 65, No. 5, May 2002, Article ID: 052327.
- [68] W. Dür and H.-J. Briegel, "Stability of macroscopic entanglement under decoherence," *Physics Review Letters*, Vol. 92, No. 18, May 2004, Article ID: 180403.
- [69] M. Hein, W. Dür and H.-J. Briegel, "Entanglement properties of multipartite entangled states under influence of decoherence," *Physical Review A*, Vol. 71, No. 3, March 2005, Article ID: 032350.
- [70] J. Calsamiglia, L. Hartmann, W. Dür and H.-J. Briegel, "Spin gases: Quantum entanglement driven by classical kinematics," *Physics Review Letters*, Vol. 95, No. 18, October 2005, Article ID: 180502.
- [71] B. Julsgaard, A. Kozhelkin and E. S. Polzik, "Experimental long lived entanglement of two macroscopic objects," *Nature*, Vol. 413, No. 6854, 2001, pp. 400-403.
- [72] S. Ghosh, T. F. Rosenbaum, G. A. Aepli and S. N. Coppersmith, "Entanglement quantum state of magnetic dipoles," *Nature*, Vol. 425, No. 6953, 2003, p. 48.
- [73] H. Xu, F. W. Strauch, S. K. Dutta, P. R. Johnson, R. C. Ramos, A. J. Berkley, H. Paik, J. R. Anderson, A. J. Dragt, C. J. Lobb and F. C. Wellstood, "Spectroscopy of three-particle entanglement in a macroscopic superconducting circuit," *Physics Review Letters*, Vol. 94, No. 2, January 2005, Article ID: 027003.
- [74] S. L. Braunstein and C. M. Caves, "Information-theoretic bell inequalities," *Physics Review Letters*, Vol. 61, No. 6, August 1988, pp. 662-665.
- [75] N. C. Cerf and C. Adami, "Entropic bell inequalities," *Physical Review A*, Vol. 55, No. 5, May 1997, pp. 3371-3374.
- [76] S. M. Korotaev, "Filtration electromagnetic field of the submarine springs," *Izvestiya Physics of the Solid Earth*, No. 8, August 1979, pp. 91-95.
- [77] M. M. Bogorodsky and E. F. Zimin, "Modern methods and tools of the geoelectric field research," *Izvestia Physics of the Solid Earth*, Vol. 32, No. 10, October, 1996, pp. 31-40.
- [78] J. G. Digurova, M. I. Soloviev and I. S. Golyak, "Determination of device temperature coefficients at long research," In: A. N. Morozov, Ed., *Irreversible Processes in Nature and Technics, Part I*, PIAS Press, Moscow, 2007, pp. 205-208

References

- (in Russian).
- [79] S. M. Korotaev, J. G. Digurova and M. I. Soloviev, "Preliminary results of investigation of cosmic ray variation influence on signals of different detector kinds," In: A. N. Morozov, Ed., *Irreversible Processes in Nature and Technique, Part I*, Bauman Moscow State Technical University Press, Moscow, 2009, pp. 18-21 (in Russian).
 - [80] D. Savage, "Time stress and other properties of time," *The Toth-Maatian Review*, Vol. 4, No. 2, April 1985. pp. 1899-1911.
 - [81] D. Savage, "Conservation of momentum at a distance," *The Toth-Maatian Review*, Vol. 4, No. 4, August 1986, pp. 2257-2262.
 - [82] D. Savage, "Measuring local time dilation using sandglass egg timers," In: A. Wesely, Ed., *Progress in Space-Time Physics*, Blumberg University Press, 1987, pp. 242-251.
 - [83] M. M. Lavrentyev, I. A. Eganova, M. K. Lutset and S. E. Fominyh, "On remote influence of the stars upon the resistor," *Physics-Doklady*, Vol. 314, No. 2, February 1990, pp. 352-355.

Abbreviations

GHZ state	Greenberger-Horne-Zeilinger state (3.30).
CKW state	Coffman-Kundu-Wootters state (3.55).

